Disorder and synchronization in nonequilibrium Bose-Einstein condensates

John Moroney

A thesis presented for the degree of
Doctor of Philosophy

School of Physics

Trinity College Dublin

2022

Declaration

I declare that this thesis has not been submitted as an exercise for a degree at this or any other university and it is entirely my own work.

I agree to deposit this thesis in the University's open access institutional repository or allow the Library to do so on my behalf, subject to Irish Copyright Legislation and Trinity College Library conditions of use and acknowledgement.

I consent to the examiner retaining a copy of the thesis beyond the examining period, should they so wish (EU GDPR May 2018).

Signed: _____
         John Moroney

Summary

In this thesis, we investigate the impact of spatial disorder on driven-dissipative Bose-Einstein condensates (BECs). Bose-Einstein condensation is a collective phenomenon where many particles spontaneously occupy a single energy level and behave as a single quantum state. In recent years, new types of BECs have been made from part-light, part-matter quasiparticles called polaritons, which occur in semiconductor microcavities. Such condensates are nonequilibrium in nature, as polaritons have finite lifetimes, and so a population must be maintained through pumping. The nonequilibrium nature of these new condensates gives rise to new and interesting behaviour, distinct from traditional equilibrium BECs.

We first consider a double well configuration where two condensates with different energies are localized on either side of a potential barrier. Depending on a number of factors including the energy detuning between wells, the density of particles in each condensate, and their ability to tunnel between wells, the frequencies of the condensates may be either desynchronized or synchronized. We extend previous work, which characterizes the synchronized and desynchronized regimes of this configuration, to include the effect of pumping of the condensates in each well with different strengths. This is done in the framework of a non-equilibrium extension of the Gross-Pitaevskii equation, where the phase difference between condensates is shown to behave like an overdamped pendulum. We find that this pump asymmetry acts as an effective detuning, shifting the position of the phase boundary between synchronized and desynchronized states.

We then generalize the analysis of the double well to the case of lattices of many localized condensates. We derive a description for this system in terms of coupled equations for the phase of the condensate at each site. We

demonstrate the similarities between this model and the Kuramoto model of coupled oscillators. Unlike the Kuramoto model, however, this lattice model permits a synchronized solution in the thermodynamic limit, and thus exhibits a phase transition. We demonstrate this through mapping to a continuum description, and outlining the connection of the model to the quantum description of a particle moving in a random potential. We produce a phase diagram characterizing the synchronized and desynchronized regimes of this system, and demonstrate the agreement between our theory and numerical simulations.

Following this, we consider whether such a synchronized lattice of condensates may exhibit superfluidity. This may be tested by applying a phase twist across the boundaries of the system and measuring its energy response. By way of numerical simulations of our lattice oscillator model of driven-dissipative condensates, we confirm previous results which find that disorder inhibits superfluidity. While a uniform lattice with no detunings between sites displays a non-zero superfluid stiffness, this disappears when disorder is present in the on-site energies. We present a further perspective on this result by discussing it in the context of the connection to the wavefunction of a particle localized in a random potential.

We also analyse correlation functions of the synchronized, disordered lattice in one dimension. By plotting the spatial correlation function of the condensate order parameter, we show that this system exhibits long-range phase order. This is contrasted with correlation functions of the same system, but with the static disorder replaced by spatio-temporal noise. These noisy correlation functions are seen to decay exponentially with distance. Finally, we consider the impact of both types of disorder simultaneously – time-independent random on-site energies, and spatio-temporal noise. We find that while the phase profiles of such systems have the same long-range structure that is seen for synchronized lattices with static disorder, the additional fluctuations cause the correlation functions to decay. These numerical results enable us to draw a phase diagram of the regimes of phase and frequency ordering in 1D as a function of the strengths of both the static disorder and the noise.

Acknowledgements

I feel incredibly fortunate to have had Paul Eastham as my supervisor for this PhD. In addition to providing countless valuable insights and helping me to improve my knowledge and understanding of physics, he has consistently been patient and generous with his time, and has always been available to provide guidance when needed. I've learned a lot from him.

I would like to thank all of the members of Paul's Quantum Theory of Light and Matter group, as well as my fellow occupants of office 2.21 in the Lloyd institute, for the lively and enlightening discussions, which were not limited to topics in physics.

I am lucky to have a wonderful group of friends who have done a great job of keeping me balanced by distracting me from matters of physics and research over the past four years. I don't have the space to name all of you, but if you're reading this thesis without a specific interest in nonequilibrium Bose-Einstein condensates, I'm probably talking about you.

Special thanks go to my parents, my sisters, and of course, Aisling. Your continuous and unwavering belief and support made this possible, and I am so grateful.

Contents

x

List of Publications

Material from this thesis appears in the following paper:

John P. Moroney and P. R. Eastham, Synchronization in disordered oscillator lattices: Nonequilibrium phase transition for driven-dissipative bosons, Physical Review Research 3, 043092 (2021)

Chapter 1

Introduction

1.1 Motivation

This project is quite generally about how things order. Despite the implications of the second law of thermodynamics, nature does not always tend towards disorder. Sometimes, it becomes favourable for systems of many components to align their behaviour with each other. Examples of such ordering include swarms of fireflies flashing in synchrony, water turning to ice as it freezes, and the magnetization of metals. This dramatic change of the properties of a system is called a phase transition. The sudden and often unexpected nature of phase transitions make them quite spectacular to observe. Arguably one of the most spectacular and unexpected examples of an ordering transition is Bose-Einstein condensation.

The phenomenon of Bose-Einstein condensation has fascinated and intrigued physicists since it was first predicted almost a century ago. A Bose-Einstein condensate (BEC) is formed when a gas of bosons is cooled below a critical temperature. At this point, a macroscopic number of the particles begin to occupy the same ground state energy level. This creates a new exotic state of matter which opens a rare window on the quantum world. Because many particles begin to behave collectively as one, BECs exhibit quantum behaviour on a macroscopic scale. Novel behaviour associated with BECs includes superfluidity, or flowing without dissipation.

Pure BECs were only first realized experimentally in 1995, when atomic gases were successfully cooled to a few hundred nanoKelvin [1, 2, 3]. In the

1

last twenty years, the field has seen a frenzy of renewed interest, due to numerous different experimental realizations of BECs of different particles [4]. Perhaps the most exciting of these was the discovery of condensation of exciton-polaritons – part-light, part-matter quasiparticles that occur in semiconductor microcavities [5, 6]. Unlike in the case of atoms, ultra-low temperatures are not required for the condensation of polaritons due to their extremely low mass. However, polaritons are short-lived particles, decaying after a few picoseconds, and as a result, the condensates they form are not in thermal equilibrium. Polariton condensates must be pumped with a laser to compensate for losses due to decay. This driven-dissipative nature of polariton condensates gives rise to some novel behaviour, distinct from that of equilibrium BECs [7, 8, 9, 10].

The work in this thesis focuses on understanding on the impact of randomness and disorder on driven-dissipative condensates. Impurities in the semiconductor material as well as features of the pump laser can lead to a disorder potential which the polariton condensates inhabit. The presence of such disorder is inevitable, particularly in the materials most suitable for room-temperature polariton condensation [11]. Strong disorder can cause multiple localized condensates to form in a single sample. We describe how these individual condensates, when organized in pairs and lattices with random energies, can synchronize their frequencies and form a single ordered state.

Remarkably, this may be described in a similar way as to how seemingly unrelated systems – such as coupled clocks – synchronize their motions. We develop a theory describing how a general class of locally-coupled oscillators synchronize their frequencies when arranged in disordered lattices. While this analysis was motivated by a desire to understand the behaviour of driven-dissipative condensates in the presence of disorder, its implications are not limited to this particular system. Our work therefore intersects the multidisciplinary field of coupled oscillators [12]. This approach provides us with accessible and tractable models which we use to probe the complex behaviour of polariton condensates. We apply results obtained from these models to characterize the impact of disorder in driven-dissipative condensates.

We begin with an overview of some of the key concepts involved in this

thesis.

1.2 Exciton-polaritons

When light is incident on a semiconductor, the material may absorb a photon, exciting an electron from the valence band to the conduction band, and creating a hole in the valence band. The Coulomb attraction between these oppositely-charged particles can lead to the formation of a bound state of an electron and a hole, called an exciton. This compound particle may be thought of as a hydrogenic atom, with a binding energy which lowers its energy below that of the bandgap. An exciton is thus the lowest-energy optical excitation of a pure semiconductor. The system may return to its ground state through decay of the exciton, where the electron and hole recombine, and a photon is emitted. Much like an atom, this excitation can couple to the electromagnetic field, and indeed, by placing quantum wells in a semi-conductor microcavity, one may have strong coupling to modes of the cavity whereby the rate at which exciton-photon transitions occur exceeds the rate at which photons are lost from the cavity. In this regime, the eigenstates of the system are no longer bare excitons or photons, but instead a quantum superposition of the two, called a polariton [5, 13].

The cavity exciton-polariton is not the only species of polariton that has been observed: other excitations such as phonons and magnons may also couple to light, and indeed polaritons may exist outside of cavities. None of these will be considered in this work, however, and so when polaritons are mentioned, it is the picture outlined in this section we have in mind.

Microcavities are typically constructed from GaAs or CdTe, although other materials such as GaN, and ZnO are also used [10, 14]. Photons are trapped using mirrors made from distributed Bragg reflectors composed of alternating dielectrics of different refractive indices, each of thickness one quarter wavelength. These cavities confine photons in two dimensions, quantizing their motion in the z-direction as $k_z = 2\pi N/L$, where L is the effective width of the cavity, and the available modes are indexed by N. The photon

dispersion may then be written as

$$\omega_{\mathbf{k}} = \frac{c}{n}|\mathbf{k}| = \left(\frac{c}{n}\right)\sqrt{k^2 + \left(\frac{2\pi N}{L}\right)^2} \tag{1.1}$$

where k is in-plane wavevector and n the refractive index. For small k, this may be expanded to give the parabolic dispersion

$$\omega_{\mathbf{k}} = \left(\frac{c}{n}\right)\left(\frac{2\pi N}{L} + \frac{k^2 L}{4\pi N}\right), \tag{1.2}$$

which we may write as

$$\omega_{\mathbf{k}} = \omega_0 + \frac{\hbar k^2}{2m_{ph}}. \tag{1.3}$$

This gives an effective mass to the photon of

$$m_{ph} = \hbar\left(\frac{n}{c}\right)\frac{2\pi N}{L}, \tag{1.4}$$

which is dependent on the size of the cavity [7].

The light-matter coupling is enhanced by placing quantum wells at the antinodes of the cavity modes. Confining electrons and holes in a transverse region of the order of magnitude of their de Broglie wavelength increases the exciton binding energies [15]. The excitons in these wells then have a dispersion relation given by

$$\varepsilon_{\mathbf{k}} = \varepsilon_0 + \frac{\hbar^2 k^2}{2m_{ex}}, \tag{1.5}$$

where $\varepsilon_0 = E_{gap} - E_{binding}$. A schematic of this microcavity configuration is shown in Fig. 1.1. The photon (1.3) and exciton (1.5) dispersions may then be tuned close to resonance with one another by varying the cavity width, L. Practically, this may be achieved by employing a wedge-shaped cavity, where various values of L may be obtained within the same sample [13].

One may write down a Hamiltonian for this system in terms of creation and annihilation operators of photons ($a_{\mathbf{k}}^{(\dagger)}$) and excitons ($D_{\mathbf{k}}^{(\dagger)}$) [7],

$$H = \begin{pmatrix} a_{\mathbf{k}}^{\dagger} & D_{\mathbf{k}}^{\dagger} \end{pmatrix}\begin{pmatrix} \omega_{\mathbf{k}} & \Omega_R/2 \\ \Omega_R/2 & \varepsilon_{\mathbf{k}} \end{pmatrix}\begin{pmatrix} a_{\mathbf{k}} \\ D_{\mathbf{k}} \end{pmatrix}. \tag{1.6}$$

The off-diagonal terms describe the exciton-photon coupling, where Ω_R is the Rabi frequency, and here, and in the remainder of this section, we have
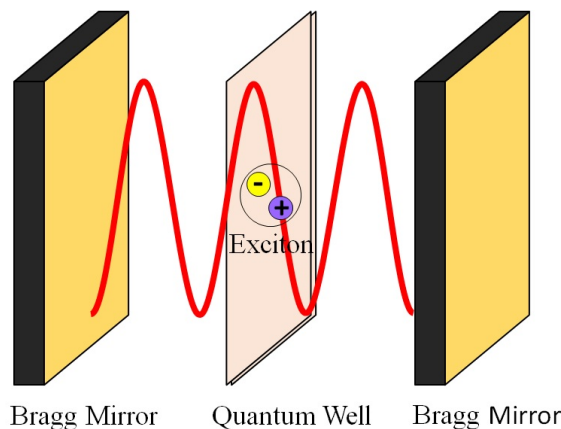
Figure 1.1: A schematic of how polaritons are formed in semiconductor microcavities.

set $\hbar = 1$, Diagonalizing this yields the eigenvalues,

$$E_{\mathbf{k}}^{LP,UP} = \frac{1}{2}\left[\omega_{\mathbf{k}} + \varepsilon_{\mathbf{k}} \pm \sqrt{(\omega_{\mathbf{k}} - \varepsilon_{\mathbf{k}})^2 + \Omega_R^2}\right], \tag{1.7}$$

where LP and UP label the two branches as 'lower polariton' and 'upper polariton' respectively. We can rewrite this expression in terms of wavevectors and the detuning between the exciton and photon bands $\delta = \omega_0 - \varepsilon_0$,

$$E_{\mathbf{k}}^{LP,UP} = \frac{1}{2}\left[\delta + \frac{k^2}{2M_{ex}} + \frac{k^2}{2m_{ph}} \pm \sqrt{\left(\delta + \frac{k^2}{2M_{ex}} + \frac{k^2}{2m_{ph}}\right)^2 + \Omega_R^2}\right], \tag{1.8}$$

where we have set the zero of our energy scale as the bottom of the exciton dispersion, ε_0, for convenience.

The above is discussed in detail in several review articles on the subject [7, 9, 16]. It should be noted, however, that this picture of polaritons is a simplification, as it assumes a perfect, infinite quantum well. In reality, there will be disorder present, which will cause localization of the exciton states. These will not have a well-defined momentum, and will not necessarily couple to a single cavity mode. A more rigorous microscopic description of polaritons is provided in [17], but although we will discuss systems with disorder, the picture outlined above is sufficient for our purposes. This is because we shall be considering the behaviour of polaritons, whose wavelengths are large compared with the length scales of the excitonic disorder.
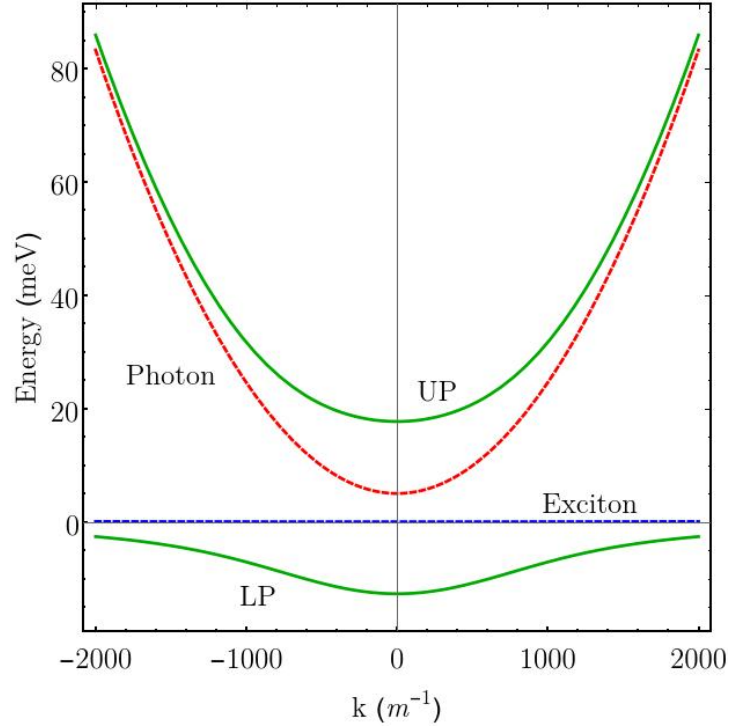
Figure 1.2: Schematic polariton dispersion, showing bare photon and exciton dispersions. Plotted for typical values of $m_{ex} = 0.1m_e$, $m_{ph} = 5 \times 10^{-5}m_e$, where m_e is the mass of an electron, $\Omega = 30$ meV and exciton-photon detuning $\delta = 5$ meV.

The dispersion of the two polariton modes (1.8) is plotted alongside the bare exciton and photon modes in Figure 1.2. As the effective mass of the photon is typically three to four orders of magnitude smaller than the exciton mass – which varies depending on the semiconductor material – the photon dispersion is far steeper than the exciton dispersion, and the latter appears flat in the plot. Condensation typically occurs in the lower polariton branch, due to its lower energy. At small wavevectors, this dispersion is approximately quadratic, and such polaritons have a significant photonic fraction. This effect can be amplified by negatively detuning the photon and exciton resonances ($\delta < 0$). This ensures that condensed polaritons will be very photon-like, with an extremely low mass. Moving out to larger k values, the dispersion has a point of inflection, before it approaches the exciton dispersion. As such, high-momentum polaritons are effectively just excitons.

1.3 Driven-dissipative condensates

The unique combination of properties of polaritons makes them ideal candidates for Bose-Einstein condensation. Photons are bosons, and – when their separations are greater than their size – so are excitons, so polaritons at low densities are composite bosons. This means that at low temperatures, a population of polaritons will experience macroscopic occupation of the ground state, and will form a BEC. The textbook description of a gas of bosons in three dimensions shows that condensation occurs below a critical temperature of

$$T_C = \frac{2\pi\hbar^2}{mk_B} \left(\frac{n}{\zeta(3/2)} \right)^{2/3}, \tag{1.9}$$

where m is the particle mass, n the particle density, k_B Boltzmann's constant, and ζ the Riemann-zeta function [18]. This does not hold for polaritons, because they exist in two dimensions, and are generally out of equilibrium, but we may still gain some insight from the form of (1.9). The lighter the particles in question, the higher the temperature at which the onset of condensation occurs. As can be seen from the polariton dispersion in Fig. 1.2, at low momenta where condensation occurs, the polariton mass is similar to that of the photon, or 10^{-4} times the bare electron mass. This is nine orders of magnitude less than the mass of a rubidium atom, and so polaritons are seen to condense at far higher temperatures than traditional atomic BECs. This removes one of the primary barriers to the observation of BECs, and permits condensation at room temperatures. In fact, the upper temperature limit for condensation is set not by the polariton mass, but rather by the binding energy of the exciton. While most early reports of polariton condensation used either GaAs or CdTe cavities, and required cryogenic temperatures of order 10K [6, 19, 20], room temperature condensation has been reported in large-bandgap materials such as GaN [21, 22, 23] and ZnO [24, 25, 26], as well as organic cavities [27, 28].

The excitonic component of polaritons is also critical for condensation. Unlike photons, excitons can interact through the Coulomb force, and this means that polaritons interact with one another. As will be discussed below, this is crucial in enabling them to thermalize and form a condensate. While polaritons undergo condensation and display macroscopic occupation of a

single energy state, there are a number of features of polariton condensates that are distinct from traditional BECs.

Generally, Bose-Einstein condensation is characterized by the onset of off-diagonal long range order (ODLRO) [29, 30]. This means that the one-body density matrix of the system

$$n^{(1)}(\mathbf{r}, \mathbf{r}') = \langle \hat{\Psi}^\dagger(\mathbf{r}) \hat{\Psi}(\mathbf{r}') \rangle, \tag{1.10}$$

has finite off-diagonal entries, or equivalently, that it has a macroscopic eigenvalue [18]. This enables the definition of a classical order parameter for the condensate, as it shows the existence of a spatially-extended, macroscopically-occupied mode. In (1.10), $\hat{\Psi}^\dagger(\mathbf{r})$ and $\hat{\Psi}(\mathbf{r}')$ are the creation and annihilation operators for a particle at position $\mathbf{r}$ and $\mathbf{r}'$, and the angular brackets indicate a quantum mechanical average over the states of the system. Experimentally, ODLRO is determined by measuring if the correlation function

$$g^{(1)}(\mathbf{r} - \mathbf{r}') = \frac{\langle \hat{\Psi}^\dagger(\mathbf{r}) \hat{\Psi}(\mathbf{r}') \rangle}{\sqrt{\langle |\Psi(\mathbf{r})|^2 \rangle \langle |\Psi(\mathbf{r}')|^2 \rangle}} \tag{1.11}$$

remains finite as $|\mathbf{r} - \mathbf{r}'| \to \infty$. Here, the angular brackets represent an expectation value.

We must stress however, that polariton condensates typically exist in two-dimensional cavities, and by the Mermin-Wagner theorem, ODLRO is suppressed by thermal fluctuations in fewer than three dimensions [31]. In contrast to the physics of condensates in three dimensions, 2D BECs undergo a Berezinskii-Kosterlitz-Thouless (BKT) transition to an ordered state [32, 33]. This phase transition is distinct from the 'standard' 3D BEC transition. In two dimensions, correlation functions of the condensate field – and therefore phase coherence – then decay algebraically, vanishing in the infinite limit. A 2D condensate is said to have quasi-long range order, with macroscopic occupation occurring on small scales. As we shall see later, the picture for polariton condensates is complicated by their non-equilibrium nature. This can cause an exponential decay of correlations, however coherence has been observed across the extent of the sample size of a polariton condensate [6], and power-law decay of correlations in line with the equilibrium theory has also been reported [34].

While the part-light, part-matter composition of polaritons gives them a suitable mix of characteristics that allow for condensation, it has another consequence. Although the Bragg mirrors in microcavities have a very high reflectivity, it is finite, and photons eventually escape from the semiconductor. This limits the lifetime of polaritons to typically be of the order of a few picoseconds [35, 36]. Lifetimes of up to 100 ps have been achieved in more recent experiments using cavities with high quality factors [37, 38], however despite the observation of quasi-equilibrium condensates of long-lifetime polaritons [39, 40], in this work, we will only consider situations where the polariton lifetimes are short enough for the system to be considered truly driven-dissipative.

Because of the finite lifetimes of polaritons, a condensate must be continually replenished, or it will vanish. There are various methods of injecting polaritons into the condensate. The most common method, and the one which we assume for the theoretical models used in this work, is that of non-resonant pumping [7]. Typically, a laser is used to excite the sample incoherently, well above the polariton energy. The high-energy excitons created by this process cool through emission of phonons until they lie on the LP dispersion. Relaxation to the ground state then occurs through stimulated scattering. This gives the polaritons the coherence that is a signature of condensation. This method involves the creation of a large population of incoherent polaritons. As these have relatively high energies and momenta, they essentially behave as excitons which interact weakly with light. We can then model the non-resonant pumping process by considering a pump creating a reservoir of excitons, which then populates the condensate.

In addition to non-resonant pumping, there are a number of experimental methods that involve exciting the sample resonantly. These generally involve creating polaritons with a specific momentum by controlling the angle at which photons are injected. This may bring about coherent scattering into the ground state, for example through an optical parametric oscillator regime. We will not go into detail on the various mechanisms and models of resonant pumping, as they are not relevant to this thesis, however, such methods are reviewed in detail in [7] and [8].

The non-equilibrium nature of polariton condensates has a number of

useful consequences. The photons which escape the cavity retain their coherence, so a polariton condensate emits laser-like coherent light. In fact, the emission of the condensate contains all the relevant information on its state. The frequency and momentum of the polaritons are conserved when they tunnel through the Bragg mirrors. One may therefore deduce the energy of the occupied modes by measuring the frequency of the emission, while the in-plane momentum may be calculated from the angle at which light is emitted. This latter feature is exploited in the resonant pumping schemes outlined above.

Because it acts as a coherent light source, and involves exciting a medium in a cavity with a pump, a polariton condensate has much in common with a laser. In fact, these systems are sometimes referred to as 'polariton lasers'. Their behaviour is distinct from that of traditional photon lasers, however. In the case of conventional lasers, photons gain coherence through stimulated emission from a gain medium. In polariton condensates however, it is the polaritons, not photons, which gain coherence, and this occurs through stimulated scattering. It can be shown that unlike photon lasers, population inversion is not required for polaritons to lase [41], and furthermore, polariton condensates are in the strong-coupling regime, which may be verified by obtaining the dispersion from the emission below condensation threshold. In truth, polariton condensates lie on a spectrum between equilibrium BECs and lasers. Driven-dissipative condensates have their own unique characteristic properties and clearly warrant individual scrutiny.

1.4 Theoretical model of non-equilibrium condensates

The dynamics of a Bose-Einstein condensate may be described at the mean-field level by the Gross-Pitaevskii equation (GPE) [18],

$$i\hbar\frac{\partial}{\partial t}\Psi(\mathbf{r}, t) = \left(-\frac{\hbar^2}{2m}\nabla^2 + V(\mathbf{r}) + U|\Psi(\mathbf{r}, t)|^2\right)\Psi(\mathbf{r}, t), \qquad (1.12)$$

where the entire condensate is described by a classical, single-particle wavefunction $\Psi(\mathbf{r}, t)$. This wavefunction is an order parameter for the condensate

in the sense that it is zero in the uncondensed phase. It is normalized such that

$$\int |\Psi(\mathbf{r}, t)|^2 d\mathbf{r} = N, \tag{1.13}$$

where N is the total number of particles in the state. The local density of the condensate is then given by

$$n(\mathbf{r}, t) = |\Psi(\mathbf{r}, t)|^2. \tag{1.14}$$

Eq. (1.12) has the form of a single-particle Schrödinger equation with an additional nonlinear term, which models the interactions between particles in the condensate, with strength U. An external potential experienced by the condensate is included as $V(\mathbf{r})$.

The GPE is a valid description of the ground state of a dilute gas of bosons at low temperatures. The introduction of the classical order parameter is justified when there are a large number of particles in the gas, and their temperature is below the critical threshold for Bose-Einstein condensation. In this case, all particles will occupy the same state. In addition to this, if the separation between particles is greater than the scattering length, the true interaction potential may be replaced by an effective psuedopotential. As a result, all interactions may be represented in terms of the s-wave scattering amplitude, which is contained in the interaction strength, U. These approximations mean that the GPE is applicable when describing phenomena that take place over a length scale much larger than that of the scattering length.

The GPE may be generalized to the case of a non-equilibrium condensate by including extra terms to model driving and dissipation. In particular, a straightforward yet effective description of a non-resonantly pumped polariton condensate is the extended Gross-Pitaevskii equation (eGPE) [42]:

$$i\hbar \frac{\partial \Psi}{\partial t} = \left[-\frac{\hbar^2}{2m} \nabla^2 + V(\mathbf{r}) + U|\Psi|^2 \right] \Psi + i \left(g - \Gamma|\Psi|^2 \right) \Psi. \tag{1.15}$$

The additional complex terms in this equation phenomenologically model the gain and loss associated with the condensate. The pump excites a gain medium, creating a reservoir of hot excitons, from which the condensate is populated through stimulated scattering events, with a rate γ. Meanwhile, the condensate continually experiences losses due to the decay of photons

from the cavity, with a rate κ. The new linear term

$$g = \gamma - \kappa, \tag{1.16}$$

describes the net result of both of these mechanisms. When the cavity is pumped strongly enough such that the gain compensates for the losses, g is positive, and this term causes the condensate to grow exponentially. On the other hand, when $\kappa > \gamma$, the condensate will decay. Thus, the threshold for condensation occurs at $g = 0$. This corresponds to the threshold pumping power that is experimentally required to observe condensation [6]. A gain saturation term, with coefficient Γ, is also required. Clearly, when pumped above threshold, a condensate cannot continue to grow exponentially. For instance, scattering into the condensate depletes the gain medium, slowing the rate of growth. This is modelled by the inclusion of the nonlinear term. The new gain and loss terms attempt to establish a steady-state density,

$$n_0 = g/\Gamma. \tag{1.17}$$

Indeed, in the absence of a potential, Equation (1.15) has the uniform steady-state solution

$$\Psi(\mathbf{r}, t) = \sqrt{n_0} \exp\{(-i\mu t/\hbar)\}, \tag{1.18}$$

where $\mu = U n_0$ is the chemical potential of the condensate. In this thesis, we mainly use units where $\hbar = 1$, in which case the chemical potential corresponds to the frequency of the wavefunction.

This 'free space' version of Eq. (1.15) where the potential term is zero, or constant in space has the form of a complex Ginzburg-Landau equation (CGLE). An extension of Landau and Ginzburg's theory of phase transitions in superconductors, the CGLE is a remarkably versatile tool for studying a multitude of different systems. Generally speaking, it describes the dynamics of extended oscillatory media [43, 44].

Another commonly-used model of polariton condensates considers a separate rate equation for the uncondensed exciton reservoir, which is coupled to a similar extended GPE through a reservoir density term n_R [45]:

$$i\hbar\frac{\partial \Psi}{\partial t} = \left[-\frac{\hbar^2}{2m}\nabla^2 + V(\mathbf{r}) + g_C|\Psi|^2 + g_R n_R + \frac{i\hbar}{2}\left(R n_R - \gamma_C\right) \right] \Psi, \tag{1.19}$$

$$\frac{\partial n_R}{\partial t} = P - \left(\gamma_R + R|\Psi|^2\right) n_R. \tag{1.20}$$

Here, as well as a term describing interactions between condensed particles, proportional to g_C, this model also explicitly contains a condensate-reservoir interaction term proportional to g_R. The pump strength or excitation power is given by P, R is the rate at which polaritons are scattered from the reservoir into the condensate, and γ_C and γ_R are the decay rates from the condensate and the reservoir respectively. This model reduces to the eGPE (1.15) in the adiabatic approximation, whereby the dynamics of the reservoir instantaneously follow those of the condensate. The rapid relaxation of n_R to its steady state enables us to eliminate the reservoir densities by writing Eq. (1.20) as

$$n_R = \frac{P}{\gamma_R + R|\Psi|^2},$$

which, close to a steady state condensate density – or alternatively, just above threshold – may be expanded to give an equation of the same form as Eq. (1.15). The specific analytic conditions necessary for the adiabatic approximation, and thus the agreement of the two models – including the restriction that only low-momentum modes of the condensate be occupied considerably – are outlined in [46]. These conditions may generally be met, and so we only consider the eGPE model given by Eq. (1.15) for our analysis in this work. In fact, this equation will be the starting point for all of our analysis of driven-dissipative condensates.

1.5 Disorder and localization of polariton condensates

1.5.1 Spatial disorder

Disorder is an inescapable feature of polariton condensates. Although modern semiconductor fabrication techniques enable the production of very clean microcavities, some level of impurities and fluctuations in the cavity width and/or reflection coefficient is inevitable [11, 47]. This is especially prevalent in wide-bandgap materials such as GaN and ZnO, which have provided the most promising results for room-temperature condensation [21, 48].

A spatial disorder potential can inhibit condensation by causing the con-

densate wavefunction to become localized. This can lead to the formation of several 'pools' of condensed particles, which are localized around minima of the disorder potential [49,50]. In general, these localized condensates will have macroscopic occupation of different modes, as may be confirmed by measuring the emission frequency. Spatially-separated modes are not generally coherent, leading to phase correlations that decay beyond the spatial extent of a single localized condensate, and an absence of long-range order.
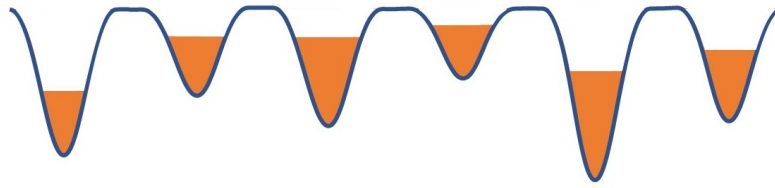
Figure 1.3: A schematic of localized condensates in a disordered potential. Note: more generally, in a disordered potential, the wells will not have equal widths, as is shown here.

Disorder-induced localization of BECs also occurs in equilibrium. In this case, however, the condensates are generally formed without disorder, and this is later introduced to the sample [51,52]. The effects of localization may be overcome by increasing the density of the condensate. The steady-state solutions of the GPE (1.12) – and indeed those of its driven-dissipative extension (1.15) – have a frequency which contains a blueshift due to interactions of the form Un. Thus, adding more particles to a condensate can increase its frequency. This blueshift, or increase in energy can then screen the disorder potential. The condensate wavefunction may extend across the entire sample, as it can 'see over' the peaks in the disorder profile.

A similar effect is described by the Bose-Glass-superfluid transition [53]. In an equilibrium bosonic system, the transition between an insulating state and a superfluid one (i.e. the onset of condensation) goes through an intermediate 'Bose glass' phase in the presence of spatial disorder. In this intermediate phase, localized puddles of superfluid form, but superfluidity does not extend across the system. There is then a phase transition from this state to a superfluid. While this picture was expected to be broadly

the same for nonequilibrium condensates [54], the addition of driving and dissipation proves to alter the physics. It has been shown that superfluidity is impossible in a disordered driven-dissipative condensate in the thermodynamic limit [55], while the observation of intensity fluctuations in the emission spectrum of a polariton condensate, even at strong excitation power (corresponding to high densities), suggests that spatial disorder may inhibit long-range order. Experiments on finite systems, however, have shown that increased excitation powers can cause initially separated, localized polariton condensates to synchronize their emission frequencies and lead to the establishment of phase coherence across the sample. [50, 56, 57].

The localization of polariton condensates due to a potential is not necessarily a nuisance. It allows for the construction of lattices and other complex structures which enable the observation of phenomena such as the Josephson effect [56]. Josephson effects may be seen when two condensates are localized close enough to one another that their wavefunctions overlap. This enables the tunnelling of particles from one condensate to another through the potential barrier between them. This tunnelling is one of the mechanisms that can bring about synchronization in the energies of spatially-separated, localized condensates. Polariton lattices have also been identified as candidates for analogue simulation, with the condensate dynamics used to solve complex problems with many degrees of freedom [58, 59]. Localizing potentials need not come from disorder intrinsic to the sample. The profile of the pump laser also contributes to the potential seen by the condensate. The pump creates hot excitons where it is incident on the sample. Condensed polaritons may interact with these excitons, so they create a repulsive potential. This effect may be exploited to create lattices where condensed polaritons are trapped between pump spots [57]. It is also possible to engineer lattices of condensates that are not trapped in potential wells. Non-uniform pumping can create spatially separated condensates at the peaks of the potential. These condensates are propagating states, and can also be seen to synchronize their frequencies and gain coherence [58, 60, 61].

We will consider lattices of the former variety, where condensates are localized in the wells of a trapping potential. In particular, we will focus on how these spatially-separated condensates synchronize their frequencies

in a lattice with random energies. This is in part facilitated by Josephson tunnelling between neighbouring condensates [56, 62]. We are particularly interested in the question of whether synchronization is possible for an infinitely large lattice. This is important for understanding if long-range order can exist for driven-dissipative condensates in the presence of disorder.

1.5.2 Spatio-temporal noise

Static disorder resulting from the microcavity is not the only type of disorder that can affect polariton condensates. Any dissipative system that is driven by a laser is expected to have some spatio-temporal fluctuations associated with this process [63]. These fluctuations are not captured by a mean-field model, and they were not initially thought to have a significant enough impact on the physics of driven-dissipative condensates to warrant consideration alongside the models outlined in the previous section. In recent years, however, it has become clear that a purely mean-field description does not suffice when calculating correlation functions of a driven-dissipative condensate [64]. In particular, analysis that includes the effect of these fluctuations predicts the exponential decay of correlations of the condensate wavefunction [65, 66].

The eGPE is straightforwardly adapted to allow for these fluctuations. Their effect is captured by the addition of a stochastic term, $\xi(\mathbf{r}, t)$ to the right-hand side of (1.12). This term is generally taken to be a zero-mean Gaussian white noise term, characterized by

$$\langle \xi^*(\mathbf{r}, t)\xi(\mathbf{r}', t')\rangle = 2\tilde{D}\delta(\mathbf{r} - \mathbf{r}')\delta(t - t'). \tag{1.21}$$

The fluctuations arise from the gain and loss, and their strength, $\tilde{D}$ is determined by the parameters g and κ. This semiclassical stochastic model may be derived using a truncated Wigner approximation [63].

The main body of work in this thesis does not go beyond the mean-field description of driven-dissipative condensates to include the impact of pump noise. We focus on lattices of localized condensates with random energies that do not change with time. This enables us to quantify the effects of purely spatial disorder, and map the system to a classical description of coupled oscillators. In chapter 5, we present some preliminary work which takes noise into account.

1.6 Synchronization of coupled oscillators

As we have mentioned above, a primary consideration of this thesis is how lattices of spatially-separated driven-dissipative condensates may synchronize their emission frequencies. This connects the field of polariton condensates to another wide-ranging area of physics: that of the synchronization of oscillators. Synchronization is a truly universal phenomenon that spans the fields of physics, chemistry, biology and social sciences [12]. Time and time again in nature, one encounters systems which display periodic behaviour being drawn to oscillate with a common frequency, and move with the same rhythm. This is seen in swarms of pulsing fireflies, pacemaker cells in our hearts, and applauding audiences. However, synchronization also occurs in inanimate objects that are not aware of their surroundings. The study of synchronization is famously said to have begun in 1673 when the Dutch physicist Christiaan Huygens serendipitously noticed that two pendulum clocks hanging from the same frame gradually synchronized the motion of their pendula [12]. In the intervening 350 years, physicists have arranged more complex and modern objects, such as lasers and Josephson junctions, in various configurations such as chains and lattices and noticed a similar effect [67, 68]. In this thesis, we will detail how lattices of localized polariton condensates may be described in the same way, and how this analysis provides insight into the physics of such nonequilibrium systems.

1.6.1 Definitions and conventions

We begin by clarifying some of the terminology and conventions used within the framework of synchronization. A more detailed and extensive review may be found in Pikovsky, Kurths and Rosenblum's book on the subject [12]. We consider systems comprising self-sustained oscillators. These are objects that have some repeating, periodic behaviour associated with them, which they carry out without being driven externally. One may consider the classical example of a pendulum clock. With the help of a spring, a weight or a battery, the pendulum will swing back and forth with a regular period. These swings are self-sustained oscillations. In turn, the motion of the pendulum then powers the clock hands to rotate around its face. We can imagine the type

of clocks whose hands don't tick, but rather rotate smoothly. In this case, motion of the hands may also be considered as an oscillation, although the period of these oscillations is many multiples of the pendulum's period.

The motion of an individual self-sustained oscillator is parameterized by a well-defined phase, θ_j. Formally, the phase variable describes the position of an oscillator along its limit cycle in phase space, however in our particular choice of self-sustained oscillator – a BEC – the phase appears naturally in its order parameter as $\Psi = \sqrt{n}\exp(-i\theta)$. The frequency of an oscillator is then the rate of change of its phase, $\dot{\theta}_j$. For well-behaved systems in the absence of external perturbations, the phase of an individual oscillator increases linearly in time. This allows us to define the natural frequency of the oscillator,

$$\omega_j = \theta_j t. \tag{1.22}$$

In the case of the steady state solution of a BEC, this natural frequency is equal to its chemical potential, μ, as $\Psi_0(\mathbf{r}, t) = \Psi_0(\mathbf{r})\exp(-i\mu t)$ (in units where $\hbar = 1$). Oscillations, by definition, are periodic. Without loss of generality, we consider oscillations with periodicity 2π, so ω_j is an angular frequency. Two phases that differ by 2π then describe the same physical state. We could choose to define the phase on a circle, however this is not necessary, as the equations that govern the dynamics of these systems encode this periodicity with sine and cosine functions.

Synchronization can occur when oscillators are coupled to one another. This coupling can have many forms, so long as it enables the motion of one oscillator to influence another. Huuygens' original pendulum clocks were connected by a common wooden frame. This allowed their motion to be coupled through vibrations, or equivalently the exchange of phonons. Localized BECs on the other hand, are coupled through the Josephson tunnelling of particles between neighbouring condensates. Once oscillators are coupled, there are different forms of synchronization that may occur.

The most general form is frequency synchronization, or entrainment, whereby a common frequency is established across a group of N oscillators: $\dot{\theta}_1 = \dot{\theta}_2 = \cdots = \dot{\theta}_N = \Omega$. This is also referred to as phase locking, because oscillators with the same frequency have a constant phase difference – their

phases are 'locked' together with a constant offset, such that

$$|\theta_j - \theta_k| = A_{jk}. \tag{1.23}$$

A special case of this frequency synchronization occurs when this phase offset is zero everywhere, and the oscillators are all *in phase* with one another. When this happens, one also has phase synchronization, or mutual coherence of the oscillators. Phase synchronization is responsible for some of the more spectacular examples of synchronization that may be commonly observed. The synchronization that occurs in an applauding crowd, or a swarm of fireflies is striking because the clapping or the flashing occurs in unison. However, it is not generally the case that oscillators with synchronized frequencies are in phase. Two clocks are entrained if one never runs slow or fast with respect to the other. Only if they continually tell the same time are their phases synchronized. (In this example, we think of the phase as describing the motion of the hands).

This language is not entirely consistent throughout the literature, but in this work, unless specified, the terms synchronization, entrainment and phase-locking will be used to refer to frequency synchronization. We will specify when phase synchronization also occurs.

1.6.2 The impact of noise on coupled oscillators

The presence of noise, or any time-dependent disorder, in a system makes the discussion of synchronization somewhat less straightforward. Few physical systems are perfect: most oscillators experience some sort of noise from their surroundings. As discussed in section 1.5.2, this is also true for driven-dissipative condensates. Noise generally causes the phase of an oscillator to jump around rather than increasing linearly, and as such it is difficult to define a natural frequency. Furthermore, when time-dependence is introduced into the couplings or natural frequencies of oscillators, situations can exist where oscillators display phase synchronization at some point in time, but in general, their frequencies are not synchronized. In this case, it makes sense to consider the average frequency of an oscillator over a certain amount of time to determine synchronization. One may then loosen the definition of synchronization, and choose an upper allowable bound on frequency differences.

Two oscillators may be considered synchronized if their average frequencies differ by less than this amount.

In the case of noisy oscillators, it can also be useful to consider the phases of the oscillators rather than their frequencies. We may generalize the definition of phase locking for noisy oscillators by replacing the equality in Eq. (1.23) with an inequality:

$$|\theta_j - \theta_k| < B_{jk}, \tag{1.24}$$

where $B_{jk} \leq 2\pi$. This allows the phase of each oscillator to fluctuate, but constrains them both to evolve with the same frequency. If the noise is strong enough, however, it may cause a 'phase slip' to occur, where the phase difference between the two oscillators rapidly jumps by $\pm 2\pi$. In fact, in the case of unbounded noise, such as the case of Gaussian noise $\eta(t)$, with $\langle \eta(t)\eta(t') \rangle = 2\tilde{\sigma}\delta(t - t')$, such phase slips are inevitable. No matter how large we choose B_{jk} to be, eventually a large enough fluctuation will occur to briefly knock the oscillators out of sync. If the noise is weak, this will happen infrequently enough that oscillators may be considered synchronized over a finite length of time. In the limit of long times, the average frequencies of oscillators subject to weak noise will also be synchronized because of the relative rarity of phase slips. Furthermore, applying a suitable bound to the noise strength may prevent slips from occurring at all, and ensure synchronization.

For most of this work, we consider noise-free systems of oscillators. The effects of noise will only be taken into account in the final chapter, when we generalize our results for clean systems to include the effects of noise.

1.6.3 Synchronization of large populations of oscillators and the Kuramoto model

Remarkably (or perhaps not, if statistical physics has taught us anything), regardless of whether one wishes to describe how groups of clocks, lasers or fireflies synchronize, a common mathematical description tends to suffice. The paradigmatic mathematical description of synchronization of groups of

oscillators was proposed by Kuramoto in 1975 [69, 70]. It reads,

$$\dot{\theta}_j = \omega_j + \sum_{j=1}^{N} K_{jk} \sin\left(\theta_k - \theta_j\right). \tag{1.25}$$

This model is quite elegant in its simplicity. A population of N oscillators, whose individual phases are given by the θ_j, each have a natural frequency of rotation ω_j, and are coupled to one another through a periodic coupling function with coefficient K_{jk}. Sine is a natural choice for the coupling function, as it is the simplest function with the same 2π-periodicity as the phase difference between oscillators, which it takes as its argument. Furthermore, this corresponds to 'diffusive' coupling: the coupling function attempts to bring neighbouring oscillators to the same state [71, 72]. One can see from the behaviour of the sine function with small arguments that when the phase of one oscillator is slightly ahead of its neighbour, the coupling function will add a 'boost' to the frequency of the trailing oscillator, while reducing the frequency of the leading oscillator by the same amount. The coupling is then zero when the oscillators have the same phase.

Typically, one considers a random distribution of natural frequencies. Then, in the absence of coupling, all oscillators will rotate at different frequencies. Increasing the coupling strength causes the oscillators to influence each other more strongly, and works to bring about synchronization. Conversely, increasing the spread of the natural frequencies makes it more difficult for oscillators to synchronize, so synchronization results from a competition between the coupling strength and the variance of the natural frequency distribution. In fact, separate parameters are not required to describe each of these effects. Eq. (1.25) is invariant under the scaling $t \to \sigma t$, so one may always consider natural frequencies with unit variance by dividing across by the original standard deviation, σ. In the simplest case of uniform coupling, the synchronization dynamics of the Kuramoto model are then controlled by a single parameter, $K' = K/\sigma$.

Typically speaking, the Kuramoto model refers to the case of all-to-all, or 'mean-field' coupling, whereby each oscillator is coupled to every other one, with a coupling strength that is proportional to the total number of oscillators, $K_{jk} = K/N, \forall j, k$. In this special case, the model may be solved analytically, and one finds a phase transition from a desychronized

state to global frequency synchronization at a K_c that is independent of the system size [69, 73]. It is therefore known that it is possible for an infinitely large number of globally coupled Kuramoto oscillators to synchronize their frequencies.

For many systems, such as the lattices of coupled condensates which we consider, the oscillators are not influenced equally by the entire ensemble – rather, each site is only coupled to its neighbours. To describe this, one takes $K_{jk} = 0$ except for the case of nearest neighbours on a regular cubic grid. In the simplest case, we take the coupling to be uniform, and write the locally-coupled Kuramoto model as

$$\dot{\theta}_j = \omega_j + K \sum_{<k>} \sin \left(\theta_k - \theta_j \right), \qquad (1.26)$$

where now the sum which appears in the coupling function has $2d$ terms (with d the dimensionality of the lattice) rather than N, as is the case in the globally coupled model.

The synchronization behaviour of this local Kuramoto model is not as easily determined as that of its more celebrated mean-field counterpart. However, locally-coupled lattices of oscillators – or at least continuous media that may be approximated as such – appear in many contexts [12], so this model has been the subject of some scrutiny. We note that locally-coupled oscillator lattices with different – and indeed, more general – coupling functions have also been studied [72, 74, 75], however it is worth reviewing the behaviour of (1.26) specifically, because it is quite well understood, and it provides a grounding to contextualize our own model (3.5), which we introduce in chapter 3, and is closely related.

Kuramoto himself, together with Sakaguchi [76] was the first to address the question of whether synchronization is possible for the locally-coupled model in the limit $N \to \infty$. It is clear from numerical simulations of small lattices in one and two dimensions that one may choose a large enough K such that all oscillators attain the same frequency. At values of K just before the onset of synchronization, one sees clusters or plateaus of oscillators entrained to a common frequency, so it would not be unreasonable to expect that some form of synchronization might occur in infinitely large systems. Sakaguchi and Kuramoto showed through a consistency argument, however,

that in the limit $N \to \infty$, global frequency synchronization is impossible in dimensions $d \leqslant 2$. Very shortly after, Strogatz and Mirollo [77] went a step further, and demonstrated that in fact, frequency synchronization cannot occur in a lattice of oscillators in any finite dimension. This statement was proved for any random distribution of natural frequencies with finite mean and variance. In fact, both of these works showed that in two or fewer dimensions, the probability of synchronized clusters existing also decays to zero in the infinite limit.

An analytic solution for the probability of global synchronization in a 1D chain of Kuramoto oscillators was also derived in [77]. By interpreting the sum of the natural frequencies along the chain as a random walk around their average, it was shown that in the limit $N \to \infty$, the probability of all of the oscillators being synchronized is equivalent to the probability of the maximum value of a pinned Wiener process being less than the coupling strength. This result is known exactly to be a Kolmogorov-Smirnov distribution [78], so we may write the probability of synchronization of a chain of N oscillators described by (1.26) with natural frequencies distributed with zero mean and unit standard deviation coupled with strength $K\sqrt{N}$ as

$$\lim_{N \to \infty} P(N, K\sqrt{N}) = \frac{\sqrt{2\pi}}{K} \sum_{m=0}^{\infty} \exp\left\{ \left(\frac{-(2m+1)^2\pi^2}{8K^2} \right) \right\}. \qquad (1.27)$$

This expression increases from zero to almost one as $K\sqrt{N}$ is varied from zero to 2, implying synchronization occurs at coupling strengths of size $\mathcal{O}(\sqrt{N})$. Thus, an infinitely large coupling strength would be required to synchronize an infinite chain.

1.7 Notes on numerical simulations

In this work, we present the results of both analytic and numerical investigations. The majority of numerical simulations were carried out using Mathematica. Differential equations were solved using the NDSolve package, while the Fourier package was employed to calculate discrete Fourier transforms. There are two exceptions to this. The two-dimensional simulations in Chapter 3 were performed in Fortran, using an adaptive Runge-Kutta

algorithm [79] originally written by my supervisor, Paul Eastham. This code was then adapted and run by me. In addition, the results for the stochastic model presented in Chapter 5 were also obtained using a Fortan code written by Paul. This employs the two-step Runge-Kutta method given in [80] to solve the coupled stochastic differential equations.

Chapter 2

Synchronization of two coupled driven-dissipative condensates

2.1   Introduction

In this chapter we consider the synchronization dynamics of the 'polariton Josephson junction': two polariton condensates, separated by a potential barrier, through which quantum tunnelling may occur. There are many ways to experimentally realize such a configuration. A 'double well' trapping potential may arise from the fabrication of micropillars through etching and/or deposition [81,82], from interactions with the excitonic reservoir [83], or from the growth-induced disorder intrinsic to the sample [56], to list but a few examples. Two different polarization states of a polariton condensate in a single trap may also behave as a polariton Josephson junction [84,85]. The double well configuration has been the subject of much experimental and theoretical investigation because it is a relatively simple platform to test quantum effects. In analogy with the DC Josephson effect in superconductors, a current may be established between the two wells that depends on their relative phase difference, and if the energies of the wells are sufficiently detuned from one another, the system undergoes a transition to an AC Josephson effect, whereby the current rapidly changes direction.

There are a number of differences between the polariton Josephson junction and the traditional superconductor equivalent. In particular, the two condensates are not part of a circuit; rather, the gain and loss due to the

pumping of each condensate attempts to balance the condensate densities. The connection to disorder is what motivates our interest in this configuration. It has been shown that disorder in a microcavity can lead to the formation of several condensates localized at different locations in the plane of the sample [50]. The double well provides an accessible starting point to understand the transition between distinct, localized condensates and a single ordered state. As we will illustrate, this problem is closely linked to the synchronization of coupled oscillators.

We will outline the theoretical description of condensates in a double well potential, starting from the extended Gross-Pitaevskii equation. We demonstrate how this may be reparameterized in terms of the phase and density of each well to illustrate the existence of both a synchronized and desynchronized regime, and how these correspond to a DC and AC Josephson effect respectively. We then focus on the boundary between these two regimes as a function of the parameters in the system to highlight the role that interactions, gain and loss play in synchronization. In particular, we study the effect of varying the pump strengths for each well. We show that asymmetrical pumping – approximated by introducing a difference between the linear gain terms in each well – shifts the position of the phase boundary between synchronized and desynchronized states, thus acting as an effective additional energy detuning. This demonstrates how pump asymmetry may combat a disorder-induced detuning between two localized condensates and bring about synchronization.

2.2 The Gross-Pitaevskii equation in the double well

As will be the case for all of our investigations of driven-dissipative condensates, we shall take the extended Gross-Pitaevskii equation (eGPE) (1.15) as our starting point,

$$i\frac{\partial \Psi}{\partial t} = \left[-\frac{1}{2m}\nabla^2 + V(\mathbf{x}) + U|\Psi|^2\right]\Psi + i\left(g - \Gamma|\Psi|^2\right)\Psi, \qquad (2.1)$$

where here and henceforth we set $\hbar = 1$. We assume two well-separated, roughly harmonic potential wells. In order to study this configuration, we
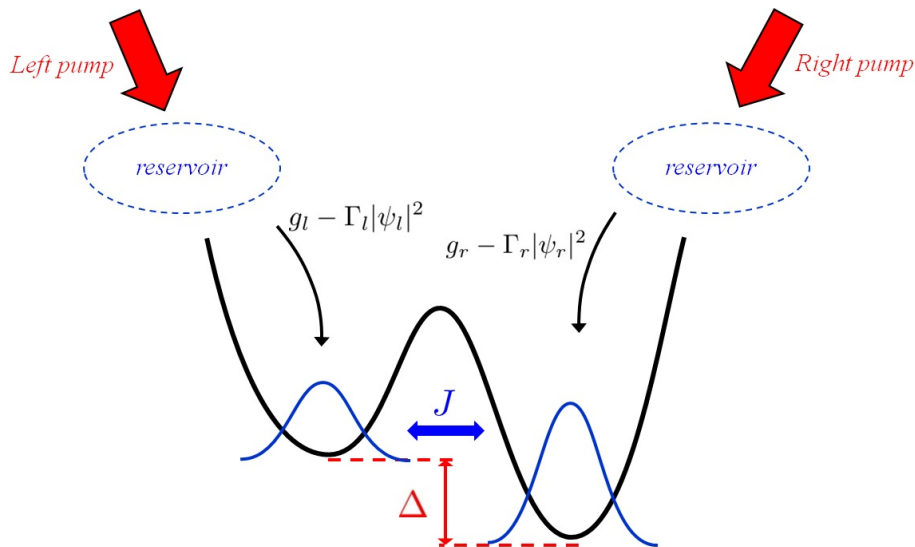
Figure 2.1: A schematic of two condensates in a double well potential.

expand the condensate wavefunction over the orbitals of the left and right wells [86],

$$\Psi(\mathbf{x}, t) = \psi_l(t)\phi_l(\mathbf{x}) + \psi_r(t)\phi_r(\mathbf{x}). \tag{2.2}$$

Here $\phi_{l,r}$ are the localized ground state wavefunctions in the left and right wells, which are normalized as $\int \phi_{l,r}^*(\mathbf{x})\phi_{l,r}(\mathbf{x})d\mathbf{x} = 1$, and $\psi_{l,r}$ are the respective amplitudes. Substituting this expression in (2.1) yields two coupled equations, one for the amplitude of each condensate:

$$
\begin{aligned}
i\frac{\partial \psi_l}{\partial t} &= \epsilon_l\psi_l - J\psi_r + U_l|\psi_l|^2\psi_l + i\left(g_l - \Gamma_l|\psi_l|^2\right)\psi_l \\
i\frac{\partial \psi_r}{\partial t} &= \epsilon_r\psi_r - J\psi_l + U_r|\psi_r|^2\psi_r + i\left(g_r - \Gamma_r|\psi_r|^2\right)\psi_r.
\end{aligned}
\tag{2.3}
$$

The above equations are obtained by multiplying the eGPE on the left by $\phi_l^*(\mathbf{x})$ and $\phi_r^*(\mathbf{x})$ respectively, and integrating over the size of the system. We have assumed that the overlap between the two wavefunctions is large relative to their size, so terms containing this quantity are exponentially small and may be neglected. ϵ_l is the ground state energy of the left well, and the polariton-polariton interaction strength in this condensate is $U_l = \int |\phi_l|^4 U \, d\mathbf{x}$. The dissipative terms $g_l = \int \phi_l^* g \, \phi_l \, d\mathbf{x}$ and $\Gamma_l = \int |\phi_l|^4 \Gamma \, d\mathbf{x}$ describe the gain and loss in the left condensate due to pumping and decay. The parameters that appear in the dynamics of the

right well are of course defined analogously. J is the tunnelling matrix element between wells. Explicitly, the tunnelling from the left well to the right is given by $J_{lr} = -\int \phi_l^*(\mathbf{x})\left[-(1/2m)\nabla^2 + V(\mathbf{x})\right]\phi_r(\mathbf{x})d\mathbf{x}$, and we make the assumption that the tunnelling is symmetric, i.e. $J_{lr} = J_{rl} = J$. This tunnelling term is real, however this is not always the case. If each well is not pumped uniformly, and the gain instead has some spatial dependence, this contributes an additional imaginary term to the tunnelling of the form $i\int \phi_l g(\mathbf{x})\phi_r d\mathbf{x}$ [87]. We will not, however, consider such a model with imaginary tunnelling strength. Furthermore, we assume that the nonlinearities in each well due to interactions and gain are the same, so we set $U_l = U_r = U$ and $\Gamma_l = \Gamma_r = \Gamma$.

In the absence of tunnelling between the wells (for example when the separation between them is large), each of the equations in (2.3) simply describes the dynamics of the amplitude of a trapped condensate. This supports the stationary solution,

$$\psi_l = \sqrt{n_{0,l}}e^{-i(\omega_l t + \Theta_l)}, \tag{2.4}$$

where again we use the example of the left well. $n_{0,l} = g_l/\Gamma$ is the steady state occupation of the well, and the solution oscillates with frequency $\omega_l = \epsilon_l + Un_{0,l}$, which is the single-particle energy of the well blueshifted by the energy arising from interactions between particles. Θ_l is an arbitrary phase factor resulting from spontaneous symmetry breaking. The overall phase has no physical significance, but as we shall see, the phase difference between coupled condensates plays a critical role in their dynamics.

It is also worth noting that our choice of normalization of the wavefunction at each site sets a dimensionless density scale such that the unit of length in this model is taken to be the spatial extent of the potential well. This follows from the definition of the total number of particles in the system,

$$\begin{aligned}
N &= \int |\Psi(\mathbf{x}, t)|^2 d\mathbf{x} \\
&= |\psi_l(t)|^2 \int |\phi_l(\mathbf{x})|^2 d\mathbf{x} + |\psi_r(t)|^2 \int |\phi_r(\mathbf{x})|^2 d\mathbf{x} \\
&= |\psi_l(t)|^2 + |\psi_r(t)|^2 \\
&= n_l + n_r.
\end{aligned} \tag{2.5}$$

Thus, the density at each site is just the number of particles in that well,

and as such, we use the terms 'density' and 'occupation' interchangeably.

In the absence of coupling, trapped condensates behave independently of one another. They generally have different energies, and their emission frequencies are set by the depth of the well, and the number of particles in each condensate, which is controlled by the pump strength. In the double well configuration however, tunnelling between sites means that it is possible to overcome detunings in energy and pump strength, and for two initially separated condensates to behave as a single state, and emit at a common frequency.

This phenomenon is best seen by reparameterizing the dynamical equations given by (2.3) in terms of the phase and density in each well. The most general form of the amplitude in each well is given by

$$\psi_{l,r}(t) = \sqrt{n_{l,r}(t)}e^{-i\theta_{l,r}(t)}. \tag{2.6}$$

Substituting this in (2.3), and separating real and imaginary parts yields coupled equations for the densities,

$$
\begin{aligned}
\frac{\dot{n}_l}{2} &= (g_l - \Gamma n_l)\, n_l - J\sqrt{n_l n_r}\sin(\theta_l - \theta_r) \\
\frac{\dot{n}_r}{2} &= (g_r - \Gamma n_r)\, n_r + J\sqrt{n_l n_r}\sin(\theta_l - \theta_r),
\end{aligned} \tag{2.7}
$$

and phases,

$$
\begin{aligned}
\dot{\theta}_l &= \epsilon_l + U n_l - J\sqrt{\frac{n_r}{n_l}}\cos(\theta_l - \theta_r) \\
\dot{\theta}_r &= \epsilon_r + U n_r - J\sqrt{\frac{n_l}{n_r}}\cos(\theta_l - \theta_r),
\end{aligned} \tag{2.8}
$$

of each well. Equations 2.7 describe the particle currents that flow between the two wells. The first terms on the right describe the net flow of particles in or out of each condensate due to pumping and decay. If the pumping succeeds in establishing a steady state density at each site, these terms cancel, and the equations are those of two coupled equilibrium condensates. The last term on the right of each equation describes the Josephson current that flows from one well to the other as a result of the phase difference between the condensates. This is the mechanism behind the remarkable DC Josephson effect: even in an ideal double well potential, where two condensates of equal energies and

densities are maintained through uniform pumping, a current will still flow through the barrier because of the differing phases between the condensates. It is because of this current that we must correct our initial assessment of the dynamics. The dissipative terms on the right of (2.7) will *not* cancel. As the phase of each condensate will in general be different, the Josephson current will act to unbalance the densities on each side. It is easy to see, in the simple case of identical pumping of each well ($g_l = g_r, \Gamma_l = \Gamma_r$), that the nonlinear term will no longer saturate the gain. In the case where the Josephson current flows from left to right, the gain terms will act as a particle source in the left well, and a sink in the right, and vice versa for a current in the opposite direction. Thus, the gain and loss mechanisms in the polariton condensate are analogous to connecting the superconductors in the traditional Josephson junction in a circuit: they prevent the condensate occupations on either side of the junction from being depleted by the Josephson current.

Of course, the DC Josephson effect relies on the phase difference, that is the argument of the sine terms, remaining constant. If this phase difference instead grows in time, the sine will rapidly and repeatedly change sign, and an alternating current occurs between the wells. This is analogous to the AC Josephson effect, which is traditionally observed when a fixed voltage is imposed across a superconducting Josephson junction. The equations (2.8) describing the phase dynamics are thus key to understanding whether a direct or alternating current is present across the junction, as we will see in the next section.

We can see evidence of the DC and AC Josephson effect in the plots of the occupations of each well in Fig. 2.2. In both plots, the left well has a slightly higher energy than the right well, and both are pumped equally. The larger occupation of the right well in plot (a) is evidence of a constant Josephson current flowing from the left well to the right to balance the energy difference. In plot (b) however, the tunnelling is not strong enough relative to the energy difference to maintain a constant phase difference between the condensates, and we see density oscillations between the two wells, characteristic of the AC Josephson effect [88]. We will characterize these two regimes further in the following section.
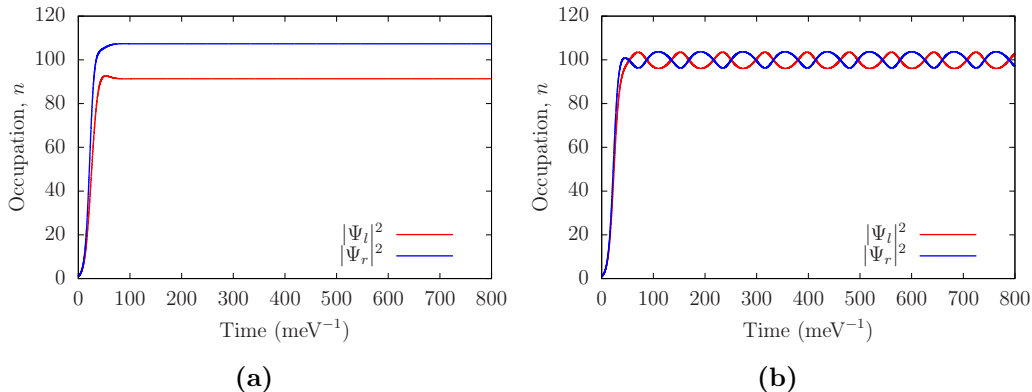
Figure 2.2: Time dependence of the density of two coupled condensates in the (a) synchronized and (b) desynchronized regimes. Josephson oscillations are evident in the densities in the desynchronized case. Densities are obtained by solving Eq. (2.3) with parameters: (a) $\Delta = 0.05$ meV, $J = 0.015$ meV, (b) $\Delta = 0.08$ meV, $J = 4$ μeV. In both cases both wells have $g = 0.1$ meV, $\Gamma = 1$ μeV, $U = 3$ μeV.

2.3 Phase dynamics and synchronization in the double well

The question of whether a driven-dissipative condensate in a double well potential exhibits a DC or an AC Josephson effect is equivalent to asking whether the condensates in each well have the same energy. From (2.7), we see that if the phase difference between the wells grows with time, the direction of the Josephson current will fluctuate. Thus, a direct current requires the frequencies of the condensates – set by (2.8) – and therefore their energies, to be synchronized. The synchronized and desynchronized phases of the double well have been studied before [86, 88, 89], and the phase boundary between the two regimes has been derived as a function of the parameters of the mean field model [85]. These investigations have considered only the cases of uniform pumping of both condensates, or pumping of a single condensate. Remarkably, the phase boundary in this case does not depend on the rate of linear gain of the condensates, g. In this section, we generalize the approach of Borgh et al. [85] to account for differing rates of linear gain in each well. This approximates asymmetric pumping of the system.
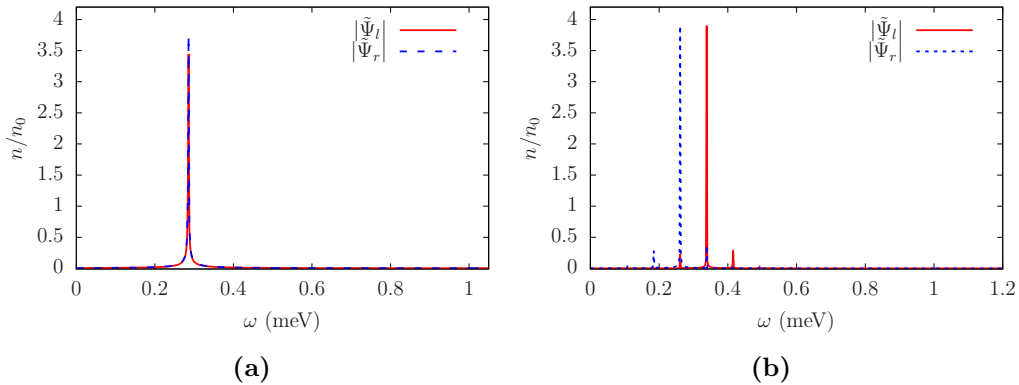
Figure 2.3: Spectra of two coupled condensates in the (a) synchronized and (b) desynchronized regimes. Parameters used are the same as for the corresponding plots in Fig. 2.2. Fourier transforms are sampled over a range of 2 ns.

To proceed, we express the equations (2.7) and (2.8) in terms of the parameters relevant to the problem. Whether the condensates are synchronized or not depends on the phase difference between the wells, $\Phi \equiv \theta_l - \theta_r$. Specifically, a synchronized state is one where this quantity is constant in time. It is also the detuning of the energies of the two wells, rather than their individual single-particle energies, that influences the dynamics, so we define this detuning as $\Delta \equiv \epsilon_l - \epsilon_r$. We expect that in general, a large detuning will inhibit synchronization, while the tunnelling strength, J, assists it. This is to be seen in Figs. 2.2 and 2.3, where we plot the densities and frequencies of each well in the two different regimes. The frequencies of each well are obtained by solving (2.3) numerically and performing a discrete Fourier transform (DFT) on the amplitudes. The frequencies of each well are then evident as peaks in these spectra when plotted. In Figs. 2.2(a) and 2.3(a), the tunnelling strength is large relative to the detuning, and both wells have the same frequency, and a constant density. In Figs. 2.2(b) and 2.3(b) on the other hand, a larger detuning and smaller tunnelling strength are chosen, and the dynamics are qualitatively different. The amplitude of each well oscillates with a different frequency, causing an alternating Josephson current to oscillate between the wells.

In order to effectively describe the synchronization dynamics of the sys-

tem, and derive an expression for the boundary between the two distinct phases, it is convenient to follow [85] in defining new variables describing the mean condensate density, and the density imbalance,

$$R = \frac{n_l + n_r}{2}, \qquad z = \frac{n_l - n_r}{2},$$

while we do likewise for the linear gain terms in each well:

$$\bar{g} = \frac{g_l + g_r}{2}, \qquad \delta g = \frac{g_l - g_r}{2}.$$

In the uniformly pumped double well, one has $g_l = g_r = \bar{g}$, and $\delta g = 0$. With these re-definitions, the dynamics of the system are then captured more concisely by adding and subtracting the pairs of equations (2.7) and (2.8) to obtain equations for the mean density, and the density and phase differences:

$$\dot{R} = 2R\bar{g} + 2z\delta g - 2\Gamma(R^2 + z^2) \tag{2.9}$$

$$\dot{z} = 2R\delta g + 2\bar{g}z - 4\Gamma Rz - 2J\sqrt{R^2 - z^2}\sin\Phi \tag{2.10}$$

$$\dot{\Phi} = \Delta + 2Uz - \frac{2z}{\sqrt{R^2 - z^2}}J\cos\Phi. \tag{2.11}$$

We note that the dynamics of the total phase are not relevant to synchronization.

At this point, we make a number of assumptions to simplify our analysis. We will assume that there is significant occupation of both wells, such that

$$R \gg z. \tag{2.12}$$

As the steady state density of a single condensate is proportional to the linear gain, in order for the above restriction to be true, we must also consider a pump asymmetry that is small relative to the overall pump strength, i.e.

$$\delta g \ll \bar{g}. \tag{2.13}$$

In general, as noted in [85], if the double well is pumped strongly enough to fulfil the above conditions, the system will be in the Josephson regime [90], where interactions dominate over tunnelling. We therefore also have

$$UR \gg J. \tag{2.14}$$

33

Finally, we restrict ourselves to studying the dynamics where the overall density is in a steady state, or $\dot{R} = 0$. This is a reasonable assumption, as numerical simulations of the eGPE in the double well show that the total density rapidly relaxes to the steady state in experimentally relevant parameter regimes. This is to be seen in Fig. 2.2, where after initial rapid transient behaviour, the total density remains constant in both synchronized and desynchronized regimes.

Taking the steady state of (2.9), dividing across by R^2, and neglecting terms of second order in (z/R) gives us the expected condition for the total occupation of the wells:

$$R = \frac{\bar{g}}{\Gamma}. \qquad (2.15)$$

Here, we have used $n_{l,r} \approx g_{l,r}/\Gamma$, so that $\delta g \approx z\Gamma$, and $z\delta g/R^2 \approx \Gamma(z/R)^2$.

Eq. (2.11) also simplifies with the condition (2.12), and by recognizing that $|\cos\Phi| \leqslant 1$, we can use (2.14) to eliminate the trigonometric term, and rewrite this equation as an expression for the density difference,

$$z = \frac{\Delta - \dot{\Phi}}{2U}. \qquad (2.16)$$

Finally, we can substitute (2.15) and (2.16) into (2.10) to eliminate all dependence on density, and obtain a dynamical equation for the system in terms of its phase difference:

$$\ddot{\Phi} + 2\bar{g}\dot{\Phi} + 4\bar{g}\frac{UJ}{\Gamma}\sin\Phi = 2\bar{g}\left(\Delta + 2\frac{U}{\Gamma}\delta g\right). \qquad (2.17)$$

This equation is a generalization of the one derived by Borgh et al. [85] for non-uniform pumping of the wells. It has the familiar form of the equation of motion of a damped, driven pendulum [91].

It is useful to analyse the behaviour of this system in the 'overdamped regime', where the second derivative term may be neglected. This corresponds to strong pumping of the system. To see this, we first reparameterize the equation by defining a dimensionless time, $\tilde{t} = (\Gamma/2UJ)t$. For the second derivative term to vanish, its coefficient must be negligibly small in these dimensionless units, which is the case if

$$\bar{g} \gg \frac{UJ}{\Gamma}. \qquad (2.18)$$

The overdamped description of the system then takes on the more approachable form,

$$\dot{\Phi} = \lambda - \sin \Phi, \tag{2.19}$$

where the derivative is now in terms of the new dimensionless time, and

$$\lambda = \frac{\Gamma}{U} \frac{\Delta}{2J} + \frac{\delta g}{J}. \tag{2.20}$$

Eq. (2.19) is often called the Adler equation [12], and its behaviour is well known. Two distinct types of solution are permitted. A synchronized solution corresponds to a steady state, $\dot{\Phi} = 0$. This is only possible if $\lambda \leqslant 1$, due to the bounded nature of the sine function. When this is the case, the phase difference will rotate from its initial condition to a fixed point at $\Phi = \arcsin(\lambda)$, where it will then remain. On the other hand, when $\lambda > 1$, a stationary solution is impossible. The phase difference will continually rotate, and the individual frequencies are desynchronized. There is thus a transition from a synchronized to a desynchronized state at $\lambda = 1$, or in terms of the parameters of the polariton double well, at

$$\Delta = \frac{2U}{\Gamma} (J - \delta g). \tag{2.21}$$

In the case of uniform pumping, $\delta g = 0$, and we recover the result from [85]. This illustrates how synchronization is a competition between detuning and tunnelling strength: the larger the energy difference between the two wells, the greater the tunnelling strength that is required to maintain synchronization. The ratio of the nonlinearities in the system affect synchronization in the same way. When the interaction strength is strong relative to the gain saturation strength, this diminishes the effect of the detuning, enabling synchronization to occur at a smaller value of tunnelling strength, and vice versa.

Two identical wells that experience the same gain and loss will always be synchronized regardless of tunnelling, as their relative detuning is zero. However, we see that this is not the case if a gain asymmetry ($\delta g \neq 0$) is introduced. This contributes an extra effective detuning of $2U\delta g/\Gamma$. Therefore, if the system is in a parameter regime that does not support synchronization under uniform pumping, introducing a gain asymmetry in the opposite direction of the energy detuning of the wells by pumping the lower well more

strongly can synchronize the energies of the condensate. This may be explained by noticing that the condensate that experiences a higher linear gain will have a greater occupation, meaning the interactions between particles will have a greater contribution to the energy of the condensate than in the more weakly pumped well.

Eq. (2.17) provides another connection between the polariton double well and the superconducting Josephson junction. The resistively and capacitively shunted junction (RCSJ) model [92, 93, 94] describes the total current flow through a Josephson junction. In addition to a supercurrent, this will typically contain contributions from a displacement current and an ordinary current. In the RCSJ model, these are accounted for by including a capacitor and a resistor in parallel with the Josephson junction in a circuit. The supercurrent is given by $I_c \sin \Phi$, where Φ is now the phase difference across the junction and I_c is the Josephson critical current. The current through the capacitor and resistor are $C\dot{V}$ and V/R respectively, with C capacitance, R resistance and V voltage. All three currents may be written in terms of the phase difference across the junction with the Josephson voltage-phase relation $\dot{\Phi} = 2eV/\hbar$, which is essentially the analogue of (2.11) for a superconducting Josephson junction. The total bias current is then given by summing the three distinct contributions:

$$\frac{\hbar C}{2e}\ddot{\Phi} + \frac{\hbar}{2eR}\dot{\Phi} + I_c \sin \Phi = I. \qquad (2.22)$$

This may be analysed in the same way as (2.17). The overdamped limit is equivalent to having a negligible dimensionless McCumber parameter, $\beta = 2eI_cR^2C/\hbar$, and in this regime, the transition between DC and AC Josephson effects is found to be simply $I = I_c$.

A useful way of visualizing the dynamics of equations such as (2.17) and (2.22) is by interpreting them as equations of motion for a particle with position Φ moving in a potential $V(\Phi)$. In terms of the parameters of our coupled condensate model in dimensionless time, this particle has low mass $UJ/(4\bar{g}\Gamma)$, and experiences a strong viscous drag force, meaning it effectively has no inertia. The potential may be calculated as

$$-\frac{dV}{dt} = \lambda - \sin \Phi, \qquad (2.23)$$

(a)

(b)
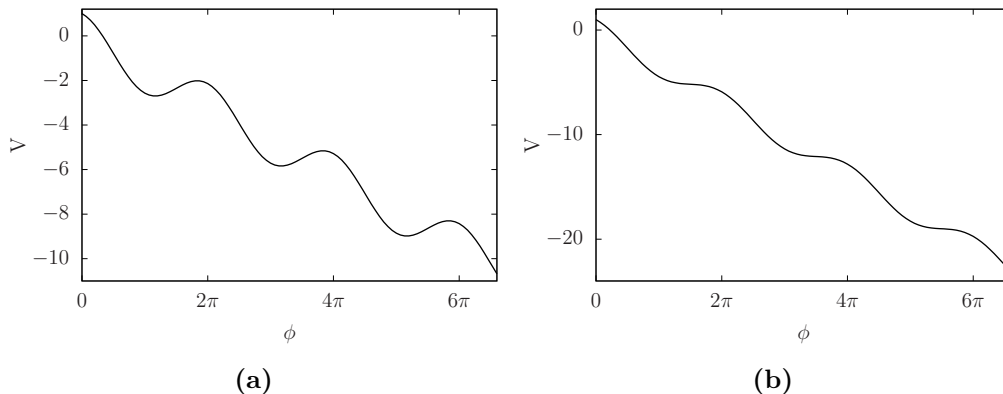
Figure 2.4: Washboard potentials for the overdamped polariton double well (2.19). In (a), $\lambda = 0.5$, and the system is synchronized. Our 'particle' will reach a stable fixed point in one of the minima of $V(\Phi)$, where Φ will remain constant. In (b), $\lambda = 1.1$, and there are no longer any stable fixed points to prevent the phase difference from increasing. The frequencies in this case are desynchronized.

so

$$V(\Phi) = -\lambda\Phi + \cos\Phi. \qquad (2.24)$$

This so-called 'washboard potential' [91, 92] is plotted for two values of λ in Fig. 2.4. When $\lambda < 1$, the particle will become trapped in one of the potential minima of the potential, and so we have the synchronized result, $\dot{\Phi} = 0$. On the other hand, at $\lambda = 1$, these potential minima become inflection points, and the particle is free to roll down the slope. Thus, this shows how Φ steadily increases (or rather rotates, as it is 2π-periodic) for a desynchronized solution corresponding to $\lambda > 1$.

2.4 Phase diagram

Our expression for the phase boundary between synchronized and desynchronized states of the double well of polariton condensates is confirmed by numerical simulations of the eGPE in the double well (2.3). In Fig. 2.5, we plot phase diagrams distinguishing the synchronized and desynchronized regimes as a function of tunnelling strength and energy detuning for both symmetric

(a), and asymmetric (b) pumping of the wells. Whether the system is synchronized or not in a given parameter regime is determined numerically by solving the coupled equations (2.3), and performing a DFT on the resulting amplitudes to determine the frequency of each condensate, as was done for Fig. 2.3. These frequencies are then compared to determine synchronization. This test is performed iteratively over a grid of points in parameter space to produce the blue (synchronized) and red (desynchronized) regions in Fig. 2.5. The analytic result (2.21) is then plotted as a white dashed line over the numerical data, and is seen to agree well.
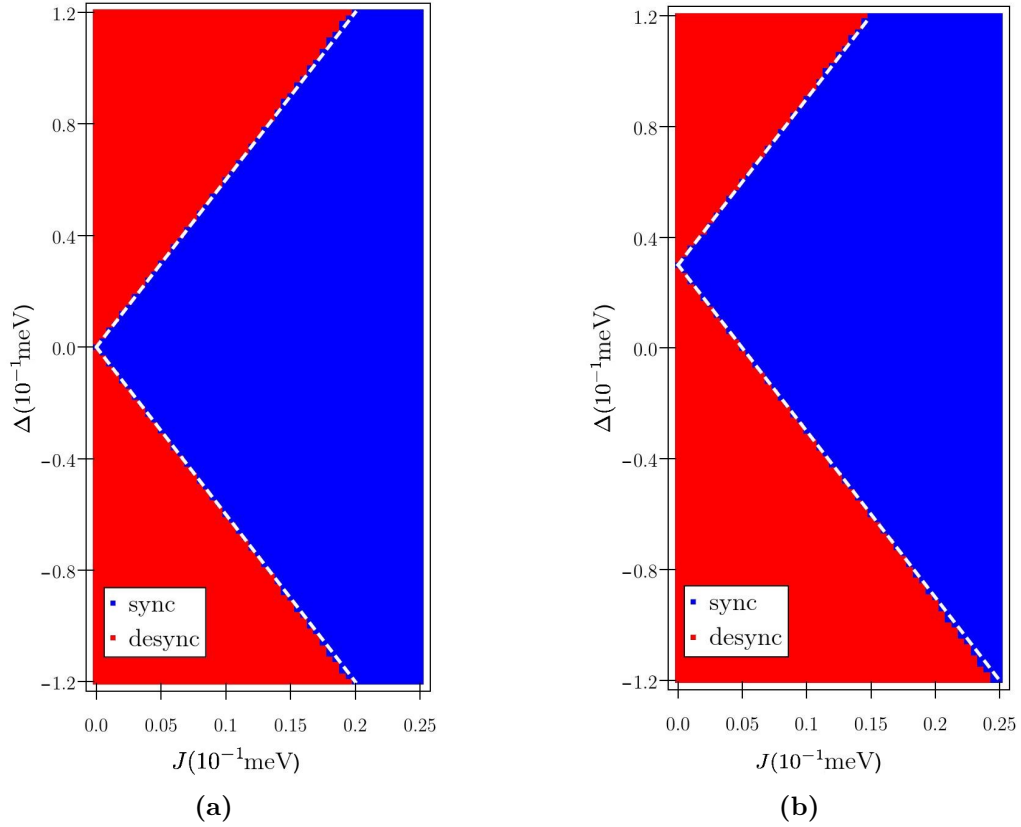
Figure 2.5: Phase diagrams for condensates in a double well potential with (a) symmetric and (b) asymmetric linear gain coefficients. Analytic results for the phase boundaries are plotted as white dashed lines. As per (2.3), a positive detuning corresponds to the minimum of the potential on the left lying above that on the right, and the converse for negative detuning. The linear gain terms for (b) are $g_l = 0.095$ meV and $g_r = 0.105$ meV, while both plots have $\Gamma = 1$ μeV, $U = 3$ μeV.

The phase diagrams are plotted for an experimentally valid range of parameters, which we justify in the following section (2.5.2). Following from our definitions of the detuning, positive values of Δ correspond to the condensate in the left having a greater single-particle energy than that on the right and vice versa. The phase diagram is symmetric with respect to this detuning when the wells are pumped uniformly (Fig. 2.5(a)). At $\Delta = 0$, the frequencies of the condensates are synchronized, regardless of tunnelling strength. However, once an energy detuning is introduced in either direction, a finite tunnelling strength is required for synchronization. Fig. 2.5(b) shows the same phase diagram, but with the right well pumped more strongly than the left. We see that now the condensates are desynchronized at the origin ($\Delta = 0, J = 0$), as the pump asymmetry effectively shifts the detuning by $2U\delta g/\Gamma$. In the top half of the plot, where Δ is positive, the direction of the pump asymmetry opposes the detuning. This implies that for a given value of J, the wells require a greater detuning to be brought into the desynchronized regime than in the symmetric case. The opposite is true when the positively-detuned condensate is pumped more strongly than the other one (negative values of Δ). We note that the condensate interaction strength, U, and gain saturation coefficient Γ, were kept constant for these phase diagrams. We know from (2.21) that varying the ratio of these two terms changes the slope of the phase boundary. Outside of the range of parameters considered in these phase diagrams, our parameters are no longer in the heavy damping and/or Josephson regimes, and we expect nonlinear effects to cause the phase boundary to deviate from a straight line [85].

2.5 Comparison with experiment

2.5.1 Approximation of asymmetric pumping

As mentioned in the previous section, our approximation of an asymmetrically pumped double well by employing different linear gain coefficients for the condensates on either side is a somewhat crude one. While varying the pump strength does change the linear gain coefficient in each well, it also affects several other parameters in our model. This can be seen by con-

sidering equations of the form (1.19) and (1.20) for each well, which model the pump reservoir explicitly [45]. Adiabatically eliminating the reservoir dynamics, and expanding the reservoir densities as in [46], or the following section 2.5.2, yields an equation of the form of the double well eGPE (2.3) in terms of parameters such as the pump strength, the reservoir relaxation and loss rates, and the strength of the interactions between polaritons in the condensate and the hot excitons in the reservoir. We may compare this expression directly with Eq. (2.3) to see the relationship between the parameters of the two models.

In particular, by doing this one finds that the pump strength from (1.20) appears in the quadratic interaction term (U in our model), and the linear oscillation frequency (our $\epsilon_{l,r}$). This is because implicit in the eGPE is the condensate-reservoir interaction energy. This depends on the reservoir density, which is set by the pump rate, and has contributions to both the interaction term, U, and the linear term, $\epsilon_{l,r}$. Pumping one well more strongly than the other will create more reservoir excitons which interact with the condensate polaritons in that well. These additional interactions will contribute an extra blueshift to the energies of the more strongly-pumped well. To account for this, we may absorb this additional difference in energies into the energy detuning, Δ. We also note that our analysis found that increasing the linear gain of one of the condensates effectively increases its energy relative to the other. The additional blueshift due to increased condensate-reservoir interactions which we neglect would appear in the same direction as the blueshift due to detuning of linear gain parameters, so even if this latter term is not absorbed into Δ, it does not qualitatively impact our result. We would therefore expect an experimental analysis of the double well to find that a small asymmetry in the pumping of the wells will have the effect of shifting the phase boundary between synchronized and desynchronized states in the direction of the pump asymmetry. For a given measured energy detuning, Δ, the shift in the position of the boundary would be greater than is predicted by (2.21) however.

In addition to changing the condensate-reservoir interaction strengths in the wells, a differing pump strength may also be expected to affect the gain saturation term, Γ. This can be seen when the two mean-field models are

compared in equations 2.31, 2.32 and 2.33 in the following section. However, it is not unreasonable to imagine a pump mechanism that affects the linear gain much more strongly than the nonlinear saturation, justifying our consideration of differing values of g between wells, while approximating Γ as uniform.

2.5.2 Choice of parameters for simulations

When choosing parameters for numerical simulations of the eGPE in the double well (2.3), we are guided by experimental results for polariton condensates. While some of the parameters in our model are experimentally measured, most are not directly accessible, and must be estimated.

We consider potential wells which confine the condensates in a region of size $\sim 10 \, \mu\text{m} \times 10 \, \mu\text{m}$. This is consistent with what is experimentally observed in confinement potentials arising from disorder [56,95], and potential wells on this scale have been engineered using spatially patterned pump lasers [83,96]. Rather than the energies of the individual wells, it is their detuning, Δ that is relevant to our theory. Detunings of ~ 0.3 meV have been reported for localized condensates in disordered samples [50], while similar values of Δ have also been achieved for 'polaritonic molecules', where condensates are localized in pairs of micropillars [82]. In the latter case, the ground state energy of one of the condensates is raised by weakly pumping its micropillar, thus creating a reservoir of excitons there, which interact with the condensed polaritons.

Pumped sufficiently above threshold, a condensate in such a potential would be expected to contain ~ 100 polaritons, based on estimates from experimental data on emission intensities [6,95]. This sets the ratio of the gain parameters, as the steady-state density in a well is $n_0 = g/\Gamma$. These individual parameters are not straightforwardly available from experimental data, as together they describe a range of different mechanisms, including stimulated scattering from reservoir to condensate, and the decay of both condensed and uncondensed polaritons through the cavity mirrors. We may however infer them from reported values of polariton decay rates and relative pumping strengths.

The linear gain coefficient g describes the net gain or loss of the condensate amplitude, and is defined as $g = \gamma - \kappa$, where κ is the decay due to losses through the cavity mirrors, and γ is the gain due to scattering from the reservoir. A value of κ may be obtained directly from experimental data. The rate of decay from the condensate is simply the inverse of the polariton lifetime, which may be calculated directly from the linewidth of the emission. The decay rate of the population is 2κ, due to the relationship between density and amplitude. We may demonstrate this with the example of an unpumped condensate (where imaginary terms are neglected):

$$\begin{aligned}
\frac{\partial n}{\partial t} &= \frac{\partial}{\partial t}|\psi|^2 \\
&= \psi^* \frac{\partial \psi}{\partial t} + \frac{\partial \psi^*}{\partial t} \psi \\
&= \psi^*(-\kappa\psi) + (-\kappa\psi^*)\psi \\
&= -2\kappa|\psi|^2 \\
&= -2\kappa n.
\end{aligned}$$

Unlike κ, a value for γ does not suggest itself as readily from available data. The linear gain, γ, and loss, κ, balance at threshold, and as g increases with pumping strength, P, one may assume a linear dependence of γ on P, as in [42], implying the gain takes the form

$$g = \kappa \left(\frac{P}{P_{th}} - 1 \right), \tag{2.25}$$

where P_{th} is the pumping at threshold. Indeed, one obtains this exact expression from the alternative Gross-Pitaevskii model of a polariton condensate (1.19, 1.20) in the adiabatic limit of instantaneously fast reservoir dynamics. In this framework, the gain in the GPE has the form

$$i\frac{\partial \psi}{\partial t} = \ldots + \frac{i}{2}\left(R\frac{P}{\gamma_R + R|\psi|^2} - \gamma_C \right)\psi, \tag{2.26}$$

where, as outlined in Section 1.4, R is the rate of scattering from the reservoir to the condensate, and γ_R and γ_C are the rates at which polaritons decay from the reservoir and condensate, respectively. From this, the steady state density is given by

$$|\psi_0|^2 = \frac{P}{\gamma_C} - \frac{\gamma_R}{R}, \tag{2.27}$$

and setting this quantity to zero gives us the threshold pumping strength:

$$P_{th} = \frac{\gamma_C \gamma_R}{R}. \tag{2.28}$$

Using this, we may rewrite the expression for the steady state density in terms of experimentally accessible parameters,

$$|\psi_0|^2 = n_s \left(\frac{P}{P_{th}} - 1 \right), \tag{2.29}$$

where $n_s = \gamma_R/R$ is the saturation density corresponding to the occupation when the system is pumped at twice the threshold value. Thus, we may rewrite the fraction in (2.26) in terms of these parameters to see that just above threshold, when the condensate occupation is small, it may be expanded as a power series (which we truncate to second order),

$$\gamma_C \frac{P}{P_{th}} \left(\frac{1}{1 + |\psi|^2/n_s} \right) = \gamma_C \frac{P}{P_{th}} \left(1 - \frac{|\psi|^2}{n_s} + \dots \right). \tag{2.30}$$

Substituting this in (2.26), we have

$$i\frac{\partial \psi}{\partial t} = \dots + \frac{i}{2} \left\{ \gamma_C \left(\frac{P}{P_{th}} - 1 \right) - \frac{\gamma_C}{n_s} \frac{P}{P_{th}} |\psi|^2 \right\} \psi. \tag{2.31}$$

This now has the same form as the damping in (2.1), where g has the form predicted in (2.25) (we recognize that $\kappa = \gamma_C/2$), and $\Gamma = (\gamma_C/2n_s)(P/P_{th}) = (R\gamma_C/2\gamma_R)(P/P_{th})$.

It is clear, however, that this result only holds just above threshold. When the occupation of the condensate is significant – similar to or greater than n_s – we should replace the expansion in (2.30) with a Taylor series expansion around the steady-state density [46]. This produces a similar result that has the same form (2.31), except in this case the gain parameters are

$$g = \frac{\gamma_C}{2} \left(1 - \frac{P_{th}}{P} \right) \tag{2.32}$$

and

$$\Gamma = \frac{\gamma_C^2}{2P} = \frac{\gamma_C}{2n_s} \frac{P_{th}}{P}. \tag{2.33}$$

While at first glance, these values of g and Γ appear similar to those in (2.31), the behaviour is markedly different when the system is pumped far above threshold. In particular, this approach gives the result that the linear

gain saturates, asymptotically approaching the condensate loss rate as the pump strength is increased. Of course, there are limitations to this model of the pump reservoir (2.26), as, much like the eGPE, it is a simplificaton of the processes that actually occur. Nevertheless, it would appear sensible to take our value of g to be roughly equal to $\gamma_C/2 = \kappa$, or half the inverse of the polariton lifetime. Polariton lifetimes are typically a few picoseconds [35,36], so this corresponds to g being of order 0.1 meV in our units. We then choose Γ to be two orders of magnitude smaller to set an appropriate steady state density.

The interaction strength, U, is also difficult to estimate from experiments because, as outlined above, both condensate-condensate and condensate-reservoir interactions contribute to the experimentally-observed blueshift. It is easier to obtain a value for the dimensionless ratio of nonlinearities U/Γ – and indeed, the interaction strength only appears in this ratio in the theory we have developed (2.17). We may estimate the magnitude of this quantity by considering the model of the population dynamics of a polariton condensate presented in [97] and [95]. This is a generalization of a description of atom lasers [98]. From this model, one may derive the dissipative part of the eGPE in terms of the condensate decay rate, the saturation density, and the interaction strength of a single condensate mode. The latter two quantities are determined from experimental results for the second-order correlation function and blueshift above threshold in [97]. The ratio of these two terms is equal to U/Γ in our parameters, and is found to be $\simeq 2$. This is in broad agreement with the estimate of the inverse of this ratio to be $\simeq 0.3$ in [42]. Therefore, a value of U between 0.001 and 0.01 meV would be consistent with our estimation of Γ of order 1 μeV. We note that an expression for U in terms of the parameters of the alternative model given by (1.19, 1.20) may be derived in the same way as was done for the gain and loss parameters above. As noted in the previous section, this will have a dependence on the pump strength, and it may be negative due to the influence of the reservoir. However, negative values of U give rise to instabilities in the condensate [99], so we will only consider positive values of U in this work.

We can estimate the inter-well tunnelling J, by assuming Gaussian wave-

functions in two harmonic potential wells. We may then solve the integral

$$J_{lr} = -\int \phi_l^*(\mathbf{x})\left[-(\hbar^2/2m)\nabla^2 + V(\mathbf{x})\right]\phi_r(\mathbf{x})d\mathbf{x} \qquad (2.34)$$

where m is the polariton mass, which we take to be 5.1×10^{-5} times the free electron mass [57], and the wavefunction has the form

$$\phi_{l,r}(\mathbf{x}) = \frac{1}{L\sqrt{\pi}}e^{-((x\pm a/2)^2 + y^2)/(2L^2)} \qquad (2.35)$$

with inter-well separation, a, and harmonic oscillator length $L = \sqrt{\hbar/(m\omega)}$. We may estimate this latter quantity from experimental results. In [57], the full-width at half maximum (FWHM) of the emission from a single well in reciprocal space is found to be $\delta k = 0.5~\mu\text{m}^{-1}$. For a Gaussian function of the form (2.35), this reciprocal-space FWHM may be written as $(2/L)\sqrt{\ln 2}$, so this corresponds to a harmonic oscillator length of $L \approx 3~\mu\text{m}$. We may thus construct a corresponding harmonic double well potential of the form

$$V(\mathbf{x}) = \begin{cases} \frac{1}{2}m\omega^2((x + a/2)^2 + y^2), & x < 0 \\ \frac{1}{2}m\omega^2((x - a/2)^2 + y^2), & x \geq 0. \end{cases} \qquad (2.36)$$

Putting this all together, one finds that J decays exponentially with well separation, a. If we restrict ourselves to separations $a \geqslant 4L$, such that we are justified in neglecting terms containing the overlap $\int \phi_l^*(\mathbf{x})\phi_r(\mathbf{x})d\mathbf{x} = \exp\{(-a^2/(4L^2))\}$, we find that J may be at most of order 0.01 meV.

The limitations of this method of estimating J are obvious: the approximations of the potentials and wavefunctions are not particularly realistic, and the resulting expression also decays exponentially with L^{-1}, so it is quite sensitive to variations in length scale. It is however useful for providing an order of magnitude estimate for the tunnelling matrix element. It also demonstrates how, physically, the effect of tunnelling is increased by moving the wells towards one another, and reduced by moving them away from one another. We also note that condensates localized in smaller traps will have a larger value of J.

Finally, in order to see the synchronization transition predicted by (2.19), our choice of parameters must place us in the Josephson regime (2.14) as well as the overdamped regime (2.18). These two constraints enforce the condition

$$\frac{J}{g} \ll \frac{U}{\Gamma} \ll \frac{g}{J}. \qquad (2.37)$$

It is not surprising that the values of parameters we have derived from experimental results above fulfil this condition: both synchronized and desynchronized phases of the polariton Josephson junction have been observed experimentally [50, 56].

2.6 Conclusions

In this chapter, we have analysed the synchronized and desynchronized phases of the polariton Josephson junction. We followed previous literature on this system [85, 86, 88] by writing the extended Gross-Pitaevskii equation in terms of the amplitudes of two spatially-separated sites, and by using this to derive a single equation in terms of the phase difference between the condensates. Connecting this to the classical description of an overdamped pendulum enabled us to distinguish between the synchronized and desynchronized phases. We went beyond the state of the art by considering the effect of pumping the condensates in each well with different strengths. This was done by introducing an asymmetry to the linear gain rates in each well. We found that this pump asymmetry behaves as an effective detuning between the energies of the wells that is equivalent to the extra blueshift due to interactions resulting from the difference in steady-state densities.

Understanding the transition between the synchronized and desynchronized regimes of the double well is crucial to the work in the remainder of this thesis. When the frequencies of the condensates in each well are synchronized, they behave as a single condensate that is not localized in either well. Thus, the synchronization transition is equivalent to a transition from localized to extended states. In the next chapter, we will extend our analysis to a large number of potential wells, to determine whether the same transition occurs.

Additionally, in this chapter we have derived reasonable values for all of the parameters that appear in the eGPE, through comparison with experimentally reported values, and through demonstrating the equivalence between the two commonly-used mean-field models of driven-dissipative condensates. These values will be used to guide numerical simulations in the rest of this thesis.

Chapter 3

Synchronization in disordered lattices of condensates

3.1 Introduction

In this chapter we extend the analysis of the polariton condensate in a double well from the previous chapter to the case of N coupled driven-dissipative condensates arranged in a chain, or a square lattice. We consider the condensates to be localized in potential wells with randomly-distributed depths. This configuration has been investigated experimentally [57], and approximates a disordered potential landscape in 1D (chain) and 2D (lattice). As in the case of the double well, tunnelling through potential barriers separating neighbouring condensates is possible. This enables pairs of condensates to overcome the detunings in their energies and synchronize their frequencies. We address the question of whether it is possible for a common frequency to be established across the entire lattice. As in the previous chapter, we show that each condensate may be described as an autonomous phase oscillator. Our problem then reduces to the more general one of whether frequency synchronization may occur in a lattice of locally-coupled oscillators with random natural frequencies in one or two dimensions.

The focus of this chapter is therefore not specific to the behaviour of polariton condensates, but more generally to all systems which may be described by the same phase oscillator model as that which we derive from the extended Gross-Pitaevskii equation on a lattice. To reflect this, much of the

language we use in this chapter is that of coupled oscillators, rather than being specific to the case of condensates. We refer to 'oscillators' having certain 'frequencies', and interacting through some 'coupling'. These terms may of course be replaced with 'condensates', 'energies' and 'tunnelling', but we do not wish to limit our descriptions to this framework. We compare our model to other theories of coupled oscillator from the literature – in particular the well-known Kuramoto model [69]. The description of our system is in fact equivalent to a nearest-neighbour generalization of the Kuramoto model with a modified coupling term. We demonstrate that the non-Kuramoto coupling has a significant effect: it allows synchronization to occur in large lattices, formed from macroscopic numbers of oscillators, for dimensions $d < 4$. This is contrary to the behaviour found in lattices of locally-coupled Kuramoto oscillators, where synchronization becomes impossible in the limit of an infinite number of sites [76, 77].

We do this by demonstrating that the continuum limit of the oscillator model is a Kardar-Parisi-Zhang equation [100] with time-independent noise [101, 102, 103, 104]. The KPZ equation is a stochastic nonlinear differential equation that was originally formulated in the context of interface growth, and may be used to describe a broad class of phenomona related to kinetic roughening [105]. This is because solutions to the equation – at least in low dimensions – are found to be rough, as a result of the noise term. In the three and a half decades since its introduction, many different physical systems have been shown to lie in the KPZ universality class. In particular, it has been very successful in describing the dynamics of nonequilibrium systems that experience disorder. Of course, polariton condensates are such systems. However, the disordered lattices of condensates that we describe in this chapter do not belong to the KPZ universality class. We consider spatial disorder rather than time-dependent noise, and as such, the continuum limit of our model may have smooth, regular solutions. Systems in the KPZ universality class are considered, however, in the final chapter of this thesis, where the impact of noise on lattices of driven-dissipative condensates is studied. In this chapter, mapping our KPZ-like model to an imaginary-time Schrödinger equation with a random potential allows us to derive the phase boundary for synchronization and characterize the frequency and phase pro-

files. These analytical predictions agree with numerical simulations in one and two dimensions.

Our results are significant in the context of driven-dissipative condensates. While experimental demonstrations of lattices of polariton condensates localized in potential wells have shown that a synchronization transition occurs for small systems [57], we show that this phenomenon persists in the thermodynamic limit. It is therefore characteristic of a non-equilibrium phase transition, where the change in character of the steady-state of the system in the thermodynamic limit gives rise to singularities in its properties. Furthermore, we demonstrate that phase and frequency ordering in a driven-dissipative gas of bosons are not always destroyed by static disorder, despite recent evidence that the superfluid-insulator transition which occurs in equilibrium [53] is not present out of equilibrium [55].

## 3.2 Derivation of phase oscillator model

We begin our analysis in the same way as we did in the case of the double well in the previous chapter; except this time, instead of considering two sites, we are considering many. We thus expand the condensate order parameter over the basis set of the wavefunctions localized in each well, labelled by index i:

$$\Psi(\mathbf{x}, t) = \sum_{i}^{N} \psi_i(t)\phi_i(\mathbf{x}). \tag{3.1}$$

We then substitute this in the extended Gross-Pitaevskii equation (1.15), and multiply on the left by $\phi_j^*(\mathbf{x})$ and integrate over the sample to obtain an equation for the amplitude of the jth site. We assume a 'tight-binding' type configuration where the wavefunctions are localized on each site, so that the overlaps between sites are small, and we may neglect terms containing this quantity [106]. As before, we take the wavefunction on each site to be normalized, so the density on each site is a dimensionless number of particles. Our N coupled equations then take the form

$$i\frac{\partial \psi_j}{\partial t} = \left[\epsilon_j + U|\psi_j|^2 + i\left(g - \Gamma|\psi_j|^2\right)\right]\psi_j - \sum_{<k>} J_{jk}\psi_k. \tag{3.2}$$

These are identical to the equations for the double well (2.3), except now, instead of a single tunnelling term, the sum over nearest neighbours (indicated by $<k>$) describes tunnelling between each site and those directly adjacent to it. This sum has two terms in 1D, and four on a two-dimensional square lattice. As before, ϵ_j is the single-particle energy of the jth well, $U_j = \int |\phi_j|^4 U \, d\mathbf{x}$ is the polariton-polariton interaction strength, $g_j = \int \phi_j^* \, g \, \phi_j \, d\mathbf{x}$ and $\Gamma_j = \int |\phi_j|^4 \Gamma \, d\mathbf{x}$ describe the gain and loss due to pumping and decay, and $J_{jk} = - \int \phi_l^*(\mathbf{x}) \left[-(1/2m)\nabla^2 + V(\mathbf{x}) \right] \phi_k(\mathbf{x}) d\mathbf{x}$.
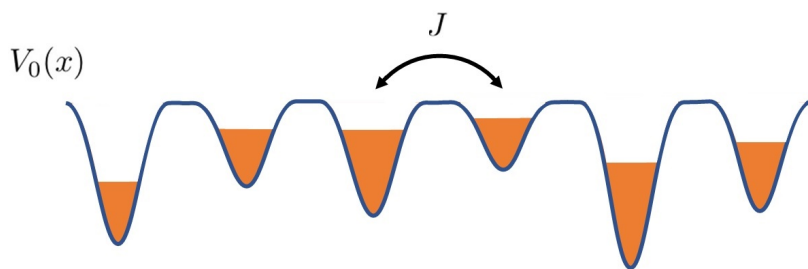
Figure 3.1: A schematic of a 1D chain of polariton condensates. Polaritons condense in the minima of the periodic potential generated by the pump. Tunneling between sites enables neighbouring condensates with different energies to synchronize their frequencies.

The physical system that we have in mind is the experimental realization of a lattice of polariton condensates described in [57]. In this experiment, the potential wells are created by a spatially-patterned pump laser. A regular grid of sites on the sample are pumped, each with the same intensity, creating reservoirs of hot excitons. These excitons relax to form condensed polaritons, which are repelled by the excitons still in the reservoirs. The polariton condensates form in the areas between pump spots. Due to the regularity of the pump profile, we may consider uniformity of the parameters, $U_j = U$, $g_j = g$, $\Gamma_j = \Gamma$ and $J_{jk} = J$ across the lattice. Due to disorder in the sample, ϵ_j varies from site to site, however this variation is small relative to the depth of the wells, so its impact on the other parameters in the model is negligible. The impact of spatio-temporal disorder arising from the pumping, which is smaller still, is not considered here, and will be discussed in Chapter 5. To account for disorder in well depths, we take the ϵ_j to be randomly distributed

with standard deviation σ. The magnitude of the standard deviation then characterizes the disorder strength.

Reparameterizing Eq. (3.2) as before in terms of the density and phase at each site yields N pairs of coupled equations of the form (2.7, 2.8):

$$\frac{\dot{n}_j}{2n_j} = g - \Gamma n_j + J \sum_{<k>} \sqrt{\frac{n_k}{n_j}} \sin(\theta_k - \theta_j) \qquad (3.3)$$

$$\dot{\theta}_j = \epsilon_j + U n_j - J \sum_{<k>} \sqrt{\frac{n_k}{n_j}} \cos(\theta_k - \theta_j). \qquad (3.4)$$

We take the same approach as in the previous chapter to simplify these expressions. One sees from Eq. (3.3) that in the absence of tunnelling, the first two terms imply that the occupation of each site relaxes to the steady-state density g/Γ with rate $2g$. Once again, we are interested in the dynamics of the system far above threshold, where this is the fastest timescale in the system. In this case, we may adiabatically eliminate the densities on each site by setting $\dot{n}_j = 0$. Furthermore, as each site is pumped far above threshold with the same strength, we may assume that the variation in densities between sites is relatively small, so that $\delta n_{jk} \equiv n_k - n_j \ll n_j$. We may therefore also set the square root factors to unity.

It is then straightforward to solve (3.3) for $\dot{n}_j$, which we substitute into (3.4) to obtain a dynamical equation for the phase at each site:

$$\frac{\partial \theta_j}{\partial t} = \epsilon_j + \frac{g}{\alpha} + J \sum_{<k>} \left[\frac{1}{\alpha} \sin(\theta_k - \theta_j) - \cos(\theta_k - \theta_j) \right]. \qquad (3.5)$$

Here, we have introduced the dimensionless parameter $\alpha \equiv \Gamma/U$. This ratio of the two nonlinearities that appear in the eGPE may be interpreted as a nonequilibrium control parameter: it is zero in an equilibrium condensate [55].

We may verify that this equation captures the behaviour of the phase dynamics of the eGPE by comparing frequency profiles obtained by solving this model and the full eGPE (reparameterized as Eqs. (3.3) and (3.4)). These are plotted in Fig. 3.2, with values of parameters consistent with the ranges determined in Section 2.5.2. The good agreement between the results obtained using both methods demonstrate the validity of the assumptions taken in simplifying (3.3) and (3.4) in an experimentally accessible parameter regime.
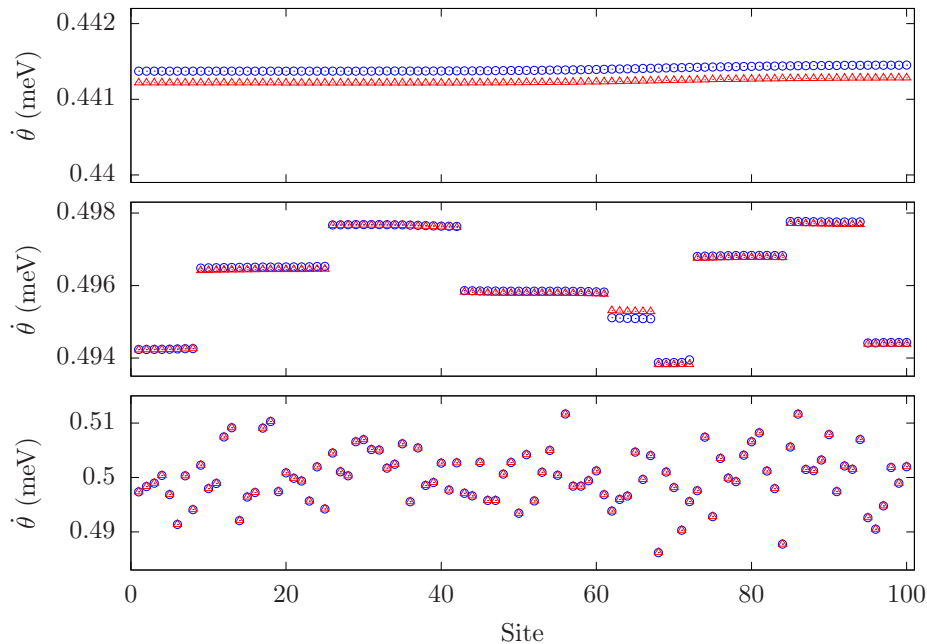
Figure 3.2: Average frequencies of a chain of 100 condensates, calculated by solving the reparameterized eGPE given by Eqs. (3.3) & (3.4) (red triangles), and the phase-only model given by Eq. (3.5) (blue circles). The same choice of random energies ϵ_j, distributed with $\sigma = 50\ \mu\text{eV}$ was used for each simulation. The values of the tunnelling matrix element were varied from plot to plot and were (from top to bottom): $J = 0.03$ meV, $J = 25\ \mu\text{eV}$, $J = 0.1\ \mu\text{eV}$. The values of the other parameters used were $g = 50\ \mu\text{eV}$, $U = 50\ \mu\text{eV}$, $\Gamma = 10\ \mu\text{eV}$. Averages were taken over 6 ns.

Eq. (3.5) is an equation which describes the phase dynamics of a system of coupled self-sustained oscillators. In the absence of tunnelling, each condensate has a frequency set by the energy of the potential well, ϵ_j, blueshifted by the interaction energy. As a result of our adiabatic elimination of the on-site occupations, this blueshift g/α is uniform across the lattice. We may therefore simplify the appearance of (3.5) by redefining the zero of our frequency scale to absorb this term into the ϵ_j. We are free to shift the scale of our energies in this way by transforming to a rotating frame in the context of oscillators. We may then visualize each condensate as a mechanical oscillator that is set to rotate at this natural frequency. However, when J is non-zero, the oscillators are coupled through the trigonometric terms, so there is a contribution to the frequency of oscillation on a given site from the

motion of the neighbouring oscillators. Physically, this occurs through an exchange of particles as the condensates tunnel through the potential barriers. In our analogy of mechanical oscillators, such as clocks, physically connecting neighbouring oscillators facilitates the coupling of their motions through exchange of phonons. This coupling enables synchronization of oscillators that initially have a range of different frequencies.

We know that for two oscillators, (3.5) has a synchronized solution for $J/\alpha > |\epsilon_1 - \epsilon_2|$, because upon setting $N = 2$ and subtracting the two equations, we have Eq. (2.19), which we derived and solved for the double well. Indeed, one can see from the numerical simulations of (3.5) in Fig. 3.2 that a 1D chain of 100 coupled oscillators may have full frequency synchronization, partial synchronization or complete desynchronization, depending on the strength of the coupling. One might again expect synchronization to depend on the other parameters in the model in a similar manner to the case of two sites. Characterizing synchronized and desynchronized states is more complicated when a large number of oscillators are involved, however. Keeping track of the natural frequency of each oscillator is no longer practical, or even possible in many cases. Instead, we treat the ϵ_j as random variables, and determine the probability of synchronization as a function of their standard deviation, σ. In fact, we can exploit the freedom of parameters in our model by dividing (3.5) by σ, and choosing $1/\sigma$ as our unit of time. This simplifies our analysis, as the model is now dimensionless, and only contains two parameters, α and J/σ.

We must consider the possibility that the number of sites and dimensionality may also impact synchronization. Our goal is to determine if any type of synchronization occurs in the thermodynamic limit ($N \to \infty, t \to \infty$), and if so, to characterize the various phases that exist in terms of the parameters in our model. At this point it is instructive to review previous work on lattices of coupled oscillators, and to compare and contrast our model with the locally-coupled Kuramoto model, which is discussed in Section 1.6.3 in the introduction.

3.3 Probability of synchronization in a chain of condensates

The similarities between our model (3.5) and the locally-coupled Kuramoto model (1.26) are clear. They only differ by the cosine term that appears in the coupling function in (3.5). The inclusion of the cosine term has the effect of making our coupling function non-odd in its arguments, and it has been suggested that this may bring about synchronization more readily than through purely odd coupling, as is the case in the Kuramoto model [72,75,76]. We see that in the limit of very small α, our model approaches the Kuramoto model, as the sine term in the coupling function dominates, and the cosine term becomes negligible. We therefore expect to see the behaviour predicted by (1.27) for finite lattices if we choose a very small value of α.
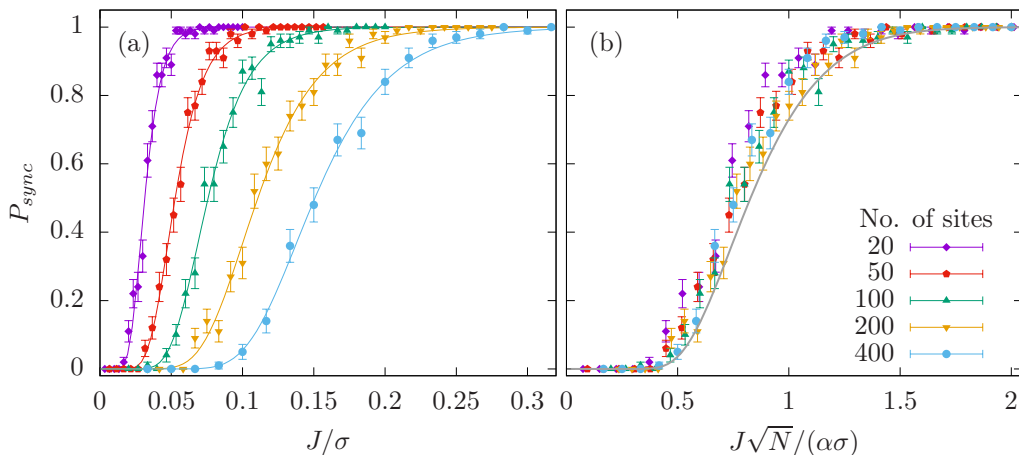
Figure 3.3: Probability of synchronization of chains of condensates of varying lengths, determined by solving Eq. (3.5) with $\alpha = 0.01$. Each probability is estimated from 100 disorder realizations, each simulated up to a time $t\sigma = 1.8 \times 10^4$. The curves in (a) are fits to the Gumbel distribution. The data plotted in each graph is the same, however in (b), each set of probabilities are plotted as a function of the coupling strength scaled by the length of the chain. The curve in (b) is the Kolmogorov-Smirnov distribution, approximated by the first 100 terms in the sum (1.27).

This is illustrated in Figure 3.3, where we plot the probability of synchronization of chains of oscillators of various lengths with normally-distributed

random on-site energies as a function of the dimensionless coupling, J/σ, with $\alpha = 0.01$. We see in Fig. 3.3(a) that for each chain length, P_{sync} increases smoothly from zero and approaches a value of one. The range of J over which this occurs is shifted progressively higher for longer chains, however. We verify that this behaviour is consistent with the Kuramoto model in Fig. 3.3(b) by re-plotting the same data, but with the x-axis now scaled by $\sqrt{N}$. The data then all collapses onto the Kolmogorov-Smirnov distribution (1.27), indicating that the results are equivalent to those of a Kuramoto model with coupling strength J/α. The unscaled data in plot (a) are fitted to Gumbel cumulative distribution functions, $\exp\{(-\exp\{(-(x-\mu)/\beta)\})\}$ with shape parameters μ and β. This has a similar form to the Kolmogorov-Smirnov distribution.

To determine the probability of synchronization across the chain for a given coupling strength, $P_{sync}(J)$, we first solve the set of coupled equations (3.5) numerically to obtain a frequency for each condensate. We employ closed boundary conditions, such that the 1st and Nth oscillators in each chain are only coupled to one neighbour. Rather than considering instantaneous frequencies, we calculate an average frequency by solving for the phase at two times, $\theta_j(t_i)$ a short time after the initial transient behaviour has decayed, and $\theta_j(t_f)$ some time later. This average frequency is then

$$\Omega_j = \frac{\theta_j(t_f) - \theta_j(t_i)}{T},\tag{3.6}$$

where $T = t_f - t_i$. We consider two neighbouring sites to be synchronized if the difference in their average frequencies is less than the smallest numerically resolvable frequency, π/T. The chain is then globally synchronized if all pairs of neighbouring sites are entrained in this way. This routine is then repeated for 100 random disorder realizations, and $P_{sync}(J)$ is estimated from the fraction of realizations that return a synchronized result. The error bars on the plots give the statistical error of this probability. A suitable value of T over which to calculate the average frequency was determined by following this routine to calculate $P_{sync}(J)$ using the same set of disorder realizations and steadily increasing T until the results converged.

The general synchronization behaviour of our model (3.5) is seen when α is large enough for us to see the contribution of the cosine term. This is
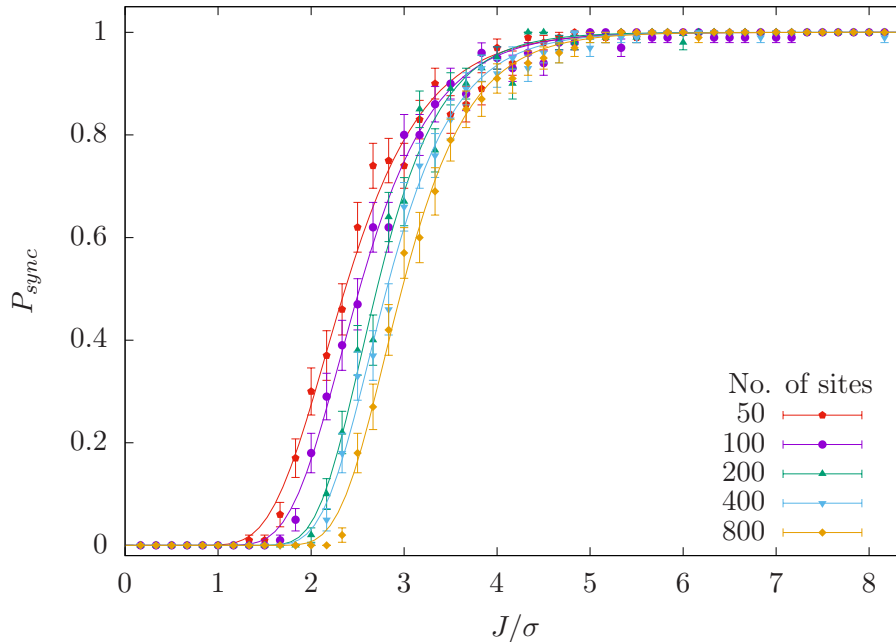
Figure 3.4: Probability of synchronization of chains of condensates of varying lengths, determined by solving Eq. (3.5) with $\alpha = 1$. As in the previous figure, each probability is estimated from 100 disorder realizations, simulated up to a time $t\sigma = 1.8 \times 10^4$, and the curves are fits to the Gumbel distribution.

generally the case for polariton condensates, where α is typically in the range $0.1-1$, as discussed in Section 2.4. We plot the probability of synchronization of chains of various lengths again in Fig. 3.4, but this time with $\alpha = 1$. P_{sync} again increases smoothly with J/σ from zero towards a value of one for each length. In contrast to the results in the small-α limit however, the position and width of these curves is almost independent of system size. The $\sqrt{N}$ scaling of the data seen in Fig. 3.3 – the signature of the 1D local Kuramoto model – is certainly absent.

The fact that the typical coupling strength at which a chain of oscillators described by (3.5) synchronizes is largely independent of system size suggests that there is a synchronization transition in the limit of thermodynamically large systems. We note that while the transition from desynchronized behaviour to synchronization in these figures is smooth and occurs gradually over a range of coupling strengths, for a single realization of disorder, the transition is a sharp one. This sharp transition occurs at slightly different

coupling strengths for different realizations, giving rise to the shape of the curves we see in Fig. 3.4. The fact that the P_{sync} follows a Gumbel distribution suggests that synchronization of an individual realization is related to an extreme value in the random natural frequencies. The reason for this will become clear in the following sections.

3.4 Continuum approximation

Further insight into the synchronization transition in our coupled oscillator model may be obtained by considering the continuum approximation of the equations (3.5) when they describe a synchronized state. To do this, we expand the trigonometric functions to second order in the phase difference [12, 107, 108]. Writing (3.5) in 1D, we have

$$\frac{\partial \theta_j}{\partial t} = \epsilon_j + \frac{J}{\alpha} \left\{ \sin(\theta_{j+1} - \theta_j) + \sin(\theta_{j-1} - \theta_j) \right\}$$
$$- J \left\{ \cos(\theta_{j+1} - \theta_j) + \cos(\theta_{j-1} - \theta_j) \right\} \quad (3.7)$$

$$\simeq \epsilon_j + \frac{Ja^2}{\alpha} \left(\frac{\theta_{j+1} + \theta_{j-1} - 2\theta_j}{a^2} \right)$$
$$- 2J + Ja^2 \left(\frac{(\theta_{j+1} - \theta_j)^2}{2a^2} + \frac{(\theta_{j-1} - \theta_j)^2}{2a^2} \right), \quad (3.8)$$

where in the second line, as well as making a Taylor expansion, we have multiplied and divided by the lattice constant, a^2. The continuum limit is valid when the phase varies slowly across the lattice. Then, the phase differences between each pair of sites are small. In this case, the terms in brackets containing the phases on different sites converge to the second derivative and first derivative squared of the phase. This is also the case in higher-dimensional lattices, where the sine and cosine terms become a Laplacian and the square of the gradient respectively in the continuum limit. We also choose the lattice constant as our new unit of length, and set $a = 1$ in our equations henceforth. We then have

$$\frac{\partial \theta(\mathbf{x}, t)}{\partial t} = \epsilon(\mathbf{x}) + \frac{J}{\alpha} \nabla^2 \theta + J (\nabla \theta)^2, \quad (3.9)$$

where $\epsilon(\mathbf{x})$ is a random function that is uncorrelated beyond the scale of the lattice constant, such that it has correlations

$$\langle \epsilon(\mathbf{x}) \epsilon(\mathbf{x}') \rangle = \sigma^2 \delta_a(\mathbf{x} - \mathbf{x}'). \quad (3.10)$$

A uniform energy shift $g/\alpha - 2Jd$ has been absorbed in the definition of $\epsilon(\mathbf{x})$, d being the dimensionality of the system. For ease of analysis however, we may consider $\epsilon(\mathbf{x})$ to have zero mean and unit variance, by resetting the zero of our energy scale through a transformation to a rotating frame, and choosing the dimensionless timescale outlined above, $t' = \sigma t$.

This continuum approximation is only valid for oscillators whose frequencies are synchronized. The sine and cosine functions are only well-approximated by a Taylor expansion when their arguments are small. If neighbouring phases are not locked to one another, their difference will grow in time, and the continuum description will not be accurate. To be precise, the phase differences must be $\mathcal{O}(a)$ in order to justify the convergence of the derivatives, and the exclusion of higher order terms from the expansions [12]. We also note that the result in (3.9) is not unique to our model. A continuum equation of this form may be derived for any model of locally coupled oscillators of the form $\dot{\theta}_k = \omega_k + \sum_{<l>} q(\theta_l - \theta_k)$, where $q(x)$ is a generic coupling function that is neither purely even nor odd. Therefore, the results derived in this chapter are relevant to a general class of coupled oscillator models.

We may gain insight into the synchronized and desynchronized phases of our model by performing a self-consistency check on the continuum approximation. The sine and cosine terms in the lattice model become $\nabla^2\theta$ and $(\nabla\theta)^2$ in this approximation. As the trigonometric functions are both bounded to have range between 1 and -1, the same must be the case for the gradient terms in order for (3.9) to accurately capture the behaviour on the lattice. This condition follows from the compactness of the phase, $\theta(\mathbf{x}, t)$, and it places a strict limit on the scale of its spatial variations. Therefore, we may analyse the solutions of (3.9) and apply this constraint to determine the parameter regimes that correspond to synchronized and desynchronized states.

Eq. (3.9) has a similar form to the Kardar-Parisi-Zhang (KPZ) equation [100,105]. As outlined in the introduction to this chapter, this stochastic differential equation has been shown to describe a wide range of nonlinear systems that experience noise or dissipation. Our model is not exactly equivalent to this, however. The difference between Eq. (3.9) and the KPZ equation

is that the random term in our model, $\epsilon(\mathbf{x})$, only has a spatial dependence, whereas the corresponding KPZ noise term is random in space and time. Of course, in the same way as we have arrived at (3.9), the KPZ equation may be derived from the eGPE describing a nonequilibrium condensate without spatial disorder, but including a space-time noise term arising from the gain and loss. Indeed, this connection between the complex Ginzburg-Landau equation and the KPZ equation has been made before in the context of polariton condensates [65, 66, 109, 110], and we will review this further when we discuss the impact of noise on our model in Chapter 5.

Although our consideration of purely spatial disorder leads to different universal behaviour, we may be guided by the KPZ equation when interpreting the behaviour of our continuous model. The phase, $\theta(x, t)$, behaves like the height of an interface, with a growth rate $\epsilon(\mathbf{x})$ which is random in space but not in time. The behaviour of the solutions to (3.9) may be understood by applying a Cole-Hopf transformation

$$Z(\mathbf{x}, t) = \exp(\alpha\theta), \tag{3.11}$$

enabling us to rewrite Eq. (3.9) in a linear form, at the cost of introducing a multiplicative disorder term:

$$\frac{\partial Z(\mathbf{x}, t)}{\partial t} = \frac{J}{\alpha}\nabla^2 Z + \alpha\epsilon(\mathbf{x})Z. \tag{3.12}$$

Equations of this form describe the evolution of a population with diffusion and random autocatalytic amplification [101, 102], as well as the partition function for a directed polymer in a random potential [103, 104]. To solve it, we recognize that it also takes the form of an imaginary-time Schrödinger equation for a particle of mass $\alpha/2J$ in a random potential $V(\mathbf{x}) = -\alpha\epsilon(\mathbf{x})$. The general solution of (3.12) can then be expressed as the linear combination of states,

$$Z(\mathbf{x}, t) = \sum_n c_n\varphi_n(\mathbf{x})e^{-E_n t}, \tag{3.13}$$

where $\varphi_n(\mathbf{x})$ are the eigenstates of an effective Hamiltonian $\hat{H} = -(J/\alpha)\nabla^2 - \alpha\epsilon(\mathbf{x})$, with corresponding energies E_n. Unlike the solutions to the Schrödinger equation in real time, each of the terms in the sum in (3.13) decays, with

rate E_n. The result of this is that $Z(\mathbf{x}, t)$ approaches the ground state wavefunction of the potential $V(\mathbf{x})$ for $t \to \infty$. For long but finite times, $Z(\mathbf{x}, t)$ will have contributions from a small number of low-energy states.

In dimensions $d < 4$, these low-lying states will be exponentially localized, about some dilute positions $\mathbf{x}_n$, with localization length ζ [102, 108, 111]:

$$\varphi_n \sim e^{-|\mathbf{x} - \mathbf{x}_n|/\zeta}. \tag{3.14}$$

We may calculate the localization length by considering how the terms in the Hamiltonian scale with the size of the wavefunction [112]. The kinetic term scales with ζ as $(J/\alpha)\zeta^{-2}$, while the potential term scales as $(\alpha\sigma)\zeta^{-d/2}$. The former scaling relation is evident from the Laplacian in the kinetic term, while the latter follows from the average value of a random function over a region of size ζ. Equating these two terms, we have the relation

$$\frac{J}{\alpha\zeta^2} \sim \frac{\alpha\sigma}{\zeta^{d/2}}, \tag{3.15}$$

which we may manipulate to find

$$\zeta \sim \left(\frac{J}{\alpha^2\sigma}\right)^{2/(4-d)}. \tag{3.16}$$

In Figs. 3.5 and 3.6 we plot some phase and frequency profiles obtained by solving the discrete coupled oscillator model (3.5) at various times. These solutions agree qualitatively with those of the continuum model, given by Eqs. (3.11) and (3.13). We include plots for both one and two dimensions because although our analysis above is valid for all $d < 4$, these are the relevant dimensionalities for polaritonic systems. In both cases, multiple peaks are evident in the phase profile at short times, each of which corresponds to a localized, low-energy state of the Hamiltonian $\hat{H}$. The corresponding energies appear as plateaus in the frequency profile. The low-lying states have negative energies, and so they grow in magnitude, corresponding to a steadily increasing phase in the region controlled by each localization centre. The ground state, with the lowest energy, grows fastest, and eventually dominates the sum in (3.13), giving a solution with a single peak in the phase profile, and a single frequency (corresponding to the ground state energy of
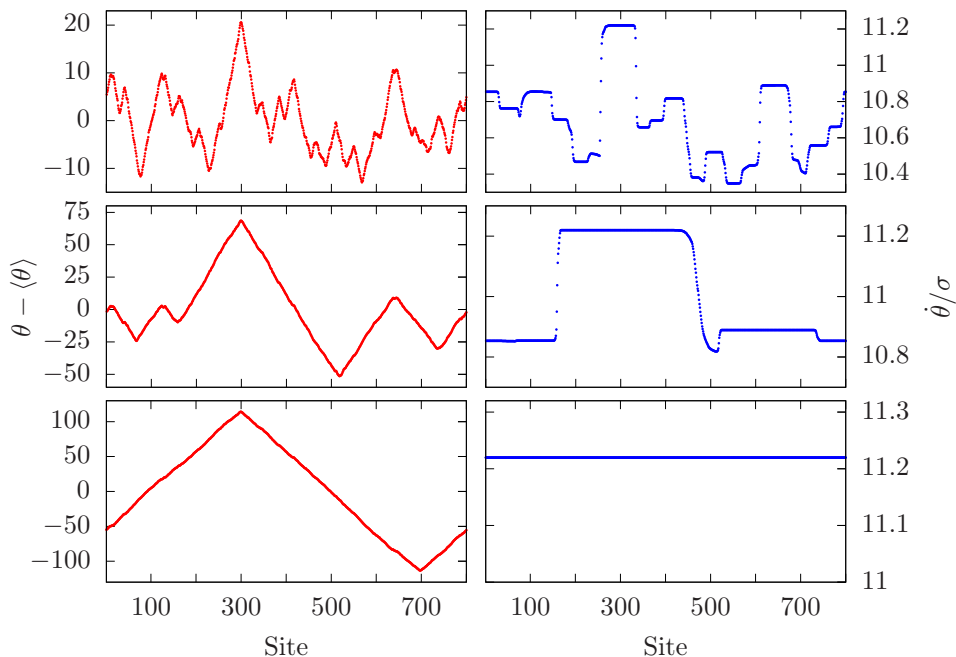
Figure 3.5: Phase (left column) and frequency (right column) profiles in a chain of 800 coupled oscillators, obtained by solving (3.5) with $J/\sigma = 3.33$ and $\alpha = 1$. The oscillators initially have a uniform phase, and periodic boundary conditions are employed. The profiles are shown after times $t\sigma = 100$ (top row), 600 (middle row), and 24000 (bottom row).

$\hat{H}$). We only see synchronization across the lattice of oscillators after enough time has passed for all but the ground state term in (3.13) to 'die off'. The phase profile of a synchronized state is then given, from (3.11), (3.13) and (3.14) by

$$\theta(\mathbf{x}, t) = \frac{1}{\alpha} \ln Z(\mathbf{x}, t)$$
$$\simeq C - \frac{1}{\alpha} \left(\frac{|\mathbf{x} - \mathbf{x}_0|}{\zeta} + E_0 t \right), \tag{3.17}$$

where C is a constant term that may be subtracted off, as the zero of the phase scale is arbitrary. We have used this phase symmetry when plotting the phase profiles in Figs. 3.5 & 3.6, where we subtracted off the average phase at each time. Of course, unlike the height of a surface described by a KPZ-like interface model such as (3.9), the phase variable is defined modulo 2π. We plot our phase profiles over a range that is much larger than this to illustrate the insights that may be gained from the behaviour of the interface model.
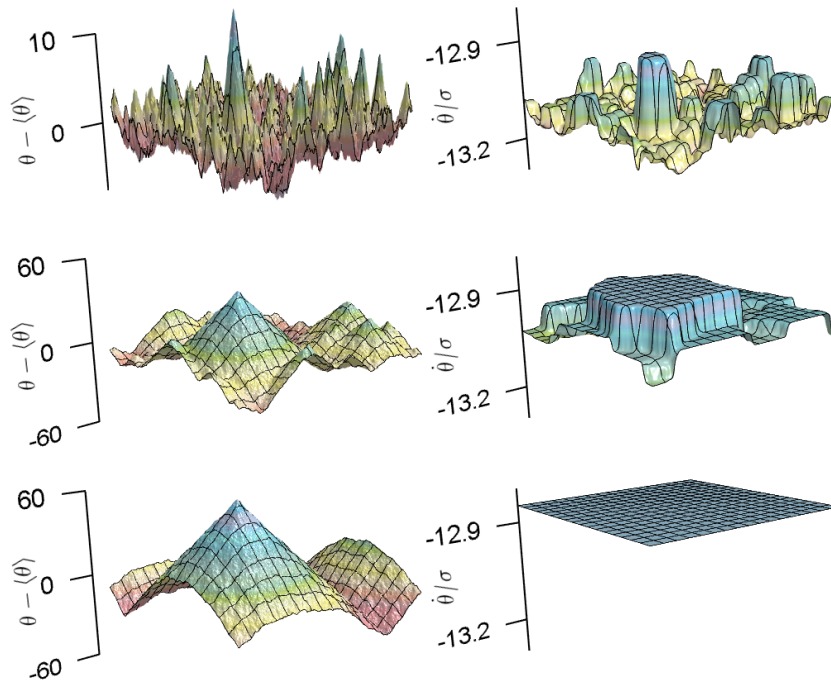
Figure 3.6: Phase (left column) and frequency (right column) profiles in a two dimensional lattice of 512×512 coupled oscillators, obtained by solving (3.5) with $J/\sigma = 3.33$ and $\alpha = 1$. The oscillators initially have a uniform phase, and periodic boundary conditions are employed. The profiles are shown after times $t\sigma = 50$ (top row), 300 (middle row), and 1700 (bottom row).

To fully capture the periodicity of the phase, one may imagine wrapping the plots around a cylinder of unit radius, although the practicality and functionality of such a visualization are debatable.

The discrepancy between the sign of the frequencies in one and two dimensions arises from the fact that for the 2D plots, the g/α term in (3.5) was removed through a transformation to a rotating frame, while this was not done for the 1D simulations. Thus, the phases in 1D behave like a surface with average growth rate $(g/\alpha - 2Jd)/\sigma = 16.67 - 6.67 = 10$, while the corresponding average growth rate in 2D is $-2Jd/\sigma = -13.3$. In both figures, the frequencies synchronize to a value that is slightly higher than these averages, which is to be expected, as from Eq. (3.17), the synchronization frequency is related to the ground state energy by

$$\dot{\theta} = -\frac{E_0}{\alpha}, \qquad (3.18)$$

with E_0 the energy of the state localized in the deepest potential well.

Periodic boundary conditions were used when solving (3.5) to obtain the phase and frequency profiles in Figs. 3.5 and 3.6, to approximate an infinite system.

3.5 Phase diagram

Following the above analysis, we can now derive the scaling form of the phase boundary between synchronized and desynchronized states in the phase oscillator model (3.5). As mentioned in the previous section, the continuum version of this model has a 'speed limit' beyond which it is no longer consistent in approximating the behaviour of a lattice of oscillators. This limit is

$$|\nabla\theta| \lesssim 1. \tag{3.19}$$

From (3.17), we have

$$|\nabla\theta| = \frac{1}{\alpha\zeta} = \left[\alpha^d \left(\frac{\sigma}{J}\right)^2\right]^{1/(4-d)}, \tag{3.20}$$

so applying the constraint (3.19) to this gives us the condition for synchronization

$$\frac{\sigma}{J}\alpha^{d/2} \lesssim 1. \tag{3.21}$$

This condition is relevant for $d < 4$, as localized solutions to Eq. (3.12) are not guaranteed otherwise. Lattices of polariton condensates may only be realized in one or two dimensions, however, so this theory suffices to describe these systems.

The above inequality is not a strict one, as we cannot say at which precise value of the phase gradient our continuum approximation will break down. We know however, from the numerical results of synchronization probabilities in 1D shown in Fig. 3.4, that attempting to derive a sharp threshold for synchronization of oscillators with random frequencies is, if not a fruitless task, then not a particularly worthwhile one. Tails on the distributions of the random natural frequencies mean that there is still a non-zero probability of a lattice being desynchronized for values of parameters that would correspond to synchronization in the vast majority of disorder realizations, and vice versa

63

in parameter regimes that tend towards synchronization. Furthermore, our analysis up to this point is not specific to a certain distribution of random frequencies, and an upper bound for synchronization may not be general to all distributions. What we do have is a description of how the phase
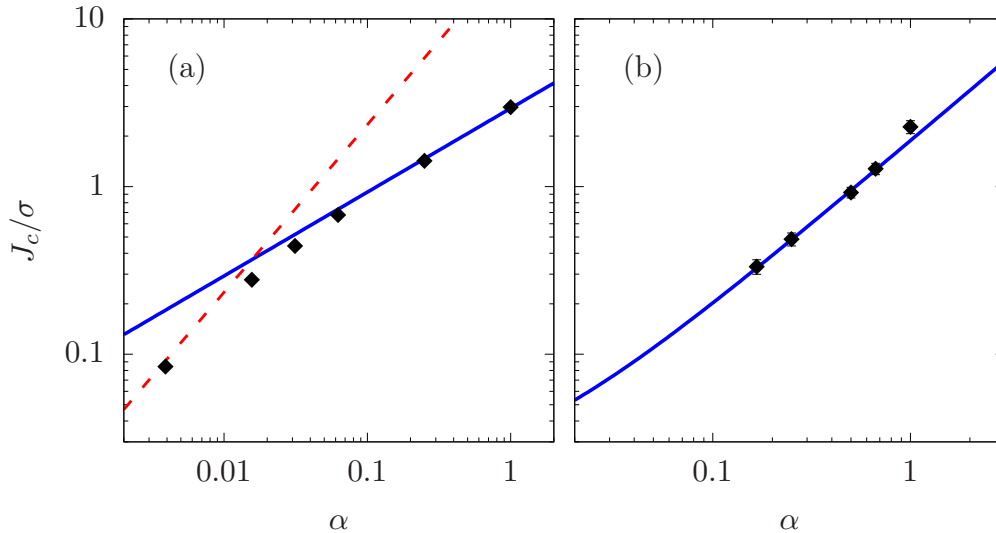
Figure 3.7: Phase boundary for synchronization for (a) a 1D chain of 800 oscillators, and (b) a 2D square lattice of 128×128 oscillators. J_c is defined as the value of J corresponding to a probability of synchronization of 0.5. The points are numerical values, computed as discussed in the text. The solid lines show fits to the predicted slopes of 0.5 (a) or 1 (b). The dashed line in (a) is the phase boundary for synchronization for a chain of 800 Kuramoto oscillators.

boundary between desynchronized and synchronized phases of our locally-coupled oscillator lattice scales with the parameters of the model in $d < 4$. We verify this scaling with numerical simulations in one and two dimensions in Fig. 3.7. We define the critical coupling strength J_c as the centre of the transition in the probability plots, such that $P_{sync}(J_c) = 0.5$. Our analysis implies this should scale as

$$J_c \sim \sigma \alpha^{d/2}. \tag{3.22}$$

This dependence of J_c on α is confirmed in Fig. 3.7. The data points are generated by simulating Eq. (3.5) for one hundred disorder realizations to obtain $P_{sync}(J)$, and fitting the resulting data to a Gumbel extreme-value

distribution, as we did for Fig. 3.4. We then use the fitted parameters to calculate J_c. This distribution is expected from the analysis above, because the probability that a given sample is synchronized is the probability that $\hat{H}$ has a ground-state localization length greater than a certain value or, equivalently, that the magnitude of its ground-state energy is less than a certain value. Since the ground-state energy is an extreme value – the lowest energy among the states – this quantity is the cumulative distribution function for an extreme-value distribution, and since the density of states in a band tail vanishes exponentially, it should be the Gumbel one.

The solid curves in Fig. 3.7 are then square-root (1D) and linear (2D) functions which are fitted to the data, to demonstrate the dependencies predicted in (3.22). On the 1D phase diagram, we also show the prediction of the local Kuramoto model (1.26) with coupling strength $K = J/(\alpha\sigma)$ for a chain of $N = 800$ sites. A critical coupling strength for this Kuramoto model is determined by numerically evaluating the sum in (1.27) to find $P_{sync} = 1/2$ when $K\sqrt{N} \simeq 0.83$. We then have $J_c^{kura}/\sigma = 0.83\sqrt{N}\alpha$. While this critical coupling – for our model without the cosine term – diverges for large N, for a small system it can nonetheless lie below Eq. (3.22) at small α. This explains the crossover seen at small α in Fig. 3.7(a), and also why the synchronization probabilities in Fig. 3.3 show scaling with $\sqrt{N}$. This is the standard finite-size behaviour if the cosine term is relevant in the renormalization group sense: such terms, even if they are small at the lattice scale, grow with distance, and control the physics in sufficiently large systems. In small systems, however, the growth can be cut off by the system size. If much larger chains were included in the small-α plots (Fig. 3.3), we would expect to see the positions of the curves saturate at a finite J/σ, as predicted by Eq. (3.22). As the leftmost data point on the 1D plot corresponds to a synchronization crossover at a coupling strength determined by the local Kuramoto model, it is not included in the fit to the line of slope 0.5.

Although our numerical results agree with Eq. (3.22) for $\alpha \lesssim 1$, they disagree in the opposite regime, where we find large sample-to-sample fluctuations and many states which are desynchronized even at large J. This may be related to dynamical instabilities in that regime [113, 114]. In any case, Eq. (3.16) holds only in the weak disorder regime where the localiza-

tion length ζ is larger than the lattice spacing $a = 1$, and the localization length at the transition is, from Eqs. (3.16) and (3.22), $\zeta_c \sim 1/\alpha$. More generally, $\zeta_c > 1$ is needed so that space can be treated as continuous, as in Eq. (3.9), at the phase boundary. Importantly, the existence of a synchronization transition in the continuum regime implies the phenomenon is universal, and independent of the details of the lattice or disorder. We note that a synchronization transition for one dimensional chains of oscillators with non-odd nearest-neighbour coupling was previously identified by Östborn [75]. That analysis, however, predicts a critical J_c which differs from Eq. (3.22), and does not agree well with our numerical results.

3.6 Discussion of results

3.6.1 Behaviour of localization length in the thermodynamic limit

Our expression for the ground-state localization length, Eq. (3.16), comes from a standard argument [102] equating the kinetic energy and the depth of a typical potential well, $\alpha\sigma/\zeta^{d/2}$. In principle one should use not the depth of a typical well, but that of the deepest of all the wells of size $\sim \zeta$ because the ground state wavefunction will generally be localized in the deepest potential well. In a system of size L, there are $\sim (L/\zeta)^d$ such wells. For a normal distribution of well depths, the typical well depth and that of the deepest well differ by a factor $\sqrt{d \ln (L/\zeta)}$, which seems to lead to the surprising conclusion that the localization length vanishes in the thermodynamic limit. This would mean, in our analysis, that J_c diverges in this limit, and there is ultimately no synchronization. However, one should bear in mind that physical systems are never infinite, although they may be very large. As was pointed out in the careful analysis of Ref. [102], this factor grows extremely slowly with $N = L^d$, and it is not large, even in a macroscopic system. For example, for $(L/\zeta)^d = N_A \sim 10^{23}$ we have $\sqrt{d \ln (L/\zeta)} \sim 7$. Thus, it does not prevent synchronization in the limit of a large physical system. Furthermore, this formal divergence arises from the assumption of an unbounded distribution of well depths, which does not occur in practice. If we consider the natural

frequencies at each site ϵ_j to have a bounded distribution, then this would imply a bound on a depth of the potential wells, and no divergence of J_c.

3.6.2 Time taken for synchronization

As outlined in Section 3.4, even when a collection of oscillators described by Eq. (3.5) has a synchronized solution, there is a transient time before which the onset of synchronization occurs. This corresponds to the timescale on which multiple low-energy states still contribute to the sum in the solution (3.13) to the imaginary-time Schrödinger equation for a particle in a random potential (3.12). This effect is clearly seen in Figures 3.5 and 3.6, where multiple frequencies are still observed for chains and lattices of oscillators up until $t\sigma \approx 500$, before synchronized solutions appear later.

The exact value of this transient time to synchronize depends on the particular random distribution of natural frequencies in an individual sample. For our numerical calculations of the probability of synchronization of a chain of oscillators, the range of time over which to perform the simulations was chosen by first solving for P_{sync} over steadily increasing time periods, until the results converged – i.e. it was clear that the transient time had been exceeded for each realisation we were considering. We concluded that $t\sigma = 1.8 \times 10^4$ was sufficiently long for the parameter regimes and system sizes under consideration. It was evident from observing the results of individual realisations, however, that some samples synchronized on timescales that were much smaller than this.

Considering the form of Eq. (3.13), one sees that the key parameter which determines the time taken for a sample to synchronize is the difference between the energies of the two lowest-lying states. We can estimate how the synchronization time scales with the parameters in our model by considering the situation where enough time has passed such that only the two lowest-lying states contribute to the sum in (3.13). The solution then has the form

$$Z(t) \approx C_0 e^{-E_0 t} + C_1 e^{-E_1 t}, \tag{3.23}$$

where all factors in the wavefunction that do not depend on time have been absorbed into the terms C_0 and C_1. Dividing across by the first (ground

state) term, we can see that the second term ($j = 1$ state) is negligible when

$$(E_1 - E_0)t \gg 1. \tag{3.24}$$

We may then say that the synchronization time scales as

$$t_{sync} \sim (E_1 - E_0)^{-1}. \tag{3.25}$$

It is possible to determine the scaling of this quantity using a similar procedure to the one employed to calculate the localisation length of these states. As before, we recognise that the depths of the potential wells will be normally distributed. The difference in magnitude of the depths of the two lowest wells is then known to be of order [102]

$$(E_1 - E_0) \sim \alpha\sigma\zeta^{-d/2}[d\ln(L/\zeta)]^{-1/2}. \tag{3.26}$$

For ease of calculations, we will once again neglect the logarithmic factor on the basis that it grows very slowly with system size. We may then substitute the expression (3.16) for the localization length in the above equation, and invert it to obtain the following scaling relation for the synchronization time:

$$t_{sync} \sim J^{d/(4-d)}\sigma^{-4/(4-d)}\alpha^{-(4+d)/(4-d)}. \tag{3.27}$$

Again, this expression is expected to be valid for dimensions $d < 4$. We must caution, however, that this result is a rough estimate. It has not been tested numerically, and some of our assumptions, such as completely neglecting the trigonometric terms, may not be justified in all cases. For example, our simplifications mean that the scaling in Eq. (3.27) does not have any dependence on system size. Previous numerical simulations to determine the probabilities of synchronization of chains of various lengths suggest, however, that systems with more sites take longer to synchronize, so a more detailed investigation into synchronization times may prove useful.

3.6.3   Comparison with continuum limit of Kuramoto model

It is interesting to compare our analysis and results with those for the nearest-neighbour Kuramoto model. One may expand the sine function in (1.26)

and take a continuum limit in the same way as we did to obtain Eq. (3.9). However, the absence of an even component to the coupling means that the nonlinear term is absent, and the continuum theory for Kuramoto oscillators is

$$\frac{\partial \theta(\mathbf{x}, t)}{\partial t} = \omega(\mathbf{x}) + K \nabla^2 \theta. \tag{3.28}$$

This equation describes a linear interface-growth model that is related to the Edwards-Wilkinson equation [107, 115] with static disorder, in the same way as Eq. (3.9) is related to the KPZ equation. It was shown in [76] that the phase-phase correlation functions for (3.28) diverge with the lattice size, for any fixed separation, when $d \leq 2$. This divergence is not consistent with the expansion of the trigonometric functions, so the assumed synchronized state does not occur.

Physical insight into the difference between this model and (3.9) can be obtained by considering the behaviour of the phase gradients. The phase gradients in a synchronized solution of the Kuramoto model can be obtained using an Imry-Ma [112] argument, similar to that previously outlined for the disordered polariton condensate in Ref. [55]. Integrating (3.28) over a region of space of linear dimension $\mathcal{L}$, we see that the first term on the right-hand side is a random walk, which scales with the size of the region as $\mathcal{L}^{d/2}$. It is related, in the polariton case, to the net random current generated in the region. This must balance the second term, which is related, by the divergence theorem, to the current flowing through the boundary. We see this second term is, at most, of order $|\nabla \theta| \mathcal{L}^{d-1}$. Comparing the two terms, we have that the phase gradients at the boundary of the region scale at least as fast as $|\nabla \theta| \sim \mathcal{L}^{(2-d)/2}$. This implies they diverge as $\sqrt{\mathcal{L}}$ in $d = 1$, which is consistent with the results from [77] described in Section 1.6.3. This scaling is also consistent with a logarithmic divergence in $d = 2$ [76]. This highlights the key difference between our model and the Kuramoto model. Synchronization is dependent on the phase gradients being bounded. The inclusion of the nonlinear term resulting from the cosine coupling in (3.5) has the result that the phase gradients in this model, given by (3.20), are independent of the size of the region considered. Thus, in that case, there can be solutions with $|\nabla \theta| \lesssim 1$ everywhere, and the synchronized state is self-consistent.

We note that these self-consistency arguments do not rule out complete synchronization for lattices of Kuramoto oscillators in three or more dimensions. However, Strogatz and Mirollo have shown that this does not occur in any finite dimension [77]. They also do not rule out the possibility of partially synchronized states, where a macroscopic number of oscillators entrain to a single frequency. Numerical studies suggest that this may occur for Kuramoto oscillators, but only in three or more dimensions [107].

3.6.4   Results in the context of polariton condensates.

We have shown how driven-dissipative condensates, initially localized with independent energies in the minima of a lattice potential, may synchronize their energies and behave as a single delocalized condensate with a well-defined energy. While experimental evidence had indicated that this crossover occurs in small systems [50, 57], we have demonstrated that there is a critical point at which a common energy is attained that is independent of the scale of the system. This point is identified in Eq. (3.22). In addition to frequency synchronization, this phase transition marks the onset of phase order across the condensate. We see from Figures 3.5 and 3.6 that the establishment of a single frequency across the lattice corresponds to a smooth phase profile with a single peak. This means that the phase correlation length is at least of order the system size – one of the signatures of condensation. We can thus say that we have shown that a driven-dissipative condensate in a static disorder potential may exhibit both phase and frequency order.

It is worth noting that the continuum model for a random lattice potential (3.9) may also be derived directly from the eGPE with a random potential. If one considers a single state, rather than many localized states in a lattice potential, Eq. (2.1) may be reparameterized by writing the order parameter in terms of a density and a phase through the Madelung transformation, $\Psi(\mathbf{x}, t) = \sqrt{n(\mathbf{x}, t)} \exp(-i\theta(\mathbf{x}, t))$. The resulting equation may then be separated into its real and imaginary parts, yielding equations for

the time dependence of the phase and density respectively,

$$\frac{\partial n}{\partial t} = \frac{1}{m}\left(n\nabla^2\theta + \nabla\theta\nabla n\right) + 2(gn - \Gamma n^2), \tag{3.29}$$

$$\frac{\partial \theta}{\partial t} = \frac{1}{2m}\left((\nabla\theta)^2 - \frac{1}{\sqrt{n}}\nabla^2(\sqrt{n})\right) + Un + V(\mathbf{x}). \tag{3.30}$$

If one then makes the assumption that the fluctuations in the density are small, so that it varies slowly in space, and rapidly relaxes to its steady state, we may neglect the spatial and temporal derivatives of n. Eq. (3.29) then becomes

$$n(\mathbf{x}, t) = \frac{g}{\Gamma} + \frac{1}{2m\Gamma}\nabla^2\theta. \tag{3.31}$$

Substituting this expression for the density in (3.30), we obtain,

$$\frac{\partial \theta}{\partial t} = \frac{1}{2m\alpha}\nabla^2\theta + \frac{1}{2m}\left(\nabla\theta\right)^2 + V(\mathbf{x}) + \frac{g}{\alpha}. \tag{3.32}$$

If the potential $V(\mathbf{x})$ seen by the condensate is a truly random δ-correlated function like the continuum version of the lattice potential $\epsilon(\mathbf{x})$, then this equation is equivalent to (3.9), where once again, the constant factor of g/α may be absorbed into the energy scale. (We can see from the definition of J on a lattice (2.34), that $J/a \approx 1/(2m)$ if we approximate the overlap integral as $\sim a$.) This manipulation of the CGLE is well-established, appearing in textbooks [12, 73], as well as contemporary papers investigating the coherence properties of driven-dissipative condensates with spatio-temporal noise [65, 66, 109].

The continuum limit of a synchronized lattice of driven-dissipative condensates therefore coincides with the description of a condensate in a random potential, so long as in both cases, spatial variations in density are small. This may be achieved through strong, uniform pumping of the system. In the case when the continuum phase model is describing a lattice of condensates, we have shown that there is a bound on the spatial variation of the phase in the continuum model. As the currents in the lattice – represented by gradient terms in (3.9) – are sine functions, they must be of order 1 or less (when the unit of length is taken to be the lattice constant). When the gradients exceed this, the lattice may no longer be described by this continuum model, and the condensate splits into regions with different energies.

This localization of a condensate does not require a lattice, however. It may occur in the minima of a random potential. Therefore, we expect a threshold disorder strength to exist above which the model (3.32) breaks down. We may gain insight into how this happens by considering the fact that the phase of the condensate order parameter is a compact variable. Solutions to (3.32) must be invariant under transformations $\theta(\mathbf{x}, t) \to \theta(\mathbf{x}, t) + 2\pi m(\mathbf{x}, t)$, where $m(\mathbf{x}, t)$ is an integer-valued function. As pointed out in the supplemental material to [113], this additional symmetry leads to cases where either the spatial or temporal derivative of the phase may not exist. This occurs when the phase varies rapidly in space and time, which can cause phase slips of magnitude 2π to appear, which may be interpreted as space-time vortices in one dimension. Such vortices are defined analogously to quantized spatial vortices in superfluids [116]. They correspond to the line integral of the gradient of the phase around a closed loop in space-time taking the non-zero value of $\pm 2\pi$. The relevant physics may then be captured by a discrete model, such as that which we derived from a lattice potential (3.5).

While it is tempting to claim that our lattice model and its continuum approximation describe how a spatially random potential causes a single driven-dissipative condensate to fracture and become localized, a full analysis of this, including the role played by vortices, would require us to consider density fluctuations. To do so, the system should be modelled by the full extended Gross-Pitaevskii equation (2.1). Despite this, the phase model does demonstrate the existence of both spatially extended and localized regimes for a condensate in a random potential, corresponding to the synchronized and desynchronized solutions to the lattice equations.

3.7 Conclusions

We have shown that a model for coupled phase oscillators, which describes a disordered lattice of polariton condensates, has a synchronized state that survives in the limit of a macroscopic number of oscillators. At the critical coupling strength, given by Eq. (3.22), tunnelling between condensates overcomes the localizing effects of the random potential, leading to a state

with a single frequency, and a stable phase profile. We have thus identified a nonequilibrium phase transition that may be observed in lattices of driven-dissipative condensates. This transition, and the existence of a synchronized state in a large lattice may be important for applications of polariton condensation in areas such as analogue simulation.

The synchronized state we find is not expected for Kuramoto oscillators on a finite-dimensional lattice with nearest-neighbour couplings [76, 77, 107]. It arises from the non-odd coupling between the phases, which gives a relevant nonlinear term in the continuum limit. That same form will appear for any system of coupled oscillators in which the coupling function is neither purely even nor odd. That will generally be the case, so that our work implies that other coupled oscillator systems can support synchronized states, notwithstanding disorder in their frequencies.

Chapter 4

Superfluid response of a disordered chain of driven-dissipative condensates

4.1 Introduction

Having determined in the previous chapter that lattices of disordered driven-dissipative condensates may exhibit phase and frequency order, and behave as a single delocalized condensate, in this chapter we address the question of whether such a delocalized condensate on a disordered lattice is a superfluid. This is in part motivated by the parallels between the nonequilibrium synchronization transition and the Bose glass-superfluid transition that occurs in equilibrium bosonic systems [53]. Superfluidity is perhaps the most spectacular phenomenon associated with Bose-Einstein condensation, although a superfluid is not necessarily a BEC, and vice versa [117]. Polariton condensates have been observed to exhibit superfluid behaviour, such as dissipation-less flow [28, 118]. A perturbative analysis has shown, however, that spatial disorder inhibits superfluidity in nonequilibrium condensates [55]. The superfluid response of a disordered driven-dissipative condensate is found to decay exponentially with system size, and thus vanishes in the thermodynamic limit.

Our lattice model of the phase dynamics of driven-dissipative condensates provides a non-perturbative framework to test this claim. We reproduce the

analysis of [55] by calculating the superfluid stiffness, or the energy response of our system to the application of a phase twist across the boundaries of a region. Numerical simulations of our model confirm the previously reported findings. In the absence of disorder, we find a finite superfluid stiffness in line with analytic predictions, however once random on-site energies are introduced, this disappears. We discuss these results in the context of the connection between the phase dynamics of a driven-dissipative condensate and the localized eigenstates of the Hamiltonian of a particle in a random potential that was outlined in the previous chapter. This description provides a framework to understand why a superfluid response is not present for a condensate in a random potential.

4.2 Definition of superfluid stiffness

To investigate if a driven-dissipative condensate is a superfluid, we measure its superfluid stiffness. This is defined as the free energy response to a slow change in the phase, θ, of the condensate order parameter. This may be calculated by imposing a phase difference of φ between two ends of a region separated by distance L. The phase must vary somehow along this region, and it will have an average gradient given by

$$\langle \nabla \theta \rangle = \frac{\varphi}{L}. \tag{4.1}$$

Using this, one may calculate the free energy cost of this phase twist. It is given by

$$\Delta F = f_s \left(\frac{\varphi}{L} \right)^2 V, \tag{4.2}$$

where the coefficient f_s is known as the superfluid stiffness, or helicity modulus of the system [119], and V is its volume.

This quantity is related to superfluidity because the gradient of the condensate order parameter is proportional to the current velocity in the condensate. One may see this by considering the extended Gross-Pitaevskii equation:

$$i\hbar \frac{\partial \Psi}{\partial t} = \left(-\frac{\hbar^2}{2m} \nabla^2 + V(\mathbf{r}) + U|\Psi|^2 \right) \Psi + i \left(g - \Gamma|\Psi|^2 \right) \Psi. \tag{4.3}$$

As the density of the condensate is given by

$$n(\mathbf{r}, t) = |\Psi(\mathbf{r}, t)|^2 = \Psi^* \Psi, \tag{4.4}$$

we may obtain the dynamics for the density by multiplying the eGPE on the left by Ψ^* and subtracting the complex conjugate. The resulting expression then has the form of a continuity equation,

$$\frac{\partial n}{\partial t} + \nabla \cdot \mathbf{j} = 2(gn - \Gamma n^2), \tag{4.5}$$

where the terms on the right-hand side are sources and sinks resulting from pumping and decay of the condensate. These cancel in the steady state when the density is $n_0 = g/\Gamma$. The quantity

$$\mathbf{j}(\mathbf{r}, t) = -\frac{i\hbar}{2m} \left(\Psi^* \nabla \Psi - \Psi \nabla \Psi^* \right) \tag{4.6}$$

is the standard expression for a quantum current density [18]. This may be simplified by substituting the explicit form of the wavefunction, $\Psi(\mathbf{r}, t) = \sqrt{n(\mathbf{r}, t)} \exp(-i\theta)$. This yields

$$\mathbf{j} = -\frac{n\hbar}{m} \nabla \theta, \tag{4.7}$$

and so the condensate velocity is

$$v = -\frac{\hbar}{m} \nabla \theta. \tag{4.8}$$

This quantity is irrotational – it has zero curl – which is characteristic of a superfluid.

Imposing a steady phase twist of φ across a superfluid thus has the effect of adding an additional boost to its velocity of $v_s = (\hbar/m)\nabla\varphi$. This raises the kinetic energy of the system by

$$\Delta E = \frac{1}{2}\rho_s v_s^2 V, \tag{4.9}$$

where V is the volume of the gas, and ρ_s is the superfluid density. Comparing Eqs. (4.2) and (4.9) gives the relation

$$f_s = \frac{\rho_s}{2m} \tag{4.10}$$

between helicity modulus and superfluid density. Thus, 'twisting' the phase of the order parameter of a system by imposing a phase difference across the boundaries is equivalent to driving a supercurrent through the system. If the system is a superfluid, the supercurrent will increase its free energy, as in (4.2). We can therefore determine if a system has a superfluid response by using Eq. (4.2) to calculate its stiffness.

4.3 Numerical results for a chain of condensates

4.3.1 Calculating the superfluid stiffness

As outlined in Section 3.6.4, the phase dynamics of a driven-dissipative condensate extended over a random potential are captured by the synchronized regime of the discrete oscillator model which we derived in the previous chapter,

$$\frac{\partial \theta_j}{\partial t} = \epsilon_j + J' \sum_{<k>} \left[\frac{1}{\alpha} \sin(\theta_k - \theta_j) - \cos(\theta_k - \theta_j) \right], \qquad (4.11)$$

where $J' = J/\sigma$, and we have set our energy scale such that the ϵ_j are distributed with zero mean and unit variance. We are also once again working in units where $\hbar = 1$. We may therefore determine whether superfluidity is possible in the presence of a random potential in one dimension by calculating the superfluid stiffness of a chain of condensates described by (4.11). We follow the method of [55] by considering a chain of length $L + 1$ sites with continuous boundary conditions, and applying a phase twist of $\theta_L - \theta_0 = \varphi$ between the boundaries. We have given the first site in the chain an index of 0 for clarity.

To measure the energy cost of a phase twist, we compare the frequency of the condensates that result from solving for the right-hand side of (4.11) both with and without twisted boundary conditions. The superfluid stiffness is then [55]

$$f_s = \lim_{\varphi \to 0} \frac{L^2}{\varphi^2} \left[\omega(\varphi) - \omega(0) \right], \qquad (4.12)$$

where $\omega(\varphi)$ is the frequency obtained by solving (4.11) with a phase twist of

φ. As we are considering a synchronized chain of condensates, this frequency is the same at each site.

We solve for these frequencies numerically by first evolving (4.11) with no twist over a sufficient time, T, for a synchronized steady state to be reached. The phases and frequencies in this steady state are then taken as the initial conditions for simulations of the twisted model. As we are investigating superfluidity for a synchronized chain, all numerical simulations are performed well inside the synchronized regime, where $J' \gg 1$. A phase twist is then applied to the boundary terms. The coupling functions on the boundaries then become

$$\frac{1}{\alpha} \left[\sin(\theta_1 - \theta_0) + \sin(\theta_L - \theta_0 + \varphi)\right]$$
$$- \left[\cos(\theta_1 - \theta_0) + \cos(\theta_L - \theta_0 + \varphi)\right] \tag{4.13}$$

and

$$\frac{1}{\alpha} \left[\sin(\theta_0 - \theta_L - \varphi) + \sin(\theta_{L-1} - \theta_L)\right]$$
$$- \left[\cos(\theta_0 - \theta_L - \varphi) + \cos(\theta_{L-1} - \theta_L)\right]. \tag{4.14}$$

The coupled equations are once again solved with the synchronized initial conditions and modified boundary terms, and the steady-state frequency of the oscillators in the twisted case is compared with the untwisted frequency to obtain the superfluid stiffness. We plot the results for the superfluid stiffness obtained numerically for both a chain with uniform on-site energies ($\epsilon_j = 0 \quad \forall j$), and one with normally-distributed random energies in Fig. 4.1.

As expected, a 'clean' chain with no disorder in the on-site energies displays a non-zero superfluid stiffness. We can see this by assuming that the phase twist takes the form of a local gauge transformation,

$$\tilde{\theta}_j = \theta_j + \varphi(j/L). \tag{4.15}$$

Applying this transformation adds a constant current to the arguments of the coupling functions: $\tilde{\theta}_{j+1} - \tilde{\theta}_j = \theta_{j+1} - \theta_j + \varphi/L$. Considering the boundary terms, one sees that writing (4.11) in terms of the transformed variables $\tilde{\theta}_j$ with periodic boundary conditions is equivalent to imposing twisted boundary conditions on the model in terms of the original variables θ_j.
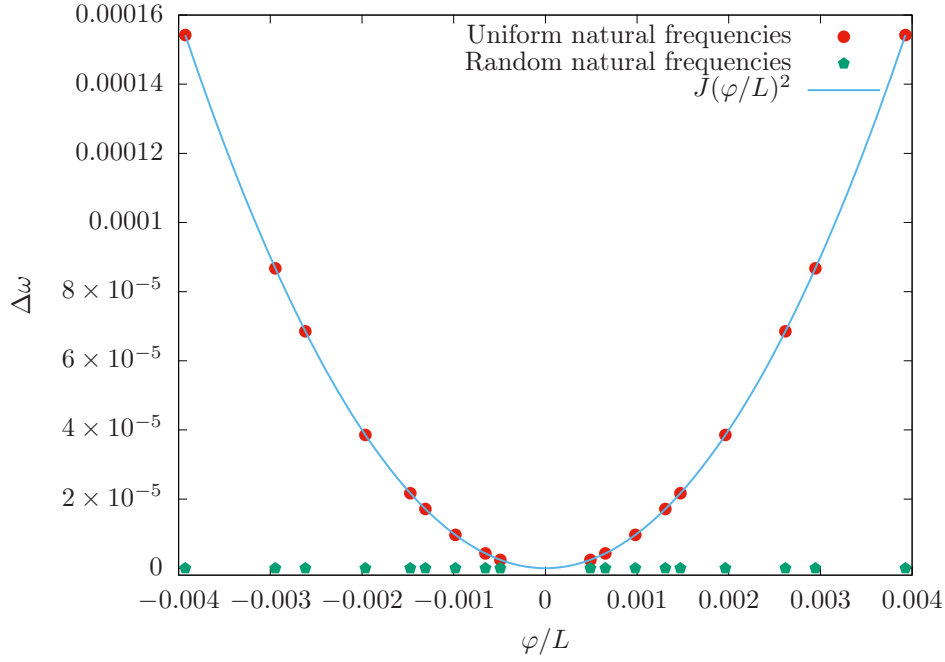
Figure 4.1: The frequency difference that results from applying a phase twist of φ across a chain of condensates with uniform (red circles) and random (green pentagons) on-site energies. The data is generated by solving (4.11) for chains of length 400, 600 and 800 sites, and twists of $\varphi = \pi/8$, $\pi/4$, $3\pi/8$, $\pi/2$. Frequencies were compared after a time $t\sigma = 15000$, when a steady state had been reached, and coupling $J' = 10$ was used throughout. The expected behaviour for stiffness in the clean case, as discussed in the text, is plotted as a blue line.

The steady state of the clean chain of condensates exhibits phase as well as frequency synchronization, so in this case, (4.11) with all $\epsilon_j = 0$ and untwisted boundary conditions reads

$$\frac{\partial \theta_j}{\partial t} = -2J'. \tag{4.16}$$

Applying the transformation (4.15), this becomes

$$\frac{\partial \theta_j}{\partial t} = -2J' \cos\left(\frac{\varphi}{L}\right), \tag{4.17}$$

which, in the limit of small twisting angle and large chains may be expanded as

$$\frac{\partial \theta_j}{\partial t} = -2J' + J'\left(\frac{\varphi}{L}\right)^2. \tag{4.18}$$

80

Subtracting (4.16) from (4.18) gives a superfluid stiffness of

$$f_s = J', \tag{4.19}$$

which is confirmed numerically by plotting $\Delta\omega = J'(\varphi/L)^2$ alongside the data in Fig. 4.1. This finite value for the stiffness is as expected for the eGPE in free space [120]. Once disordered energies are added to the system, the superfluid stiffness collapses to zero, however. This is in agreement with what has been previously observed in [55].

4.3.2 Analysis of phase profiles with twisted boundary conditions

The contrasting results for the stiffness in clean and disordered chains may be better understood by comparing the phase profiles that result from solving (4.11) both with and without a phase twist across the boundaries. These profiles are plotted in Figure 4.2. A phase twist across the boundaries attempts to drive a current through the condensate. This occurs in the clean case, where we see a constant phase gradient appear in the phase profile when a twist is applied. This current raises the energy of the chain because of the stiffness, $f_s = J'$, as seen in Fig. 4.1.

The disordered chain of condensates is resistant to the establishment of such a current, however. Unlike in the case of the clean chain, without applying a twist to the boundaries, the phase profile of the synchronized chain already has a current flowing in it. The shape of this profile was predicted by the connection between the phase oscillator model (4.11) and the imaginary-time Schrödinger equation for a particle in a random potential in Section 3.4. As described by Eq. (3.17), in the continuum limit, the phase profile is proportional to the natural logarithm of the exponentially-localized ground state wavefunction. The random potential 'seen' by the particle is essentially the continuum limit of the on-site energies, but inverted, and scaled by α. The point around which the wavefuction is localized therefore corresponds to the largest 'hill' that appears in the energy landscape (or the deepest well, when flipped upside-down). This results in a peak-like structure to the phase profile: the phase decreases linearly in either direction
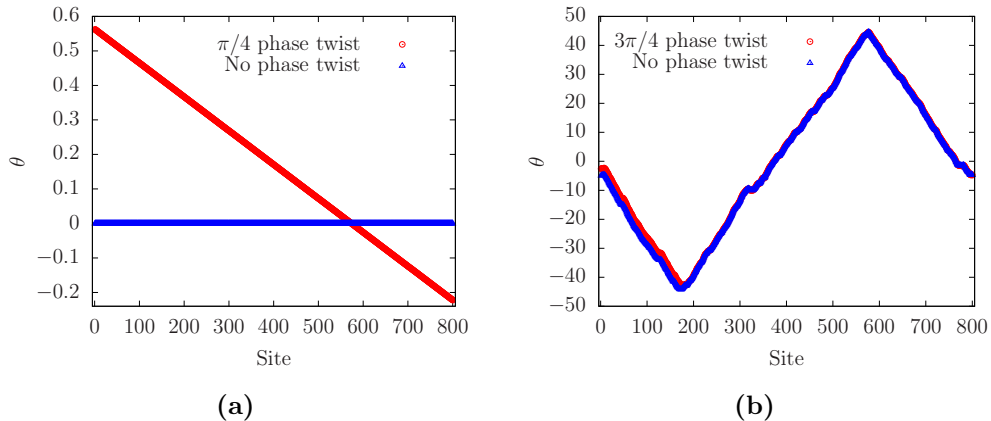
Figure 4.2: Phase profiles of clean (a) and disordered (b) chains of oscillators with twisted and untwisted boundary conditions. Profiles are obtained by evolving (4.11) for $t\sigma = 15000$ until a steady state is reached, with the resulting phases and frequencies for the untwisted simulations then used as initial conditions for the simulations with phase twists.

away from the position of the ground state. As the current is proportional to the gradient of the phase, a synchronized chain of condensates has a current of constant magnitude. This current always flows away from the position of the ground state, so this localization centre acts as a current source.

Imposing periodic boundary conditions on the chain is equivalent to considering a periodically repeating energy landscape, and therefore multiple identical ground state wavefunctions, separated by distance L. The phase on each site is influenced by its nearest ground state. Halfway between neighbouring localization centres, we must then have a current sink where the phase gradients change sign. An example of this may be seen near the 180th site in Fig. 4.2(b).

Unlike in the clean case, the application of a phase twist between the boundaries of the disordered chain does not produce a homogeneous response of the form (4.15). Instead, only the phases of the sites between a boundary and the nearest current sink (bottom of a valley in the phase profile) are shifted. In Fig. 4.2(b), due to the position of the ground state, and the direction of the phase twist, the phases of the leftmost sites are all shifted above their values in the untwisted case by a magnitude of φ. If the random

energies of the sites produced a phase peak in the left half of the chain, the current sink would appear on the right of the chain, and the phases of sites to the right of this would instead be reduced by this amount. The current in the chain then remains unchanged by a phase twist except in the immediate vicinity of the sink that appears $L/2$ sites from the ground state, where there is a localized response corresponding to a slight shift in the position of the sink. This is in agreement with results from [55], where the current response to a phase twist is found to be localized within a narrow domain wall.

We note that the results in [55] were derived for a 2D condensate, while our simulations were carried out on a one-dimensional chain. Our analysis in the previous chapter shows that the phase profiles of delocalized condensates in 2D have the same general shape as in 1D, with currents flowing away from a ground state localization centre. This can be seen in Fig. 3.6. The discussion above then straightforwardly generalizes to two dimensions.

4.4 Conclusions

In this chapter, we have verified the results of [55] in one dimension by numerically calculating the superfluid stiffness of a chain of driven-dissipative condensates. Once disorder is introduced into the chain through random on-site energies, the stiffness vanishes. This implies that a nonequilibrium condensate in a disordered potential is not a superfluid. Although we did not systematically consider arbitrarily small disorder strengths in our simulations, no energy response to a phase twist was observed over a range of parameter values. In the context of the results of [55], we do not expect such systems with any magnitude of disorder to exhibit superfluid stiffness.

The phase profile of a synchronized chain of condensates which we derived in the previous chapter is useful for furthering our understanding of the reaction of a non-equilibrium condensate to phase twists. An extended condensate in a random potential – or equivalently, a synchronized lattice of condensates – has a peak in the phase profile that corresponds to the position of the ground state wavefunction of particle which is localized in a random potential. This peak acts as a current source, and applying a phase twist across the boundaries of a region of the lattice does not change the magni-

tude of this current, which will be constant throughout any sample. Instead, the current response is localized in a narrow domain wall corresponding to a current sink.

The absence of superfluidity in driven-dissipative condensates in the presence of disorder is in contrast with the behaviour of equilibrium condensates. There are clear similarities between a desynchronized disordered lattice of condensates containing several different regions of common frequencies and the equilibrium Bose glass phase. As a synchronized chain of condensates with random on-site energies is not a superfluid, however, the phase transition which we identified in the previous chapter is not merely a non-equilibrium analogue of the Bose glass-superfluid transition.

Chapter 5

Phase correlations and the impact of noise on condensates in one dimension

5.1   Introduction

In this chapter, we examine the first-order field correlation functions of lattices of disordered driven-dissipative condensates, or equivalently, condensates in random potentials. We show that in addition to being entrained to a common frequency, synchronized lattices exhibit phase coherence – that is, the fields at each site are perfectly correlated.

We then examine the impact of time-dependent noise on both phase and frequency order in one-dimensional systems. First, we consider 'clean' lattices with no static disorder. We review the connection between the complex Ginzburg-Landau equation describing a clean condensate in the presence of noise and the Kardar-Parisi-Zhang (KPZ) equation of growing interfaces. As a result of this, phase correlations in one-dimensional condensates decay exponentially, and therefore phase order is not present in a chain of condensates which are subject to time-dependent disorder. Such chains nevertheless exhibit frequency synchronization.

We also examine the behaviour of chains of condensates subject to only time-dependent disorder, whose phase dynamics may not be mapped to a continuum KPZ equation. In a way, this is the noisy analogue of the desyn-

chronized regime for the lattices discussed in Chapter 3; however, the frequencies of such oscillators remain synchronized in this case. This regime is characterized by the presence of space-time vortices, which occur at large noise strengths. These are equivalent to phase slips of 2π occurring between neighbouring sites.

In the final section of the chapter, we reintroduce a static disorder profile, and consider disordered chains that are also subject to random, time-dependent noise. Our numerical simulations show that while the phase profiles of such systems still retain the characteristic peaked shape of the synchronized chain with static disorder, the presence of noise causes exponential decay of the visibility of the phase correlation functions. This behaviour is characteristic of the kinetically roughened phase profiles of the KPZ and Edwards-Wilkinson universality classes. We note also that noise may cause desynchronization to occur at lower static disorder strengths than predicted for the clean model in Chapter 3. Finally, we propose a phase diagram characterizing the phase- and frequency-ordered parameter regimes of one-dimensional lattices of coupled driven-dissipative condensates.

5.2 Phase correlations in disordered chains

It is evident from the phase profile of a synchronized chain of oscillators described by the model (3.5) outlined in Chapter 3 (see Figures 3.5, 3.6 or 4.2(b) for example), that in addition to frequency synchronization, there is phase order across the system. This is not phase synchronization: as we found in the continuum limit, any amount of disorder in the on-site energies gives rise to a constant phase gradient of $|\nabla\theta| = [\alpha^d(\sigma/J)^2]^{1/(4-d)}$. This quantity must be less than one, so for a synchronized lattice with random on-site energies, the phase at each site is offset from its neighbours by a small, constant amount.

We may quantify this phase order by considering a first-order spatial correlation function of the condensate wavefunction over the length of the chain. The standard general form of a correlation function is

$$C(\mathbf{x}, \mathbf{x}'; t, t') = \frac{\langle \Psi^*(\mathbf{x}, t)\Psi(\mathbf{x}', t') \rangle}{\sqrt{\langle |\Psi(\mathbf{x}, t)|^2 \rangle \langle |\Psi(\mathbf{x}', t')|^2 \rangle}} \tag{5.1}$$

where $\Psi(\mathbf{x}, t)$ is the condensate order parameter, and the angular brackets represent an average over disorder.

We will only consider one-dimensional chains of condensate for our analysis in this chapter. The amplitude of the condensate wavefunction on each site of the chain is given by $\psi_j(t) = \sqrt{n_j(t)} \exp(-i\theta_j(t))$. In the regime where our phase-only model is valid, the density n_j is uniform across the chain, so the normalization is trivial, and the correlation function simplifies to

$$C(x, x'; t, t') = \langle \exp(-i[\theta_j(t) - \theta_l(t')]) \rangle, \qquad (5.2)$$

where $x' - x = a(l - j)$, with a the lattice constant.

As we are interested in spatial correlations, we take an equal-time correlation function, $C(\mathbf{x}, \mathbf{x}')$. It is not necessary for us to consider an average over static disorder realizations because we are interested in the features of individual samples, as may be accessed experimentally. Furthermore, the shape of the phase profile in a synchronized steady state is always the same, regardless of the random distribution of energies. All that differs from one realization to another is the position of the peak. In experiments, such correlation functions are typically determined by sending the condensate emission to a Mach-Zender interferometer, which interferes the emission with an image of itself that is reflected through an origin point $\mathbf{x} = 0$ at the centre of the sample [57]. This gives the correlator $C(\mathbf{x}, -\mathbf{x})$. One may also take the origin to be the first site on the left of the chain, and interfere the emission from every other site with this one to obtain the function $C(\mathbf{x}, 0)$.

We plot both of these correlation functions for a single realization of random energies across a chain of 800 sites in Figure 5.1. The sinusoidal shape of the real part of the correlation functions corresponds to bright and dark fringes in an interference pattern. This is the expected emission from a smooth, sloped phase profile. Such fringes are typically observed experimentally when two coherent, spatially separated sources of light are interfered with one another. These fringes appear across the length of the chain, indicating coherence across the entire sample. This pattern is also seen experimentally for a 2D lattice of polariton condensates, in the regime where the frequencies of the sites are synchronized [57].

The data points in Fig. 5.1(b) and (c) are joined with lines for ease of
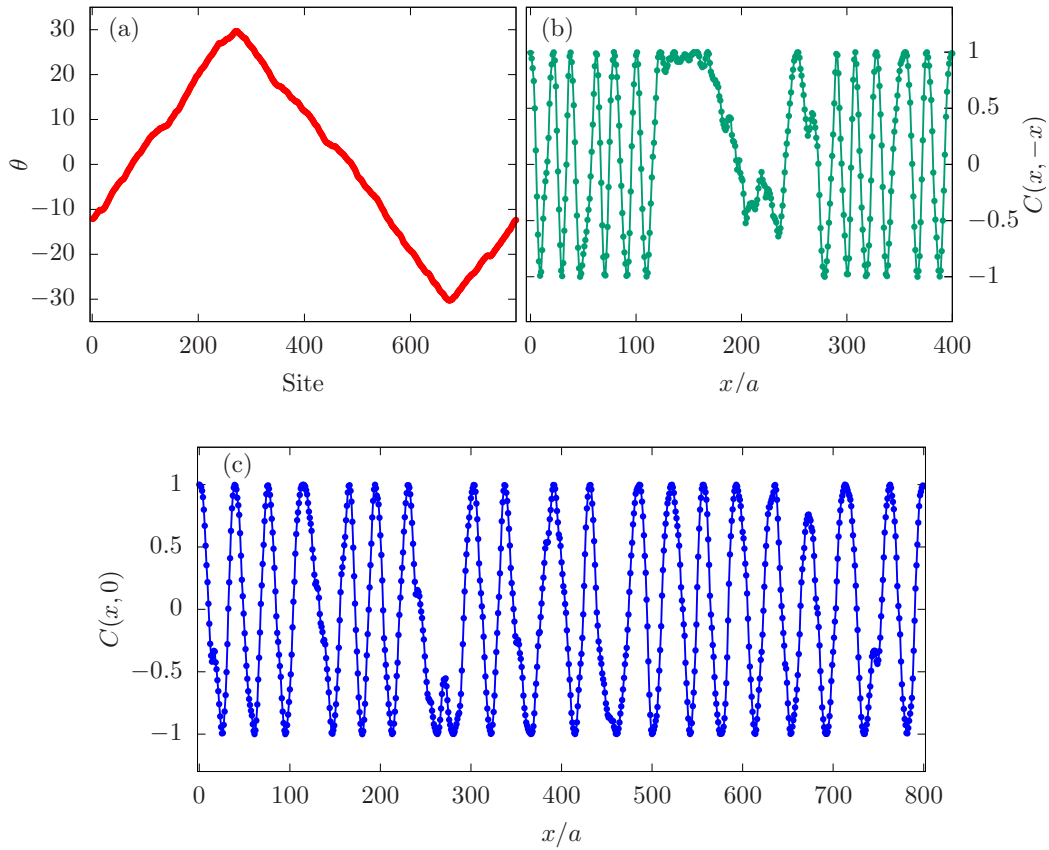
Figure 5.1: (a) Phase profile of a synchronized chain of 800 driven-dissipative condensates, obtained by solving Eq. (3.5) with $J/\sigma = 10$ and $\alpha = 1$. The real parts of the correlation functions $C(x, -x)$ (b) and $C(x, 0)$ (c) of the amplitudes on the chain corresponding to this phase profile are also shown. For the correlation function in (b), the origin was chosen to be the centre of the chain, $n = 400$, while for (c) it was chosen to be the leftmost site, $n = 1$.

visibility. We note that the density of fringes will be greater for larger phase gradients. The imaginary part of these correlation functions (not shown) is also sinusoidal in shape, due to the complex exponential form of Eq. (5.2). A relatively large coupling strength, J/σ, was chosen for our simulation so that the fringes may be easily distinguished from one another.

In Fig. 5.1(b), the fringe pattern is interrupted in the region $x/a = (120 - 250)$. This is caused by the peaks in the phase profile, where the gradient switches sign. This is consistent with the form of the correlation function (5.2). It behaves sinusoidally when the argument – given by the difference

in phases at two sites – increases linearly. In the locality of a peak, this argument is no longer linear, and the correlation function deviates from its sinusoidal behaviour. This has less of an effect in the correlation function $C(x, 0)$, shown in Fig. 5.1(c), however interruptions to the regular pattern are also visible at the positions of the peaks at sites ~ 280 and ~ 680. This effect would be less evident in larger samples, where there is still only a single peak. The visibility of the fringes may be obtained from the amplitude of the correlation function, or $|C|$. As there is no time-dependent disorder to average over, C is simply a complex exponential function, so the visibility is constant and equal to one across the chain.

We have labelled the x-axis of the plots of correlation functions in Fig. 5.1 with x/a. In the case of Fig. 5.1(c) (and other plots of $C(x, 0)$ in this chapter), this is the same as the 'Site' label which we employ for phase profiles (such as Fig. 5.1(a)), as the origin of this coordinate system is chosen to be the leftmost site. However, for the correlation function $C(x, -x)$ in Fig. 5.1(b), we choose the origin to be the centre of the chain, $n = 400$, so that half of the sites in the chain have a negative value of x. For consistency, we will follow the convention of labelling the x-axes of phase plots with 'Site', and correlation functions with x/a for the remainder of the chapter.

5.3 Condensates in the presence of noise

So far we have only considered lattices of condensates with spatial disorder in their on-site energies. However, as mentioned in the introduction, there is inevitably some spatio-temporal noise associated with the gain and loss in a driven-dissipative system [63]. This may be modelled by considering a stochastic extended Gross-Pitaevskii equation (seGPE):

$$i\frac{\partial \Psi}{\partial t} = \left[-\frac{1}{2m}\nabla^2 + V(\mathbf{x}) + U|\Psi|^2\right]\Psi + i\left(g - \Gamma|\Psi|^2\right)\Psi + \xi(\mathbf{x}, t). \quad (5.3)$$

Here, the new stochastic term, $\xi(\mathbf{x}, t)$ is a Gaussian white noise term such that

$$\langle \xi^*(\mathbf{x}, t)\xi(\mathbf{x}', t')\rangle = 2\tilde{D}\delta(\mathbf{x} - \mathbf{x}')\delta(t - t'), \quad (5.4)$$

where, as mentioned in Section 1.5.2, the strength of the fluctuations, $\tilde{D}$ is set by the the parameters g and κ. In models that explicitly consider the

reservoir dynamics, the noise strength is often taken to be approximately equal to the single particle loss rate [65, 109]. In terms of the parameters of our model, we consider $\tilde{D} \approx g$.

The impact of noise on a clean condensate, where $V(\mathbf{x}) = 0$ in (5.3), has been the subject of much research in recent years [109, 121]. In particular, it has been shown that when fluctuations in the density are small, the condensate phase obeys a Kardar-Parisi-Zhang (KPZ) equation [65, 66, 110, 113].

This may be seen by following a similar procedure to that outlined in Section 3.6.4, keeping track of the additional noise term, which we assume to have both real and imaginary components. This yields the KPZ equation,

$$\frac{\partial \theta(\mathbf{x}, t)}{\partial t} = \nu \nabla^2 \theta + \frac{\lambda}{2} (\nabla \theta)^2 + \eta(\mathbf{x}, t), \tag{5.5}$$

where $\nu = 1/(2m\alpha)$, $\lambda = 1/m$, and $\eta(\mathbf{x}, t)$ is the rescaled Gaussian noise, with strength

$$D = \frac{\Gamma}{2g} \left(1 + \frac{1}{\alpha^2} \right) \tilde{D}. \tag{5.6}$$

A more detailed derivation of the KPZ equation from the complex Ginzburg-Laundau equation may be found in [65].

The KPZ equation has a very similar form to the continuum model of the phase dynamics, (3.9), which we derived in Chapter 3. The only difference is that the true KPZ equation, which we consider here, has a time-dependent noise term in place of the static disorder from Eq. (3.9). This leads to generally different universal behaviour, which we will outline here.

5.3.1 KPZ physics

While the KPZ equation was initially formulated to describe the dynamics of growing interfaces [100], it has since been shown that a wide range of nonequilibrium processes involving disorder, from burning paper to polymer growth, lie in the KPZ universality class [105, 122, 123]. This class is characterized by the scaling behaviour of the interface width, or roughness function, defined as

$$W(L, t) = \left\langle \frac{1}{L} \int \left(\theta(\mathbf{x}, t) - \bar{\theta}(t) \right)^2 d\mathbf{x} \right\rangle^{1/2}, \tag{5.7}$$

where L is linear size of the sample, $\bar{\theta} = (1/L) \int \theta(\mathbf{x}, t) d\mathbf{x}$ is the spatial average of the phase (or interface height), and the angular brackets, as usual,

represent an ensemble average over disorder realizations. The KPZ width has been shown to obey a Family-Vicsek scaling relation [100, 124],

$$W(L,t) \sim L^{\chi} f(t/L^z), \tag{5.8}$$

where the scaling function is defined as

$$f(u) = \begin{cases} u^{\beta}, & u < 1 \\ 1, & u > 1. \end{cases} \tag{5.9}$$

In one dimension, the exponents are related by $z = \chi/\beta$, so two distinct regimes exist: a transient or dynamic regime in which the roughness increases with time as $W \sim t^{\beta}$, and a stationary regime, when the roughness has saturated to a value of $W \sim L^{\chi}$. The crossover from the former regime to the latter then occurs when $t = L^z$ [122].

We will focus on 1D systems, where the values of the scaling exponents are known exactly to be $\chi = 1/2$, $\beta = 1/3$, and $z = 3/2$ [100]. In fact, one dimension is a special case, where the static scaling behaviour is identical to that of the Edwards-Wilkinson model, which is the linear equation obtained by setting $\lambda = 0$ in (5.5).

This enables the straightforward calculation of the static correlation function, $C(x, x')$. The linear nature of the Edwards-Wilkinson equation means that it may be solved through Fourier decomposition. As the noise is Gaussian, its Fourier components are independent random processes, which are also δ-correlated in time. The Fourier modes of the phase, θ_k, are then also independent processes, obeying

$$\frac{\partial \theta_k}{\partial t} = -\nu k^2 \theta_k + \eta_k(t). \tag{5.10}$$

From this, we can show that these modes have variance

$$\langle |\theta_k|^2 \rangle = \frac{D}{\nu k^2} \tag{5.11}$$

in the long-time, stationary limit. As the Fourier modes of the phase are related to the random variables $\eta_k(t)$ through a linear transformation, the stationary distribution of phase modes is also Gaussian [105]. As a result of this, the equal-time field correlation function may be written as

$$C(x,0) \approx \exp\left(-\frac{1}{2}\langle [\theta(x,t) - \theta(0,t)]^2 \rangle\right). \tag{5.12}$$

The field correlator in the exponent may then be determined from the Fourier modes [122], yielding the result

$$C(x,0) \approx \exp\left(-\frac{D}{2\nu}x\right).$$

(5.13)

This exponential decay of correlations mean that long-range phase order is absent in 1D driven-dissipative condensates. Of course, in the case of weak noise (small D), the phases may appear correlated over the extent of a finite system. This statement may be formalized by defining the phase correlation length, $\mathcal{L} = 2\nu/D$ as the distance over which the correlation function decreases by $\exp(-1)$.

The above result is expected from the scaling properties of the 1D KPZ interface width (5.8). As the static and dynamic scaling exponents are positive, the phase profile becomes rougher as both $L \to \infty$ and $t \to \infty$. In general, a smooth profile, such as the solution to (3.5) or (3.9) (and as shown in Figure 5.1(a)) exhibits phase order, while a rough one (such as those in Figure 5.2) does not. When $\mathcal{L}$ is greater than the system size, the phase profile may look smooth; however, larger random features will appear if one considers larger systems.

5.3.2   Noisy coupled oscillators

As in the case of static disorder, driven-dissipative condensates in the presence of noise are closely related to coupled noisy oscillators. As discussed in Section 3.6.4, Eq. (5.5) is distinct from the traditional KPZ equation describing the dynamics of the height of an interface, because the phase θ is a compact variable. This implies the possibility of the existence of phase defects, specifically space-time vortices [113]. Once again, to fully capture this aspect of the physics, it is instructive to consider a discrete model. Of course, discretizing (5.5) yields the phase oscillator model (3.5) which we derived from the eGPE in Chapter 3, with the time-independent random energies ϵ_j replaced by a discrete version of $\eta(x,t)$. We will write this using the parameters from the eGPE on a lattice, as

$$\frac{\partial \theta_j}{\partial t} = J \sum_{<k>} \left[\frac{1}{\alpha} \sin(\theta_k - \theta_j) - \cos(\theta_k - \theta_j) \right] + \eta_j(t).$$

(5.14)
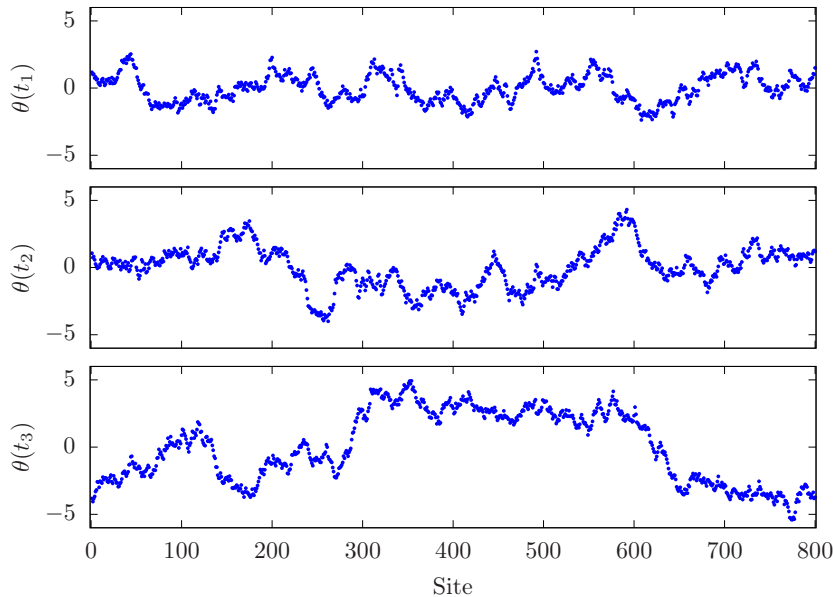
Figure 5.2: Phase profiles obtained by solving (5.14) for a chain of length $N = 800$, with $D/J = 0.08$, and $\alpha = 1$. Phases are shown at $t_1 = 100/J$, $t_2 = 4000/J$ and $t_3 = 10000/J$.

Here, η_j is a random on-site energy that also fluctuates randomly in time as

$$\langle \eta_j(t)\eta_l(t') \rangle = 2D\delta(t-t')\delta_{jl}, \tag{5.15}$$

and we have absorbed all constant terms into the energy scale such that this noise has zero mean. For our numerical simulations of noisy systems, we reduce the number of parameters in the system by transforming to dimensionless units, where $t' = Jt$ and $D' = D/J$.

In Figures 5.2 and 5.3, we plot the phases, θ_j, and field correlators, $C(x,0) = \langle \psi_j \psi_1 \rangle = \langle \text{Re}[\exp(-i(\theta_j - \theta_1))] \rangle$ obtained from solving (5.14) over a chain of 800 sites. The jagged, rough nature of the phase profile is immediately evident, and as we can see from the profiles at different times, its shape is constantly changing. These features are characteristic of a dynamically roughened surface in one dimension. The phase width in the first plot in Fig. 5.2 appears smaller than in the subsequent two, and it appears to have saturated by $t_2 = 4000/J$.

Correspondingly, exponential decay is clearly visible in the plot of the field correlation function in Fig. 5.3. Unlike the static-disorder field correlators we plotted in Section 5.2, these noisy correlation functions do require
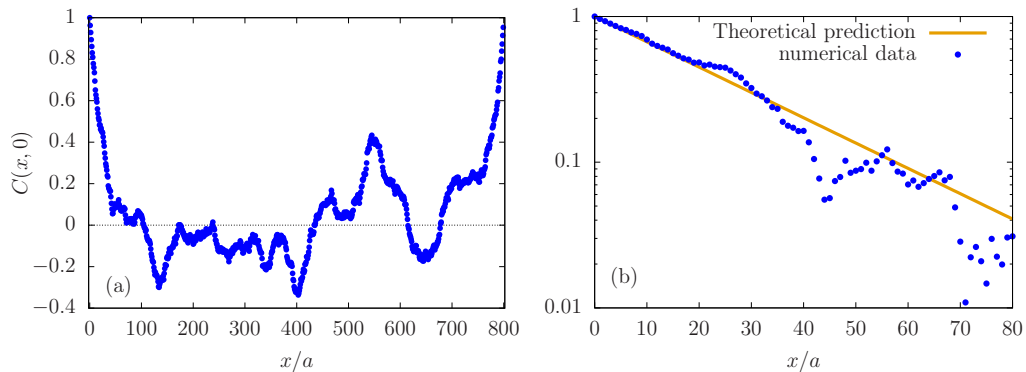
Figure 5.3: (a) Equal-time field correlation function of the system whose phases are plotted in Fig. 5.2. An ensemble average is calculated by taking the mean of 500 correlators calculated at equally-spaced times between $t = 6000/J$ and $t = 16000/J$. (b) The same data plotted on a log scale over the first 80 lattice sites. The data is seen to exhibit the exponential decay predicted by Eq. (5.13). Only the real part of the correlation function is plotted because as predicted by Eq. (5.12), the imaginary part is negligibly small in comparison.

averaging over disorder. This is achieved by evolving (5.14) from a flat initial condition for a long time (up to $t = 16000/J$), and calculating the equal-time correlation functions at 500 different times, separated by $20/J$, once the stationary regime is reached. As the disorder realizations given by $\eta_j(t)$ are independent at different times, if sufficient time is allowed to elapse between equal-time correlators for the phase profile to evolve significantly, taking the average of these correlation functions is equivalent to an ensemble average. $C(x, 0)$ is seen to decay exponentially before fluctuating around zero for large values of x/a. These fluctuations represent uncorrelated behaviour, and we suggest that their magnitude could be reduced by taking a disorder average over a greater number of stochastic trajectories.

The decay of spatial correlations is confirmed to be exponential, with correlation length $\mathcal{L} = 2J/(D\alpha) = 25$ sites, by plotting the data alongside $\exp(-x/25)$ in Fig. 5.3(b). These are in good agreement with one another over a short range. We see from Fig. 5.3(a) that $C(x, 0)$ approaches a value of one exponentially again as x approaches the system size. This is due to the periodic boundary conditions employed in our numerical simulations.

Of course, as well as modelling the phase dynamics of a driven-dissipative condensate, Eq. (5.14) is also a model of a chain of noisy coupled oscillators. It is clear from the discussion above that the phases of these oscillators do not exhibit any long-range order, but what about their frequencies? Perhaps surprisingly, given the appearance of the phase profiles in Fig. 5.2, such chains of oscillators are synchronized. This may be seen by considering the average frequency of each oscillator:

$$\Omega_j(t) = \frac{\theta_j(t) - \theta_j(0)}{t}. \tag{5.16}$$

We may rearrange this to write the phase at each site as a function of time in terms of its average frequency up to that time as

$$\theta_j(t) = t\Omega_j(t) + \theta_j(0). \tag{5.17}$$

Now, the spread of the average frequencies as a function of time may be defined analogously to that of the phases (which is given by a discretized version of Eq. (5.7)) as

$$W_\Omega(t) = \left\langle \frac{1}{N} \sum_j^N \left(\Omega_j(t) - \bar{\Omega}(t) \right)^2 \right\rangle^{1/2}, \tag{5.18}$$

for a chain of N oscillators [114]. The spatial mean of the average frequencies is $\bar{\Omega}(t) = (1/N) \sum_j^N \Omega_j(t)$. If, for simplicity, we consider a flat phase profile for the initial conditions, the phase at each site may be written as $\theta_j(t) = t\Omega_j(t)$. It is then clear that the spread of the phases may be written as $W_\theta(t) = tW_\Omega(t)$. As (5.14) is a discretized KPZ equation, $W_\theta(t)$ has the same scaling behaviour as its continuous counterpart, $W(L,t)$, so $W_\theta(t) \sim t^{1/3}$, before saturating at $W_\theta \sim \sqrt{Na}$. The frequency width then behaves as $W_\Omega(t) \sim t^{-1/3}$, so even in the case of an infinitely large chain, all frequencies will tend to a common value as $t \to \infty$. We note that the above holds true regardless of initial conditions.

This result should not be totally unexpected. After all, there is no disorder in the natural frequencies of the oscillators. While the dynamics of the phases at each individual site are erratic, they all still evolve at the same average rate. (This rate is zero as Eq. (5.14) is written, but we can add any constant term to this equation and see the same general behaviour.) In

fact, even if all forms of coupling are removed, the oscillators will still be synchronized. In this case, their dynamics are described by

$$\frac{\partial \theta_j}{\partial t} = \bar{\omega} + \eta_j(t), \tag{5.19}$$

where $\bar{\omega}$ is a common natural frequency, which we are free to set to zero. Eq. 5.19 simply describes a random walk of a phase θ_j around a mean position of $\bar{\omega}t$. The variance of a random walk process in $1D$ with δ-correlated noise of strength D is given by

$$\langle (\theta_j - \bar{\omega}t)^2 \rangle = 2Dt. \tag{5.20}$$

In this case, we may say that each phase diffuses around its expected value, and D may be referred to as a diffusion constant [12]. The standard deviation of each phase from its expected value is then $\sqrt{2Dt}$, and as each oscillator has the same natural frequency, this is also the value of the phase width, W_θ. Therefore, even in the absence of any coupling, the frequency width for noisy oscillators still obeys $W_\Omega(t) \sim t^{-1/2}$, and their average frequencies are synchronized.

5.3.3   Physics beyond the KPZ regime

Just as in the lattice with static disorder, the continuum approximation of Eq. (5.14) is not always valid. As discussed in Chapter 3, the limited range of the trigonometric functions implies that in the continuum, one has the condition $|\nabla \theta| \lesssim 1$. Thus, the discrete lattice model given by (5.14) has behaviour that is not described by the KPZ equation.

Specifically, this behaviour is seen when the noise is strong enough to 'kick' the phase of one of the oscillators enough such that it rapidly slips by an amount 2π relative to its neighbours. Such a phase slip appears as a vertical gap of $\sim 2\pi$ in a phase profile plot such as Figure 5.2. As mentioned in Chapter 3, these phase slips may be interpreted as space-time vortices in a continuum theory [113]. If one treats time as a second spatial dimension, and calculates the line integral of the gradient of the phase around a closed loop containing a single such event, the result will be non-zero, specifically $\pm 2\pi$. These features are a direct result of the compactness of the phase.

Unlike in the case of the static disorder, phase slips do not bring about desynchronization. The temporally random nature of the noise means that such phase slips are isolated events. Furthermore, even though they will occur more frequently at larger noise strengths, without static disorder in the natural frequencies of the oscillators, slips of $+2\pi$ and -2π between any given pair of oscillators are equally likely to occur. This has the result that the phases do not 'run away' from one another as they do in the case of desynchronized lattices with static disorder. An equivalent statement is that although the space-time vortex density in the system increases with noise strength, as long as no static disorder is present, there will be an equal number of vortices and antivortices.

For unbounded noise, the probability of a phase slip occurring is never zero [12], however at low noise strengths, they will occur so infrequently that very large systems and/or very long times are required to see them. In this case, the KPZ equation is still a reasonable continuum approximation, and the phase width has the scaling given by (5.8) with KPZ exponents. However, as D is increased, the vortex density increases, and a gradual transition from KPZ-like $t^{1/3}$ scaling to diffusive $t^{1/2}$ scaling of the phase width is observed [113,114]. This is consistent with the noise overcoming the coupling so that each phase behaves like that of a single noisy oscillator. Despite the existence of these two distinct regimes, frequency synchronization is present in both, as per the discussion above.

In [113] and [114], a third regime is also reported, where turbulent phase dynamics are observed. This corresponds to the sudden increase in frequencies at individual sites, or a rapid increase in space-time vortex density, and is observed to occur at large nonlinearities. This is similar to our observations for lattices with static disorder, where expected synchronization was not observed for values of $\alpha > 1$. Although we have restricted our investigations to the regime where $\alpha \leq 1$, it would appear from the results reported in [114] that this turbulent behaviour occurs when the KPZ correlation length – $\mathcal{L} = 2J/(\alpha D)$ in terms of the lattice parameters – is less than one lattice site. If this turbulence is merely a transient effect, as suggested [113,114], it will not destroy synchronization in the long-time limit, however the issue warrants further scrutiny beyond the scope of this thesis.

5.4 Impact of both spatial disorder and noise on driven-dissipative condensates

We are now ready to combine the models considered in the previous two sections, and examine the behaviour of the extended Gross-Pitaevskii equation with both static disorder and stochastic noise. We will do this by numerically solving the discrete phase-only approximation to the eGPE on a one-dimensional chain. This is a set of coupled differential equations for noisy, disordered oscillators:

$$\frac{\partial \theta_j}{\partial t} = J \sum_{<k>} \left[\frac{1}{\alpha} \sin(\theta_k - \theta_j) - \cos(\theta_k - \theta_j) \right] + \epsilon_j + \eta_j(t). \tag{5.21}$$

Here, ϵ_j and η_j are as they were defined in Eqs. (3.5) and (5.14), with strengths σ and D respectively. As before, this model is expected to describe the phase dynamics of a one-dimensional lattice of localized, driven-dissipative condensates, in the regime where fluctuations in the condensate densities are small. To this end, we have once again assumed uniformity in the pumping and disorder strengths. The noise η is taken to fluctuate on the scale of the lattice spacing, which is the smallest length scale in the model. Eq. 5.21 may also be viewed as a discrete model of a one-dimensional condensate in a random δ-correlated static potential. In addition to this, it is a generalization of the locally-coupled oscillator model (3.5) to include the impact of noise. As in the previous section, for numerical simulations, we will choose J^{-1} as our unit of time, so that the system only depends on the two dimensionless disorder strengths, σ/J and D/J, as well as the nonequilibrium control parameter α. We will take α to be one for our calculations in this section, as we have done up until now in this chapter.

As in the clean case studied in Chapter 3, solutions to this model may be either synchronized or desynchronized. The synchronized solutions of (5.21) are different to those in the clean case, however. While the phase profiles in this regime display the long-range peaked structure found in the case of static disorder, because of the noise term, the phase of each oscillator is no longer constant in time. This may be seen in Figure 5.4, where phases from three different times have been overlaid on one another. These fluctuations around the noise-free result mean that on short length scales, the phases resemble a
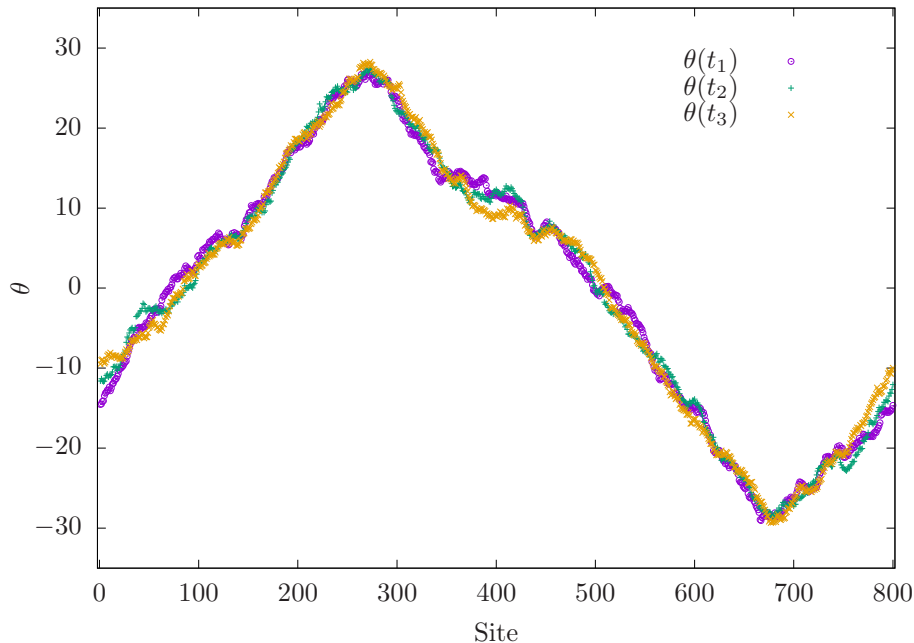
Figure 5.4: Phase profiles obtained by solving (5.21) for a chain of 800 oscillators, with $\sigma/J = 0.05$ and $D/J = 0.08$. $t_1 = 11200/J$, $t_2 = 11200/J$ and $t_3 = 11400/J$

kinetically roughened surface.

This is confirmed by calculating the spatial field correlation function, $C(x,0)$, which is plotted in Figure 5.5. While – as in the static case – interference fringes are evident in this plot, the visibility of these fringes decays exponentially. This may be seen in Figure 5.6, where the initial decay of the visibility is shown to match that of a KPZ surface with equivalent noise strength. Regardless of static disorder, the phases have correlation length $\mathcal{L} = 2J/(D\alpha)$. This suggests that while finite chains of oscillators described by the full model with noise (5.21) may exhibit phase order for sufficiently small D, phase correlations will vanish in the thermodynamic limit. This would be in line with the behaviour of the clean system, where noise destroys the phase correlations. Indeed, the correlation functions in Figures 5.5 and 5.6 are in line with the previously-discussed experimental results for a 2D lattice [57]. While interference fringes are observed in that case, their visibility is found to decay exponentially.

We note, however, that the decay in Fig. 5.6 slows down after its initially

99
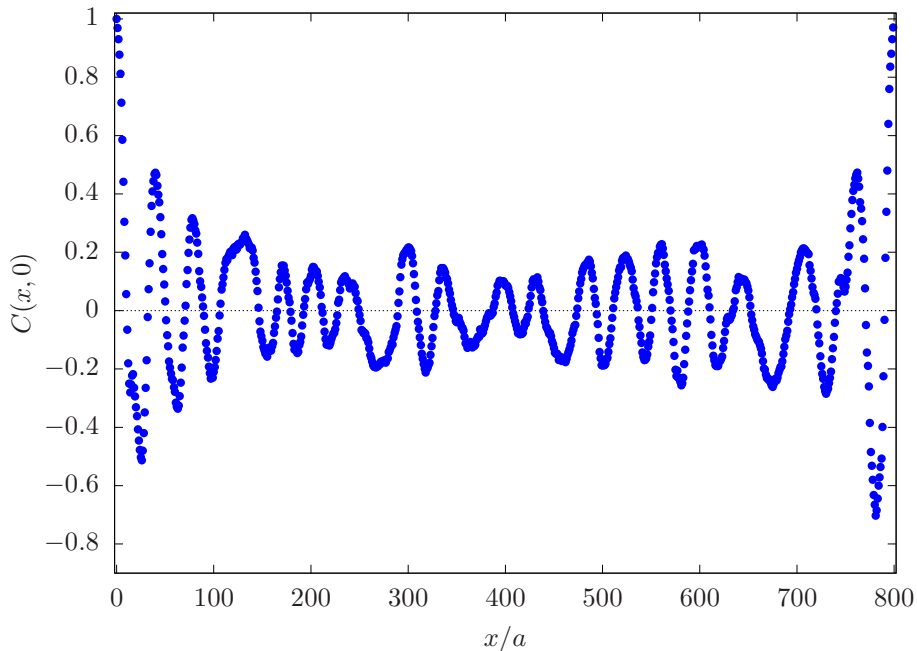
Figure 5.5: Real spatial correlation function of fields with the phases plotted in Fig. 5.4. An ensemble average is taken over noise, but not static disorder by taking the mean of 500 static correlation functions at equally-spaced times between $t = 6000/J$ and $t = 16000/J$.

exponential behaviour, and the visibility of the fringes does not go to zero. There could be a number of explanations for this – for example, we may not have averaged over enough independent realizations of the noise – but further investigations would be needed to definitively rule out the existence of phase order.

A more interesting question is how noise affects frequency synchronization. Much of the discussion in Sections 5.3.2 and 5.3.3 still holds. When Eq. (5.21) has a valid continuum approximation, the phases of neighbouring oscillators are locked to one another, and are therefore synchronized. However, as in the clean case, the noise may induce phase slips between neighbouring oscillators. Now, however, these slips are not equally likely to occur in each direction. As every oscillator is now being driven with a different frequency, oscillators with greater natural frequencies than their neighbours will accumulate extra rotations when provided with enough of a 'kick' by the noise. This may be understood for a pair of oscillators by considering the
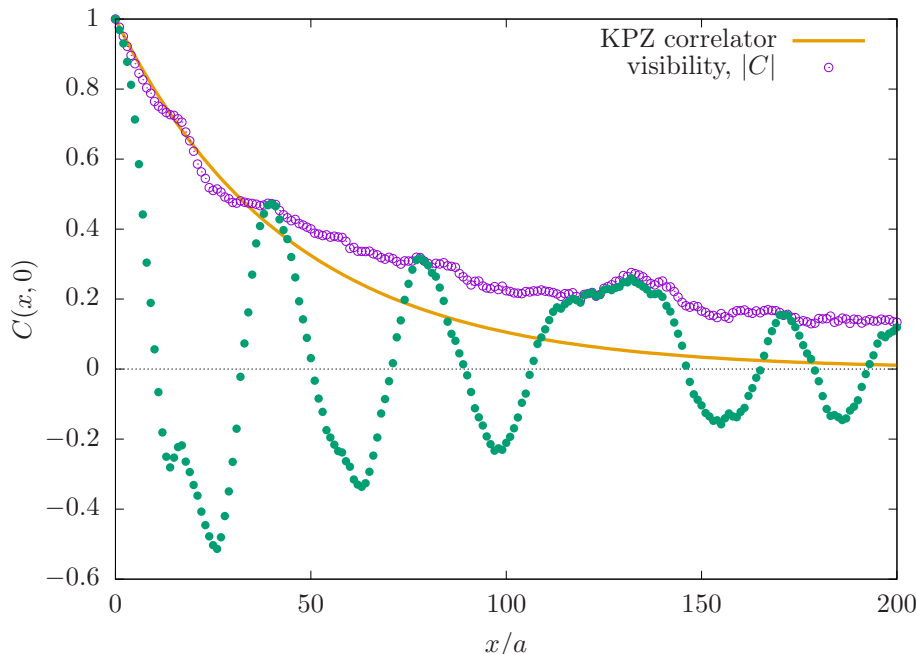
Figure 5.6: The correlation function from Fig. 5.5 is replotted over a shorter range. The visibility of this correlation function is plotted over this, and compared with the theoretical prediction for the clean KPZ equation with the same noise strength, $C(x,0) = \exp(-\alpha D x/(2J))$.

potential plotted in Fig. 2.4(a). Noise can give the 'particle' in this picture enough energy to overcome the potential barrier and hop into one of the neighbouring potential minima. A difference in natural frequencies means that this potential is sloped, so the particle is far more likely to jump over the smaller potential barrier, and proceed down the slope, increasing the phase difference between the oscillators [12].

When both static disorder and noise are weak, phase slips are rare, and the average frequencies of the oscillators will remain synchronized. However, for example if $|\nabla\theta| = \alpha\sigma/J$ is just less than one for a chain with static disorder, the addition of noise may be just enough to tip the system over into a desynchronized regime. Unlike in the clean case where the phase width of uncoupled oscillators scales as $\sqrt{t}$, an equivalent disordered system has $W_\Omega =$ a constant, so $W_\theta \sim t$, and a true desynchronized regime exists.

While our numerical simulations of Eq. (5.21) have demonstrated that noise may cause desynchronization in parameter regimes that give synchro-
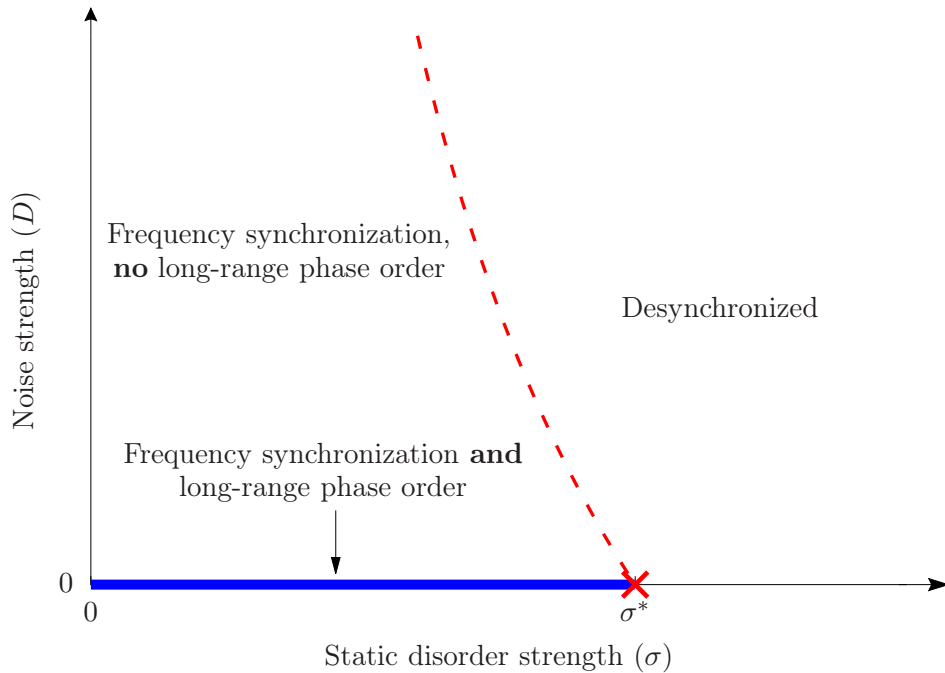
Figure 5.7: Phase diagram showing the three distinct regimes permitted by the noisy, disordered phase oscillator model in 1D (5.21), as a function of the strengths of each type of disorder. The phase transition for solely static disorder is as defined in Chapter 3: $\sigma^* = J/\sqrt{\alpha}$.

nized results in its absence, we have not formally established its impact on the phase boundary that we derived for the noise-free case (3.21). Nevertheless, we have enough information to suggest a phase diagram characterizing the distinct classes of solution permitted by (5.21) in 1D, as a function of the strengths of the static and time-dependent disorders.

This phase diagram is shown in Figure 5.7. There are generally three regimes in this diagram. From our analysis in Chapter 3, and the numerical results for correlation functions presented in Section 5.2, the behaviour of a chain of condensates subject to only static disorder is known exactly. This regime lies on the x-axis of the figure. For any given static disorder realisation there is a critical disorder strength, below which the frequencies of each site will be synchronized. Additionally, in this synchronized regime, the amplitudes of spatial correlation functions of the condensate wavefunction are found to remain constant across the sample. This indicates that the phases of the condensates in this regime are all ordered. We refer to this

as 'long-range phase order', although it is worth noting that in contrast to the off-diagonal long range order that is characteristic of 2D equilibrium BECs, the driven-dissipative systems that we are considering are not also superfluids. This was established in Chapter 4. This synchronized, phase-ordered regime is indicated by the thick blue line on the x-axis. Above the critical disorder strength, σ^*, frequency synchronization breaks down, as does phase order.

We also know what behaviour to expect for 'clean' chains which experience noise, but no spatial disorder. Such systems lie on the y-axis of the diagram. As outlined in Section 5.3, these chains always have synchronized frequencies in the long-time limit, regardless of noise strength. Spatial correlations of the wavefunction, on the other hand, are found to decay exponentially, and so there is no phase order in this regime. We therefore refer to this regime as exhibiting frequency order, but no phase order.

This leaves the the more general behaviour of a lattice of condensates subject to both types of disorder, or the area of the plot that is away from both axes. From the discussion above and the decay of spatial correlations seen in Fig. 5.6, we do not expect any long-range phase ordering in such systems. Furthermore, as our simulations indicate that adding noise to chains with spatial disorder makes desynchronization more likely, the right hand side of the diagram describes systems with no order in phases or frequencies. We label this as 'Desynchronized', and it also includes systems without noise which lie on the x-axis. There must then be some crossover from the region of frequency synchronization along the y-axis (no static disorder) to this desynchronized region. Unlike the sharp synchronization transition that we have shown to exist for a lattice with purely spatial disorder, we anticipate that this crossover occurs gradually. We have therefore indicated its presence by a dashed line in the figure. Moving up or right off either axis will see an increasing density of space-time vortices, and as discussed above, when both types of disorder are present, these lead to desynchronization. It is possible that the y-axis of the diagram is the only region with true frequency order and no phase order, and further analysis is needed to determine the exact nature of this desynchronization crossover in the presence of noise.

Finally, we note that this is just a two-dimensional slice of a three-

dimensional phase space. This work has not considered the behaviours of the different phases under large variations in α, however that is an avenue of future research.

5.5   Conclusions

In this chapter we have studied a number of generalizations to, and implications of, the phase oscillator model which we derived in Chapter 3. We have established that disordered lattices described by this model have long-range phase order in addition to synchronized frequencies. We have also, however, shown that this phase order is only present in the special case of no spatio-temporal noise.

We demonstrated this by generalizing the phase oscillator model to include a white noise term. In the absence of spatial disorder, this model is then a discretized KPZ equation. This is characterized by dynamically roughened phase profiles, and exponentially decaying spatial field correlation functions.

The addition of noise to our model also brings about desynchronization more readily when combined with static disorder, however no synchronization occurs in a clean, noisy chain of oscillators. The various regimes of this model are characterized in the phase diagram plotted in Figure 5.7. This picture of the various phases may be expanded by considering how they vary with the nonequilibrium control parameter, α.

Our results in this chapter are focused on the case of one-dimensional systems. It would be interesting to extend the analysis in this chapter to two dimensions, not least because polariton condensates typically occur in 2D, but also because the extension is not necessarily a trivial one. The KPZ scaling differs from 1D to 2D, while the physics beyond the KPZ regime in 2D is also the subject of much ongoing research, with a Berezinskii-Kosterlitz-Thouless (BKT)-like transition from a disordered state to an ordered one expected to occur [125, 126].

Chapter 6

Conclusions and future directions

In this thesis, we have investigated aspects of the phase dynamics of disordered driven-dissipative condensates using the framework of the complex Ginzburg-Landau equation. From this starting point, we have developed a phase oscillator model which, in its continuous limit, is related to the Kardar-Parisi-Zhang equation. Using this model, we have derived results for driven-dissipative condensates in disordered systems, particularly in the area of synchronization. We will summarize these below. While working only with the phase of the order parameter and neglecting the dynamics of the condensate densities is an approximation, and does not capture all the physics of the system, this enables us to connect the description of driven-dissipative condensates with that of coupled classical oscillators, and nonlinear models such as the KPZ equation. We were thus able to exploit the universality of our model, and use techniques developed for these different systems to gain a greater understanding of the physics of nonequilibrium condensates. Furthermore, the parameter regimes within which our approximations are valid coincide with those often found in experiments, and results derived using our model appear to be in line with experimentally reported findings.

We first considered synchronization of two spatially separated condensates in a double well. We extended previous analytic results which classified the synchronized and desynchronized regimes of this system, by considering asymmetric pumping of the two wells. This was achieved by following

a previous analysis [85] for two different spin states of a single condensate, and generalizing it to consider spatially separated modes, each experiencing differing linear gain terms. We found that asymmetry in the pumping contributes an additional effective detuning of the condensate energies, and acts to shift the position of the phase boundary between the two phases in parameter space. Our analytic work was supported by numerical simulations of the extended Gross-Pitaevskii equation in the double well. At this point, we also determined suitable values for the parameters in our model through calculations involving experimentally reported results. This guided our numerical simulations throughout the project.

In the third chapter, we extended the synchronization dynamics of the double well to the case of a square lattice of condensates with random on-site energies. We derived a connection between the Gross-Pitaevskii equation describing N condensates localized in a lattice potential, and a locally-coupled phase oscillator model. While this model has a similar structure to the well-known Kuramoto model, the additional nonlinear cosine term in the coupling function of our model means that it exhibits a synchronization phase transition. In the thermodynamic limit, it is possible for all of the oscillators on such a lattice to entrain their frequencies, despite the disorder. This contrasts with the behaviour of the locally-coupled Kuramoto model, where no such macroscopic synchronized state exists [77]. We derived the phase boundary analytically for lattices of dimension $d < 4$ by demonstrating that the continuum limit of our oscillator model is equivalent to a Schrödinger equation, which describes the dynamics of a single particle in a random potential in imaginary time. This system is known to have localized solutions. By connecting the expression for the localization length with the upper bound that exists for currents that may flow on a lattice, we derived a condition for synchronization in terms of the relevant parameters in the model.

This result is important in a number of contexts. It demonstrates that an arbitrarily large disordered lattice of condensates may synchronize its energies and act as one mode, emitting at a single frequency. This is useful for experimental realizations of polariton condensates and their proposed application as classical or quantum simulators [58,59]. Furthermore, it shows that a static random potential does not necessarily destroy long-range order

in a driven-dissipative condensate. More generally, however, the main result of this chapter holds for the large class of systems which may be described by our oscillator model. We have shown that a non-odd trigonometric coupling function is sufficient for entrainment of locally coupled oscillators on a regular lattice. To our knowledge, conclusive evidence had not previously been shown for a true synchronization transition in large populations of locally coupled oscillators, although previous works have presented numerical simulations and other arguments suggesting that this may occur in the 1D case [75, 108].

While our identification of the synchronization phase transition shows that a single, ordered state may exist across a disordered lattice of driven-dissipative condensates, in the following section, we demonstrated that this state is not a superfluid. This was achieved by numerically calculating the superfluid stiffness of a synchronized state of our lattice model. In contrast to a clean lattice, applying a phase twist across the boundaries of our model does not change the energy of the system, and so it does not support a superfluid current. This verifies previous analytic and numerical results [55]. Despite the absence of superfluidity, we demonstrated that a synchronized lattice of condensates with random on-site energies does have long-range phase order by calculating first order correlation functions of the condensate field.

Finally, we generalized the previous results for disordered lattices to include the effect of spatio-temporal noise. This was done for the case of one spatial dimension. We showed that the addition of such a stochastic term to our equations with static disorder causes the visibility of spatial field correlations to decay exponentially. This decay is also seen for clean systems with noise. Therefore, it appears that the correlation functions of a driven-dissipative condensate are not significantly affected by a static disordered potential, and that the long-range phase order we identified in synchronized lattices of condensates is not robust against noise. Despite this, noise is not expected to destroy the synchronization transition identified in Chapter 3, and a lattice of oscillators described by our model that experience both spatial disorder and noise may have synchronized frequencies.

A number of extensions to the work in Chapter 5 immediately suggest themselves. We have not yet conclusively determined the behaviour of the phase boundary between synchronized and desynchronized regimes in the

presence of both spatio-temporal and static disorder. The existence of both synchronized and desynchronized states separated by a phase boundary in the case of static disorder, and the absence of a desynchronization for solely spatio-temporal fluctuations, enabled us to propose a phase diagram as a function of both types of disorder. However, despite preliminary numerical results demonstrating that the addition of noise to systems with static disorder can bring about desynchronization more readily, the exact form of the phase boundary in the presence of noise has yet to be determined. A more comprehensive numerical analysis of the system, coupled with further analytic work may prove fruitful.

In addition to this, our phase diagram does not completely span the three-dimensional parameter space of the lattice model. The parameter α controls the strength of the nonlinearity in the continuum phase model, while in terms of driven-dissipative condensates, it quantifies how far out of equilibrium the system is. As noted in Chapter 3, we had difficulty verifying our analytic results for the phase boundary numerically when $\alpha > 1$, and remarked that this corresponds to the localization length, ζ becoming smaller than the spacing between sites on the lattice. Furthermore, recent work [113] has reported a phase transition at low noise strength for the clean version of this model as this parameter is increased. Although values of α in excess of one lie outside the experimentally accessible parameter regime for polariton condensates, this may not be the case for other systems that are described by this model. It would therefore be of interest to further study the synchronization properties of the system at large values of α, and produce a complete phase diagram of the system.

Finally, our analysis of the impact of noise on our system in the final chapter was limited to one dimension. While we showed in Chapter 3 that solutions to our model of disordered oscillators look broadly the same in one and two dimensions, this is not the case for noisy systems. Phase correlations are also found to decay for the KPZ universality class in 2D [65], however the scaling exponents are not identical to those in 1D. Furthermore, the physics beyond the KPZ regime in two dimensions is also different to the 1D case. The role of spatial vortices must be considered, as a Berezinskii-Kosterlitz-Thouless (BKT)-like transition from a disordered state to an ordered one is

expected to occur [125]. Although polariton condensates may be experimentally realized in one dimension, they typically occur in 2D. It would therefore be useful to fully extend the analysis in this chapter to two dimensions.

A more general potential extension to this work would be to consider different forms of coupling between condensates on a lattice. As mentioned earlier in this work, lattices of polariton condensates which are propagating states have recently been the subject of some interest, both theoretically and experimentally. These have been proposed as simulators of many complex systems, such as the XY model [58,127]. In these configurations, the coupling between sites has a significant dissipative component. It may be interesting to see how the inclusion of complex terms in the coupling functions in our model would affect our results.

Bibliography

[1] M. H. Anderson, J. R. Ensher, M. R. Matthews, C. E. Wieman, and E. A. Cornell, "Observation of Bose-Einstein Condensation in a Dilute Atomic Vapor," *Science*, vol. 269, pp. 198–201, July 1995.

[2] C. C. Bradley, C. A. Sackett, J. J. Tollett, and R. G. Hulet, "Evidence of Bose-Einstein Condensation in an Atomic Gas with Attractive Interactions," *Physical Review Letters*, vol. 75, pp. 1687–1690, Aug. 1995.

[3] K. B. Davis, M. O. Mewes, M. R. Andrews, N. J. van Druten, D. S. Durfee, D. M. Kurn, and W. Ketterle, "Bose-Einstein Condensation in a Gas of Sodium Atoms," *Physical Review Letters*, vol. 75, pp. 3969–3973, Nov. 1995.

[4] N. P. Proukakis, D. W. Snoke, and P. B. Littlewood, eds., *Universal Themes of Bose-Einstein Condensation*. Cambridge: Cambridge University Press, 2017.

[5] J. J. Hopfield, "Theory of the Contribution of Excitons to the Complex Dielectric Constant of Crystals," *Physical Review*, vol. 112, pp. 1555–1567, Dec. 1958.

[6] J. Kasprzak, M. Richard, S. Kundermann, A. Baas, P. Jeambrun, J. M. J. Keeling, F. M. Marchetti, M. H. Szymańska, R. André, J. L. Staehli, V. Savona, P. B. Littlewood, B. Deveaud, and L. S. Dang, "Bose–Einstein condensation of exciton polaritons," *Nature*, vol. 443, pp. 409–414, Sept. 2006.

[7] J. Keeling, F. M. Marchetti, M. H. Szymańska, and P. B. Littlewood, "Collective coherence in planar semiconductor microcavities," *Semiconductor Science and Technology*, vol. 22, pp. R1–R26, Apr. 2007.

[8] I. Carusotto and C. Ciuti, "Quantum fluids of light," *Reviews of Modern Physics*, vol. 85, pp. 299–366, Feb. 2013.

[9] H. Deng, H. Haug, and Y. Yamamoto, "Exciton-polariton Bose-Einstein condensation," *Reviews of Modern Physics*, vol. 82, pp. 1489–1537, May 2010.

[10] T. Byrnes, N. Y. Kim, and Y. Yamamoto, "Exciton–polariton condensates," *Nature Physics*, vol. 10, pp. 803–813, Nov. 2014.

[11] M. Thunert, A. Janot, H. Franke, C. Sturm, T. Michalsky, M. D. Martín, L. Viña, B. Rosenow, M. Grundmann, and R. Schmidt-Grund, "Cavity polariton condensate in a disordered environment," *Physical Review B*, vol. 93, p. 064203, Feb. 2016.

[12] A. Pikovskij, M. Rosenblum, and J. Kurths, *Synchronization: A Universal Concept in Nonlinear Sciences*. No. 12 in Cambridge Nonlinear Science Series, Cambridge: Cambridge University Press, 2003.

[13] C. Weisbuch, M. Nishioka, A. Ishikawa, and Y. Arakawa, "Observation of the coupled exciton-photon mode splitting in a semiconductor quantum microcavity," *Physical Review Letters*, vol. 69, pp. 3314–3317, Dec. 1992.

[14] R. I. Kaitouni, O. El Daïf, A. Baas, M. Richard, T. Paraiso, P. Lugan, T. Guillet, F. Morier-Genoud, J. D. Ganière, J. L. Staehli, V. Savona, and B. Deveaud, "Engineering the spatial confinement of exciton polaritons in semiconductors," *Physical Review B*, vol. 74, p. 155311, Oct. 2006.

[15] M. Fox, *Optical Properties of Solids*. Oxford Master Series in Physics, Oxford, New York: Oxford University Press, second ed., May 2010.

[16] A. Kavokin, "Exciton-polaritons in microcavities: Recent discoveries and perspectives," *physica status solidi (b)*, vol. 247, no. 8, pp. 1898–1906, 2010.

[17] P. R. Eastham and P. B. Littlewood, "Bose condensation of cavity polaritons beyond the linear regime: The thermal equilibrium of a model microcavity," *Physical Review B*, vol. 64, p. 235101, Nov. 2001.

[18] L. P. Pitaevskij and S. Stringari, *Bose-Einstein Condensation*. No. 116 in International Series of Monographs on Physics, Oxford: Clarendon Press, repr ed., 2010.

[19] E. Wertz, L. Ferrier, D. D. Solnyshkov, P. Senellart, D. Bajoni, A. Miard, A. Lemaître, G. Malpuech, and J. Bloch, "Spontaneous formation of a po-

lariton condensate in a planar GaAs microcavity," *Applied Physics Letters*, vol. 95, p. 051108, Aug. 2009.

[20] R. Balili, V. Hartwell, D. Snoke, L. Pfeiffer, and K. West, "Bose-Einstein Condensation of Microcavity Polaritons in a Trap," *Science*, vol. 316, pp. 1007–1010, May 2007.

[21] S. Christopoulos, G. B. H. von Högersthal, A. J. D. Grundy, P. G. Lagoudakis, A. V. Kavokin, J. J. Baumberg, G. Christmann, R. Butté, E. Feltin, J.-F. Carlin, and N. Grandjean, "Room-Temperature Polariton Lasing in Semiconductor Microcavities," *Physical Review Letters*, vol. 98, Mar. 2007.

[22] J. J. Baumberg, A. V. Kavokin, S. Christopoulos, A. J. D. Grundy, R. Butté, G. Christmann, D. D. Solnyshkov, G. Malpuech, G. Baldassarri Höger von Högersthal, E. Feltin, J.-F. Carlin, and N. Grandjean, "Spontaneous Polarization Buildup in a Room-Temperature Polariton Laser," *Physical Review Letters*, vol. 101, p. 136409, Sept. 2008.

[23] G. Christmann, R. Butté, E. Feltin, J.-F. Carlin, and N. Grandjean, "Room temperature polariton lasing in a GaN/AlGaN multiple quantum well microcavity," *Applied Physics Letters*, vol. 93, p. 051102, Aug. 2008.

[24] T. Guillet, M. Mexis, J. Levrat, G. Rossbach, C. Brimont, T. Bretagnon, B. Gil, R. Butté, N. Grandjean, L. Orosz, F. Réveret, J. Leymarie, J. Zúñiga-Pérez, M. Leroux, F. Semond, and S. Bouchoule, "Polariton lasing in a hybrid bulk ZnO microcavity," *Applied Physics Letters*, vol. 99, p. 161104, Oct. 2011.

[25] F. Li, L. Orosz, O. Kamoun, S. Bouchoule, C. Brimont, P. Disseix, T. Guillet, X. Lafosse, M. Leroux, J. Leymarie, G. Malpuech, M. Mexis, M. Mihailovic, G. Patriarche, F. Réveret, D. Solnyshkov, and J. Zúñiga-Pérez, "Fabrication and characterization of a room-temperature ZnO polariton laser," *Applied Physics Letters*, vol. 102, p. 191118, May 2013.

[26] Y.-Y. Lai, Y.-P. Lan, and T.-C. Lu, "Strong light–matter interaction in ZnO microcavities," *Light: Science & Applications*, vol. 2, pp. e76–e76, June 2013.

[27] S. Kéna-Cohen and S. R. Forrest, "Room-temperature polariton lasing in an organic single-crystal microcavity," *Nature Photonics*, vol. 4, pp. 371–375, June 2010.

[28] G. Lerario, A. Fieramosca, F. Barachati, D. Ballarini, K. S. Daskalakis, L. Dominici, M. De Giorgi, S. A. Maier, G. Gigli, S. Kéna-Cohen, and D. Sanvitto, "Room-temperature superfluidity in a polariton condensate," *Nature Physics*, vol. 13, pp. 837–841, Sept. 2017.

[29] C. N. Yang, "Concept of Off-Diagonal Long-Range Order and the Quantum Phases of Liquid He and of Superconductors," *Reviews of Modern Physics*, vol. 34, pp. 694–704, Oct. 1962.

[30] O. Penrose and L. Onsager, "Bose-Einstein Condensation and Liquid Helium," *Physical Review*, vol. 104, pp. 576–584, Nov. 1956.

[31] N. D. Mermin and H. Wagner, "Absence of Ferromagnetism or Antiferromagnetism in One- or Two-Dimensional Isotropic Heisenberg Models," *Physical Review Letters*, vol. 17, pp. 1133–1136, Nov. 1966.

[32] V. L. Berezinskiĭ, "Destruction of Long-range Order in One-dimensional and Two-dimensional Systems Possessing a Continuous Symmetry Group. II. Quantum Systems," *Soviet Journal of Experimental and Theoretical Physics*, vol. 34, p. 610, Jan. 1972.

[33] J. M. Kosterlitz and D. J. Thouless, "Ordering, metastability and phase transitions in two-dimensional systems," *Journal of Physics C: Solid State Physics*, vol. 6, pp. 1181–1203, Apr. 1973.

[34] G. Roumpos, M. Lohse, W. H. Nitsche, J. Keeling, M. H. Szymańska, P. B. Littlewood, A. Löffler, S. Höfling, L. Worschech, A. Forchel, and Y. Yamamoto, "Power-law decay of the spatial correlation function in exciton-polariton condensates," *Proceedings of the National Academy of Sciences*, vol. 109, pp. 6467–6472, Apr. 2012.

[35] G. Roumpos, M. D. Fraser, A. Löffler, S. Höfling, A. Forchel, and Y. Yamamoto, "Single vortex–antivortex pair in an exciton-polariton condensate," *Nature Physics*, vol. 7, pp. 129–133, Feb. 2011.

[36] P. Cristofolini, A. Dreismann, G. Christmann, G. Franchetti, N. G. Berloff, P. Tsotsis, Z. Hatzopoulos, P. G. Savvidis, and J. J. Baumberg, "Optical Superfluid Phase Transitions and Trapping of Polariton Condensates," *Physical Review Letters*, vol. 110, p. 186403, May 2013.

[37] B. Nelsen, G. Liu, M. Steger, D. W. Snoke, R. Balili, K. West, and L. Pfeiffer, "Dissipationless Flow and Sharp Threshold of a Polariton Condensate with Long Lifetime," *Physical Review X*, vol. 3, p. 041015, Nov. 2013.

[38] D. Tanese, H. Flayac, D. Solnyshkov, A. Amo, A. Lemaître, E. Galopin, R. Braive, P. Senellart, I. Sagnes, G. Malpuech, and J. Bloch, "Polariton condensation in solitonic gap states in a one-dimensional periodic potential," *Nature Communications*, vol. 4, p. 1749, Apr. 2013.

[39] Y. Sun, P. Wen, Y. Yoon, G. Liu, M. Steger, L. N. Pfeiffer, K. West, D. W. Snoke, and K. A. Nelson, "Bose-Einstein Condensation of Long-Lifetime Polaritons in Thermal Equilibrium," *Physical Review Letters*, vol. 118, p. 016602, Jan. 2017.

[40] D. Caputo, D. Ballarini, G. Dagvadorj, C. Sánchez Muñoz, M. De Giorgi, L. Dominici, K. West, L. N. Pfeiffer, G. Gigli, F. P. Laussy, M. H. Szymańska, and D. Sanvitto, "Topological order and thermal equilibrium in polariton condensates," *Nature Materials*, vol. 17, pp. 145–151, Feb. 2018.

[41] M. D. Fraser, S. Höfling, and Y. Yamamoto, "Physics and applications of exciton–polariton lasers," *Nature Materials*, vol. 15, pp. 1049–1052, Oct. 2016.

[42] J. Keeling and N. G. Berloff, "Spontaneous rotating vortex lattices in a pumped decaying condensate," *Physical Review Letters*, vol. 100, p. 250401, June 2008.

[43] V. García-Morales and K. Krischer, "The complex Ginzburg–Landau equation: An introduction," *Contemporary Physics*, vol. 53, pp. 79–95, Mar. 2012.

[44] I. S. Aranson and L. Kramer, "The world of the complex Ginzburg-Landau equation," *Reviews of Modern Physics*, vol. 74, pp. 99–143, Feb. 2002.

[45] M. Wouters and I. Carusotto, "Excitations in a Nonequilibrium Bose-Einstein Condensate of Exciton Polaritons," *Physical Review Letters*, vol. 99, Oct. 2007.

[46] N. Bobrovska and M. Matuszewski, "Adiabatic approximation and fluctuations in exciton-polariton condensates," *Physical Review B*, vol. 92, p. 035311, July 2015.

[47] M. Richard, J. Kasprzak, R. André, R. Romestain, L. S. Dang, G. Malpuech, and A. Kavokin, "Experimental evidence for nonequilibrium Bose condensation of exciton polaritons," *Physical Review B*, vol. 72, p. 201301, Nov. 2005.

[48] H. Franke, C. Sturm, R. Schmidt-Grund, G. Wagner, and M. Grundmann, "Ballistic propagation of exciton–polariton condensates in a ZnO-based microcavity," *New Journal of Physics*, vol. 14, p. 013037, Jan. 2012.

[49] D. N. Krizhanovskii, K. G. Lagoudakis, M. Wouters, B. Pietka, R. A. Bradley, K. Guda, D. M. Whittaker, M. S. Skolnick, B. Deveaud-Plédran, M. Richard, R. André, and L. S. Dang, "Coexisting nonequilibrium condensates with long-range spatial coherence in semiconductor microcavities," *Physical Review B*, vol. 80, p. 045317, July 2009.

[50] A. Baas, K. G. Lagoudakis, M. Richard, R. André, L. S. Dang, and B. Deveaud-Plédran, "Synchronized and desynchronized phases of exciton-polariton condensates in the presence of disorder," *Physical Review Letters*, vol. 100, p. 170401, Apr. 2008.

[51] T. Nattermann and V. L. Pokrovsky, "Bose-Einstein Condensates in Strongly Disordered Traps," *Physical Review Letters*, vol. 100, p. 060402, Feb. 2008.

[52] J. E. Lye, L. Fallani, M. Modugno, D. S. Wiersma, C. Fort, and M. Inguscio, "Bose-Einstein Condensate in a Random Potential," *Physical Review Letters*, vol. 95, p. 070401, Aug. 2005.

[53] M. P. A. Fisher, P. B. Weichman, G. Grinstein, and D. S. Fisher, "Boson localization and the superfluid-insulator transition," *Physical Review B*, vol. 40, pp. 546–570, July 1989.

[54] G. Malpuech, D. D. Solnyshkov, H. Ouerdane, M. M. Glazov, and I. Shelykh, "Bose Glass and Superfluid Phases of Cavity Polaritons," *Physical Review Letters*, vol. 98, p. 206402, May 2007.

[55] A. Janot, T. Hyart, P. R. Eastham, and B. Rosenow, "Superfluid stiffness of a driven dissipative condensate with disorder," *Physical Review Letters*, vol. 111, p. 230403, Dec. 2013.

[56] K. G. Lagoudakis, B. Pietka, M. Wouters, R. André, and B. Deveaud-Plédran, "Coherent oscillations in an exciton-polariton Josephson junction," *Physical Review Letters*, vol. 105, p. 120403, Sept. 2010.

[57] H. Ohadi, Y. del Valle-Inclan Redondo, A. J. Ramsay, Z. Hatzopoulos, T. C. H. Liew, P. R. Eastham, P. G. Savvidis, and J. J. Baumberg, "Synchronization crossover of polariton condensates in weakly disordered lattices," *Physical Review B*, vol. 97, p. 195109, May 2018.

[58] N. G. Berloff, M. Silva, K. Kalinin, A. Askitopoulos, J. D. Töpfer, P. Cilibrizzi, W. Langbein, and P. G. Lagoudakis, "Realizing the classical XY Hamiltonian in polariton simulators," *Nature Materials*, vol. 16, pp. 1120–1126, Nov. 2017.

[59] A. Amo and J. Bloch, "Exciton-polaritons in lattices: A non-linear photonic simulator," *Comptes Rendus Physique*, vol. 17, pp. 934–945, Oct. 2016.

[60] H. Ohadi, R. L. Gregory, T. Freegarde, Y. G. Rubo, A. V. Kavokin, N. G. Berloff, and P. G. Lagoudakis, "Nontrivial Phase Coupling in Polariton Multiplets," *Physical Review X*, vol. 6, p. 031032, Aug. 2016.

[61] J. D. Töpfer, J. D. Töpfer, I. Chatzopoulos, H. Sigurdsson, H. Sigurdsson, T. Cookson, Y. G. Rubo, P. G. Lagoudakis, and P. G. Lagoudakis, "Engineering spatial coherence in lattices of polariton condensates," *Optica*, vol. 8, pp. 106–113, Jan. 2021.

[62] M. Wouters, "Synchronized and desynchronized phases of coupled nonequilibrium exciton-polariton condensates," *Physical Review B*, vol. 77, p. 121302(R), Mar. 2008.

[63] M. Wouters and V. Savona, "Stochastic classical field model for polariton condensates," *Physical Review B*, vol. 79, p. 165302, Apr. 2009.

[64] L. M. Sieberer, S. D. Huber, E. Altman, and S. Diehl, "Dynamical Critical Phenomena in Driven-Dissipative Systems," *Physical Review Letters*, vol. 110, p. 195301, May 2013.

[65] E. Altman, L. M. Sieberer, L. Chen, S. Diehl, and J. Toner, "Two-dimensional superfluidity of exciton polaritons requires strong anisotropy," *Physical Review X*, vol. 5, p. 011017, Feb. 2015.

117

[66] L. He, L. M. Sieberer, E. Altman, and S. Diehl, "Scaling properties of one-dimensional driven-dissipative condensates," *Physical Review B*, vol. 92, p. 155307, Oct. 2015.

[67] K. Wiesenfeld, P. Colet, and S. H. Strogatz, "Frequency locking in Josephson arrays: Connection with the Kuramoto model," *Physical Review E*, vol. 57, pp. 1563–1569, Feb. 1998.

[68] S. Y. Kourtchatov, V. V. Likhanskii, A. P. Napartovich, F. T. Arecchi, and A. Lapucci, "Theory of phase locking of globally coupled laser arrays," *Physical Review A*, vol. 52, pp. 4089–4094, Nov. 1995.

[69] Y. Kuramoto, "Self-entrainment of a population of coupled non-linear oscillators," in *International Symposium on Mathematical Problems in Theoretical Physics* (H. Araki, ed.), Lecture Notes in Physics, (Berlin, Heidelberg), pp. 420–422, Springer, 1975.

[70] J. A. Acebrón, L. L. Bonilla, C. J. Pérez Vicente, F. Ritort, and R. Spigler, "The Kuramoto model: A simple paradigm for synchronization phenomena," *Reviews of Modern Physics*, vol. 77, pp. 137–185, Apr. 2005.

[71] D. Aronson, G. Ermentrout, and N. Kopell, "Amplitude response of coupled oscillators," *Physica D: Nonlinear Phenomena*, vol. 41, pp. 403–449, Apr. 1990.

[72] N. Kopell and G. B. Ermentrout, "Symmetry and phaselocking in chains of weakly coupled oscillators," *Communications on Pure and Applied Mathematics*, vol. 39, pp. 623–660, Sept. 1986.

[73] Y. Kuramoto, *Chemical Oscillations, Waves, and Turbulence*. Courier Corporation, Jan. 1984.

[74] N. Kopell and G. B. Ermentrout, "Phase Transitions and Other Phenomena in Chains of Coupled Oscillators," *SIAM Journal on Applied Mathematics*, vol. 50, pp. 1014–1052, June 1990.

[75] P. Östborn, "Frequency entrainment in long chains of oscillators with random natural frequencies in the weak coupling limit," *Physical Review E*, vol. 70, p. 016120, July 2004.

[76] H. Sakaguchi, S. Shinomoto, and Y. Kuramoto, "Local and global self-entrainments in oscillator lattices," *Progress of Theoretical Physics*, vol. 77, pp. 1005–1010, May 1987.

[77] S. H. Strogatz and R. E. Mirollo, "Phase-locking and critical phenomena in lattices of coupled nonlinear oscillators with random intrinsic frequencies," *Physica D: Nonlinear Phenomena*, vol. 31, pp. 143–168, June 1988.

[78] J. L. Doob, "Heuristic Approach to the Kolmogorov-Smirnov Theorems," *The Annals of Mathematical Statistics*, vol. 20, pp. 393–403, Sept. 1949.

[79] W. H. Press, S. A. Teukolsky, W. T. Vetterling, and B. P. Flannery, *Numerical Recipes 3rd Edition: The Art of Scientific Computing*. Cambridge University Press, Sept. 2007.

[80] A. Rößler, "Runge–Kutta methods for Stratonovich stochastic differential equation systems with commutative noise," *Journal of Computational and Applied Mathematics*, vol. 164–165, pp. 613–627, Mar. 2004.

[81] M. Galbiati, L. Ferrier, D. D. Solnyshkov, D. Tanese, E. Wertz, A. Amo, M. Abbarchi, P. Senellart, I. Sagnes, A. Lemaître, E. Galopin, G. Malpuech, and J. Bloch, "Polariton condensation in photonic molecules," *Physical Review Letters*, vol. 108, p. 126403, Mar. 2012.

[82] M. Abbarchi, A. Amo, V. G. Sala, D. D. Solnyshkov, H. Flayac, L. Ferrier, I. Sagnes, E. Galopin, A. Lemaître, G. Malpuech, and J. Bloch, "Macroscopic quantum self-trapping and Josephson oscillations of exciton polaritons," *Nature Physics*, vol. 9, pp. 275–279, May 2013.

[83] A. Askitopoulos, H. Ohadi, A. V. Kavokin, Z. Hatzopoulos, P. G. Savvidis, and P. G. Lagoudakis, "Polariton condensation in an optically induced two-dimensional potential," *Physical Review B*, vol. 88, p. 041308, July 2013.

[84] I. A. Shelykh, D. D. Solnyshkov, G. Pavlovic, and G. Malpuech, "Josephson effects in condensates of excitons and exciton polaritons," *Physical Review B*, vol. 78, p. 041302, July 2008.

[85] M. O. Borgh, J. Keeling, and N. G. Berloff, "Spatial pattern formation and polarization dynamics of a nonequilibrium spinor polariton condensate," *Physical Review B*, vol. 81, June 2010.

[86] P. Eastham and B. Rosenow, "Disorder, synchronization, and phase-locking in nonequilibrium Bose-Einstein condensates," in *Universal Themes of Bose-Einstein Condensation*, pp. 462–476, Cambridge University Press, 2017.

[87] I. L. Aleiner, B. L. Altshuler, and Y. G. Rubo, "Radiative coupling and weak lasing of exciton-polariton condensates," *Physical Review B*, vol. 85, p. 121301, Mar. 2012.

[88] M. Wouters, I. Carusotto, and C. Ciuti, "Spatial and spectral shape of inhomogeneous nonequilibrium exciton-polariton condensates," *Physical Review B*, vol. 77, p. 115340, Mar. 2008.

[89] F. Bello and P. R. Eastham, "Localization and self-trapping in driven-dissipative polariton condensates," *Physical Review B*, vol. 95, p. 245312, June 2017.

[90] A. J. Leggett, "Bose-Einstein condensation in the alkali gases: Some fundamental concepts," *Reviews of Modern Physics*, vol. 73, pp. 307–356, Apr. 2001.

[91] S. H. Strogatz, *Nonlinear Dynamics and Chaos: With Applications to Physics, Biology, Chemistry, and Engineering.* Studies in Nonlinearity, Cambridge, Mass: Perseus Books, 2. print ed., 2001.

[92] M. Tinkham, *Introduction to Superconductivity.* Dover Books on Physics Series, Dover Publications, 2004.

[93] W. C. Stewart, "Current-voltage characteristics of Josephson junctions," *Applied Physics Letters*, vol. 12, pp. 277–280, Apr. 1968.

[94] D. E. McCumber, "Effect of ac Impedance on dc Voltage-Current Characteristics of Superconductor Weak-Link Junctions," *Journal of Applied Physics*, vol. 39, pp. 3113–3118, June 1968.

[95] A. P. D. Love, D. N. Krizhanovskii, D. M. Whittaker, R. Bouchekioua, D. Sanvitto, S. A. Rizeiqi, R. Bradley, M. S. Skolnick, P. R. Eastham, R. André, and L. S. Dang, "Intrinsic Decoherence Mechanisms in the Microcavity Polariton Condensate," *Physical Review Letters*, vol. 101, p. 067404, Aug. 2008.

[96] G. Tosi, G. Christmann, N. G. Berloff, P. Tsotsis, T. Gao, Z. Hatzopoulos, P. G. Savvidis, and J. J. Baumberg, "Sculpting oscillators with light within a nonlinear quantum fluid," *Nature Physics*, vol. 8, pp. 190–194, Mar. 2012.

[97] D. M. Whittaker and P. R. Eastham, "Coherence properties of the microcavity polariton condensate," *EPL (Europhysics Letters)*, vol. 87, p. 27002, July 2009.

[98] L. K. Thomsen and H. M. Wiseman, "Atom-laser coherence and its control via feedback," *Physical Review A*, vol. 65, p. 063607, June 2002.

[99] F. Baboux, D. D. Bernardis, V. Goblot, V. N. Gladilin, C. Gomez, E. Galopin, L. L. Gratiet, A. Lemaître, I. Sagnes, I. Carusotto, M. Wouters, A. Amo, and J. Bloch, "Unstable and stable regimes of polariton condensation," *Optica*, vol. 5, pp. 1163–1170, Oct. 2018.

[100] M. Kardar, G. Parisi, and Y.-C. Zhang, "Dynamic scaling of growing interfaces," *Physical Review Letters*, vol. 56, pp. 889–892, Mar. 1986.

[101] W. Ebeling, A. Engel, B. Esser, and R. Feistel, "Diffusion and reaction in random media and models of evolution processes," *Journal of Statistical Physics*, vol. 37, pp. 369–384, Nov. 1984.

[102] T. Nattermann and W. Renz, "Diffusion in a random catalytic environment, polymers in random media, and stochastically growing interfaces," *Physical Review A*, vol. 40, pp. 4675–4681, Oct. 1989.

[103] J. Krug and T. Halpin-Healy, "Directed polymers in the presence of columnar disorder," *Journal de Physique I*, vol. 3, pp. 2179–2198, Nov. 1993.

[104] M. E. Cates and R. C. Ball, "Statistics of a polymer in a random potential, with implications for a nonlinear interfacial growth model," *Journal de Physique*, vol. 49, pp. 2009–2018, Dec. 1988.

[105] T. Halpin-Healy and Y.-C. Zhang, "Kinetic roughening phenomena, stochastic growth, directed polymers and all that. Aspects of multidisciplinary statistical mechanics," *Physics Reports*, vol. 254, pp. 215–414, Mar. 1995.

[106] I. Zapata, F. Sols, and A. J. Leggett, "Josephson effect between trapped Bose-Einstein condensates," *Physical Review A*, vol. 57, pp. R28–R31, Jan. 1998.

[107] H. Hong, H. Park, and M. Y. Choi, "Collective synchronization in spatially extended systems of coupled oscillators with random frequencies," *Physical Review E*, vol. 72, p. 036217, Sept. 2005.

[108] H. Sakaguchi, S. Shinomoto, and Y. Kuramoto, "Mutual Entrainment in Oscillator Lattices with Nonvariational Type Interaction," *Progress of Theoretical Physics*, vol. 79, pp. 1069–1079, May 1988.

[109] V. N. Gladilin, K. Ji, and M. Wouters, "Spatial coherence of weakly interacting one-dimensional nonequilibrium bosonic quantum fluids," *Physical Review A*, vol. 90, p. 023615, Aug. 2014.

[110] D. Squizzato, L. Canet, and A. Minguzzi, "Kardar-Parisi-Zhang universality in the phase distributions of one-dimensional exciton-polaritons," *Physical Review B*, vol. 97, p. 195453, May 2018.

[111] F. Domínguez-Adame and V. A. Malyshev, "A simple approach to Anderson localization in one-dimensional disordered lattices," *American Journal of Physics*, vol. 72, pp. 226–230, Feb. 2004.

[112] Y. Imry and S.-k. Ma, "Random-Field Instability of the Ordered State of Continuous Symmetry," *Physical Review Letters*, vol. 35, pp. 1399–1401, Nov. 1975.

[113] L. He, L. M. Sieberer, and S. Diehl, "Space-time vortex driven crossover and vortex turbulence phase transition in one-dimensional driven open condensates," *Physical Review Letters*, vol. 118, p. 085301, Feb. 2017.

[114] R. Lauter, A. Mitra, and F. Marquardt, "From Kardar-Parisi-Zhang scaling to explosive desynchronization in arrays of limit-cycle oscillators," *Physical Review E*, vol. 96, p. 012220, July 2017.

[115] S. F. Edwards and D. R. Wilkinson, "The surface statistics of a granular aggregate," *Proceedings of the Royal Society of London. A. Mathematical and Physical Sciences*, vol. 381, pp. 17–31, May 1982.

[116] D. Thouless, *Topological Quantum Numbers In Nonrelativistic Physics*. World Scientific, Mar. 1998.

[117] J. Keeling, L. M. Sieberer, E. Altman, L. Chen, S. Diehl, and J. Toner, "Superfluidity and Phase Correlations of Driven Dissipative Condensates,"

in *Universal Themes of Bose-Einstein Condensation* (D. W. Snoke, N. P. Proukakis, and P. B. Littlewood, eds.), pp. 205–230, Cambridge: Cambridge University Press, 2017.

[118] A. Amo, J. Lefrère, S. Pigeon, C. Adrados, C. Ciuti, I. Carusotto, R. Houdré, E. Giacobino, and A. Bramati, "Superfluidity of polaritons in semiconductor microcavities," *Nature Physics*, vol. 5, pp. 805–810, Nov. 2009.

[119] M. E. Fisher, M. N. Barber, and D. Jasnow, "Helicity Modulus, Superfluidity, and Scaling in Isotropic Systems," *Physical Review A*, vol. 8, pp. 1111–1124, Aug. 1973.

[120] M. Wouters and I. Carusotto, "Superfluidity and Critical Velocities in Nonequilibrium Bose-Einstein Condensates," *Physical Review Letters*, vol. 105, p. 020602, July 2010.

[121] A. Chiocchetta and I. Carusotto, "Non-equilibrium quasi-condensates in reduced dimensions," *EPL (Europhysics Letters)*, vol. 102, p. 67007, June 2013.

[122] J. Krug, "Origins of scale invariance in growth processes," *Advances in Physics*, vol. 46, pp. 139–282, Apr. 1997.

[123] T. Halpin-Healy and K. A. Takeuchi, "A KPZ Cocktail-Shaken, not Stirred...: Toasting 30 Years of Kinetically Roughened Surfaces," *Journal of Statistical Physics*, vol. 160, pp. 794–814, Aug. 2015.

[124] F. Family and T. Vicsek, "Scaling of the active zone in the Eden process on percolation networks and the ballistic deposition model," *Journal of Physics A: Mathematical and General*, vol. 18, pp. L75–L81, Feb. 1985.

[125] P. Comaron, I. Carusotto, M. H. Szymańska, and N. P. Proukakis, "Non-equilibrium Berezinskii-Kosterlitz-Thouless transition in driven-dissipative condensates (a)," *EPL (Europhysics Letters)*, vol. 133, p. 17002, Jan. 2021.

[126] V. N. Gladilin and M. Wouters, "Noise-induced transition from superfluid to vortex state in two-dimensional nonequilibrium polariton condensates," *Physical Review B*, vol. 100, p. 214506, Dec. 2019.

[127] K. P. Kalinin and N. G. Berloff, "Polaritonic network as a paradigm for dynamics of coupled oscillators," *Physical Review B*, vol. 100, p. 245306, Dec. 2019.